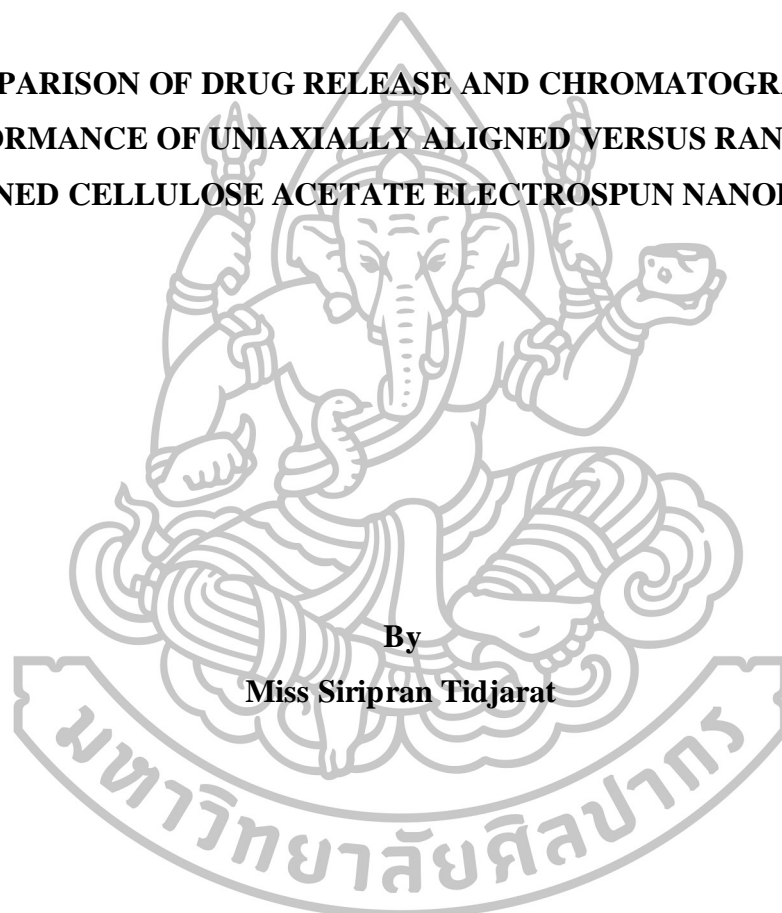




**COMPARISON OF DRUG RELEASE AND CHROMATOGRAPHIC
PERFORMANCE OF UNIAXIALLY ALIGNED VERSUS RANDOMLY
ALIGNED CELLULOSE ACETATE ELECTROSPUN NANOFIBERS**



**By
Miss Siripran Tidjarat**

**A Thesis Submitted in Partial Fulfillment of the Requirements for the Degree
Doctor of Philosophy Program in Pharmaceutical Technology
Graduate School, Silpakorn University
Academic Year 2015
Copyright of Graduate School, Silpakorn University**

**COMPARISON OF DRUG RELEASE AND CHROMATOGRAPHIC
PERFORMANCE OF UNIAXIALLY ALIGNED VERSUS RANDOMLY
ALIGNED CELLULOSE ACETATE ELECTROSPUN NANOFIBERS**



**By
Miss Siripran Tidjarat**

**A Thesis Submitted in Partial Fulfillment of the Requirements for the Degree
Doctor of Philosophy Program in Pharmaceutical Technology
Graduate School, Silpakorn University
Academic Year 2015
Copyright of Graduate School, Silpakorn University**

การเปรียบเทียบการปลดปล่อยยาและสมรรถนะในการแยกสารโดยวิธีโครมาโทกราฟีของเส้นใย
นาโนอิเล็กทรอนิกส์บนเซลลูโลสอะซิเตตชนิดเรียงตัวเป็นแนวเดียวกับชนิดเรียงตัวอย่างไร้แบบแผน



วิทยานิพนธ์นี้เป็นส่วนหนึ่งของการศึกษาตามหลักสูตรปริญญาเภสัชศาสตรดุษฎีบัณฑิต

สาขาวิชาเทคโนโลยีเภสัชกรรม

บัณฑิตวิทยาลัย มหาวิทยาลัยศิลปากร

ปีการศึกษา 2558

ลิขสิทธิ์ของบัณฑิตวิทยาลัย มหาวิทยาลัยศิลปากร

The Graduate School, Silpakorn University has approved and accredited the thesis title of “Comparison of drug release and chromatographic performance of uniaxially aligned versus randomly aligned cellulose acetate electrospun nanofibers” submitted by Miss Siripran Tidjarat as a partial fulfillment of the requirements for the degree of Doctor of Philosophy in Pharmaceutical Technology.

.....
(Associate Professor Panjai Tantatsanawong, Ph.D.)

Dean of Graduate School
...../...../.....

The Thesis Advisors

1. Associate Professor Praneet Opanasopit, Ph.D.
2. Associate Professor Theerasak Rojanarata, Ph.D.

The Thesis Examination Committee

..... Chairman
(Associate Professor Tanasait Ngawhirunpat, Ph.D.)
...../...../.....

..... Member
(Assistant Professor Warisada Sila-on, Ph.D.)
...../...../.....

..... Member
(Associate Professor Praneet Opanasopit, Ph.D.)
...../...../.....

..... Member
(Associate Professor Theerasak Rojanarata, Ph.D.)
...../...../.....

53354808 : MAJOR : PHARMACEUTICAL TECHNOLOGY

KEY WORDS : NANOFIBERS / ELECTROSPINNING / CELLULOSE ACETATE / ARBUTIN / THIN LAYER CHROMATOGRAPHY / HYDROQUINONE / RETINOIC ACID

SIRIPRAN TIDJARAT : COMPARISON OF DRUG RELEASE AND CHROMATOGRAPHIC PERFORMANCE OF UNIAXIALLY ALIGNED VERSUS RANDOMLY ALIGNED CELLULOSE ACETATE ELECTROSPUN NANOFIBERS. THESIS ADVISORS : ASSOC. PROF. PRANEET OPANASOPIT, Ph.D. AND ASSOC. PROF. THEERASAK ROJANARATA, Ph.D. xxx pp.

In this study, arbutin (AR)-loaded cellulose acetate (CA) electrospun nanofibers were fabricated by electrospinning process. The morphological, physical, chemical and mechanical properties of obtained nanofibers were studied. The effect of the speed of drum collector that affected on the arrangement of nanofibers, degree of swelling (%), weight loss (%), AR loading efficiency (%) and AR release were investigated. The results indicated that the increasing rotation speed of drum collector from 350 to 2000 and 6000 rpm resulted in the nanofibers with random, semi-aligned and mostly aligned orientation, respectively. The diameters of AR-loaded nanofibers were in the range of 616 - 624 nm without the AR crystals in the structure. The layer thickness of the nanofibers slightly decreased as increasing alignment. The mostly aligned nanofiber mats had the lowest tensile strengths when they were stretched in the direction perpendicular to the fiber alignment. On the contrary, if the mats were pulled along the fiber alignment direction, it showed the highest tensile strength value. No difference of tensile strength was observed for the random nanofibers even they were pulled in the different directions. For semi-aligned nanofibers, this mechanical behavior was in between those of the random and mostly aligned nanofibers. At 24 h, the degree of swelling of random, semi-aligned and mostly aligned nanofibers was 381%, 270% and 202%, respectively. The random nanofibers were much fluffier than other types whereas the mostly aligned nanofibers well remained its appearance as the intact sheet. The percent weight loss was about 8 %w/w and not significantly different among the types of differently aligned nanofibers. The drug loading efficiencies were found to be more than 90 %, demonstrating that most AR was successfully loaded into the nanofibers. In term of drug release, all types of nanofibers rapidly released AR and reached 80% of drug release in 1.7, 4.2 and 9.4 min for the mostly aligned, semi-aligned and random nanofibers, respectively. From these results, it can be concluded that the fastest AR release can be obtained by fabricating CA nanofibers in highly aligned orientation. This finding indicates the feasibility to use highly aligned nanofibers for delivery of certain drugs in fast-releasing formulations. For the comparison of thin-layer chromatographic (TLC) performance, CA nanofibers with different degree of alignment were fabricated by using different collector rotation speeds. Chromatographic separation ability of CA nanofibers, appearance and detectability level of spots on CA nanofibers, migration rate of solutes on CA nanofibers were evaluated and application of CA nanofibers to screening of adulterated substances in cosmetics was investigated. The average diameters of nanofibers ranged from 500 - 730 nm. Tested by using 3 analytes i.e. hydroquinone (HQ), retinoic acid (RA) and vitamin C (VC) and methanol/water/acetic acid (65:35:2.5) as the mobile phase, good resolution was obtained from mostly aligned and random nanofibers electrospun for 6 h and 4 h, respectively. The initial spots of samples on the mostly aligned nanofibers were more elliptical than those on random ones. After the separation, the spots appearing on the mostly aligned nanofibers were twice smaller and darker compared to those on the random ones. The masses of HQ and RA which could be visually detected on the mostly aligned CA nanofiber plates were twice lower than those on the random nanofibers. Moreover, the masses of both compounds which could be detected on the mostly aligned CA nanofibers were five times lower than those on typical silica plates. The solvent migration on the mostly aligned nanofibers was more rapid than that on the random ones. The applicability of the mostly aligned CA nanofibers was evaluated by the analysis of cosmetic creams. HQ and RA were efficiently separated from the substances which could form colored spots with phosphomolybdic acid. Also, it was found that the screening performed by using the mostly aligned CA nanofibers gave results in agreement with the confirmatory HPLC method according to ASEAN guidelines.

Program of Pharmaceutical Technology

Graduate School, Silpakorn University

Student's signature.....

Academic Year 2015

Thesis Advisors' signature 1..... 2.....

53354808 : สาขาวิชาเทคโนโลยีเกษตรกรรม

คำสำคัญ : เส้นใยนาโน / อิเล็กโตรสปินนิ่ง / เซลลูโลสอะซิเตต / อาร์บูติน / ทินเลเซอร์โครมาโทกราฟี / ไฮโดรควิโนน / กรดเรทิโนอิก

ศิริพรหม ทิศจรัส : การเปรียบเทียบการปลดปล่อยยาและสมรรถนะในการแยกสาร โดยวิธีโครมาโทกราฟีของเส้นใยนาโนอิเล็กโตรสปินเซลลูโลสอะซิเตตชนิดเรียงตัวเป็นแนวเดียวกับชนิดเรียงตัวอย่างไร้แบบแผน. อาจารย์ที่ปรึกษาวิทยานิพนธ์ : ภาณุ.รศ.ดร. ปราณีต โอปณะโสภิต และ ภาณุ.รศ.ดร.ธีรศักดิ์ ใจจนราธา. xxx หน้า.

ในการศึกษานี้เตรียมเส้นใยนาโนจากเซลลูโลสอะซิเตต (ซีเอ) ที่บรรจุอาร์บูติน (เออาร์) ด้วยวิธีอิเล็กโตรสปินนิ่ง ศึกษาสัณฐานวิทยา สมบัติเชิงกายภาพ เหนียว และเชิงกล ของเส้นใยที่เตรียมได้ ศึกษาผลของความเร็วรอบของวัตุรองรับที่ส่งผลต่อการจัดเรียงตัวของเส้นใย ประเมินสมบัติการพองตัวและการสูญเสียน้ำหนักของแผ่นเส้นใย หาปริมาณยาในแผ่นเส้นใย และการปลดปล่อยยาผลการทดลองพบว่าเมื่อเพิ่มความเร็วรอบของวัตุรองรับสูงขึ้นจาก 350 ถึง 2000 และ 6000 รอบต่อนาที พบว่าเส้นใยมีการจัดเรียงตัวในแนวเดียวกันมากขึ้น ได้เส้นใยที่จัดเรียงตัวอย่างไร้แบบแผน กึ่งเป็นแนวเดียว และเป็นแนวเดียว ตามลำดับ ขนาดเส้นผ่านศูนย์กลางของเส้นใยที่บรรจุเออาร์อยู่ในช่วง 616 ถึง 624 นาโนเมตร โดยปราศจากผลึกเออาร์ในโครงสร้าง ชั้นความหนาของเส้นใยลดลงเล็กน้อยเมื่อเส้นใยจัดเรียงตัวเป็นแบบแนวเดียวกันมากขึ้น ทดสอบคุณสมบัติเชิงกลของแผ่นเส้นใยทั้งสามชนิดโดยดึงด้วยแรงสองแนว คือ ทิศการดึงตั้งฉากกับแนวเส้นใยและทิศการดึงขนานกับแนวเส้นใย พบว่าเส้นใยแบบแนวเดียว เมื่อดึงในทิศตั้งฉากจะมีค่าความทนต่อแรงดึงน้อยที่สุดในทางกลับกันเมื่อดึงในทิศขนานกับแนวเส้นใยจะมีค่าความทนต่อแรงดึงสูงสุด ส่วนเส้นใยแบบกึ่งเป็นแนวเดียวจะมีค่าความทนต่อแรงดึงอยู่ในช่วงระหว่างของเส้นใยแบบไร้แบบแผนและเส้นใยแบบแนวเดียวและค่าความทนต่อแรงดึงที่ได้จากการดึงเส้นใยแบบไร้แบบแผน ทั้งสองแนว นั้นได้ค่าที่ใกล้เคียงกัน ค่าร้อยละการพองตัวในน้ำที่เวลา 24 ชั่วโมง ของแผ่นเส้นใยทั้งสามชนิด ไร้แบบแผน กึ่งเป็นแนวเดียว และเป็นแนว คือ 381 270 และ 202 ตามลำดับ แผ่นเส้นใยแบบไร้แบบแผนมีลักษณะพุ่มากกว่าเส้นใยอีกสองชนิดซึ่งคงลักษณะความเป็นแผ่นแบบเดิมอยู่ การสูญเสียน้ำหนักของแผ่นเส้นใยทั้งสามชนิดมีค่าไม่แตกต่างกัน คือ ประมาณ ร้อยละ 8 เมื่อวิเคราะห์หาปริมาณยาเออาร์ในแผ่นเส้นใยพบว่าแผ่นเส้นใยทั้งสามชนิดมีค่าการบรรจุยาได้มากกว่าร้อยละ 90 ซึ่งแสดงถึงความสำเร็จในการบรรจุเออาร์ ลงในแผ่นเส้นใย การทดสอบการปลดปล่อยยาพบว่าแผ่นเส้นใยบรรจุเออาร์ทั้งสามชนิดให้ การปลดปล่อยยาเออาร์อย่างรวดเร็วภายใน 10 นาทีแรกของการทดสอบ และที่ปริมาณยาที่ปลดปล่อยสะสมเท่ากันคือ ร้อยละ 80 พบว่าแผ่นเส้นใยที่จัดเรียงตัวอย่างไร้แบบแผน กึ่งเป็นแนวเดียว และเป็นแนวเดียว ใช้เวลาในการปลดปล่อยยา 1.7 4.2 และ 9.4 นาที ตามลำดับ ผลที่ได้นี้สามารถสรุปได้ว่าเออาร์สามารถปลดปล่อยได้เร็วที่สุดจากแผ่นเส้นใยแบบที่มีการจัดเรียงตัวในแนวเดียวกัน การค้นพบนี้เป็นอีกข้อดีของแผ่นเส้นใยแบบที่มีการจัดเรียงตัวในแนวเดียวกันเพื่อนำไปประยุกต์ใช้ในการนำส่งยาที่ต้องการให้ปลดปล่อยยาเร็วได้ สำหรับการเปรียบเทียบสมรรถนะในการแยกสาร โดยวิธีโครมาโทกราฟีคิวบาง (ทีแอลซี) นั้น เตรียมแผ่นเส้นใยนาโนจากเซลลูโลสอะซิเตต (ซีเอ) ที่มีการจัดเรียงตัวของเส้นใยตั้งกันทั้งสามแบบ ศึกษาความสามารถในการแยกสาร ลักษณะของสเปกตรัมและความสามารถในการตรวจพบสาร อัตราการเคลื่อนที่ของสารบนแผ่นเส้นใย และการประยุกต์ใช้แผ่นเพื่อตรวจวิเคราะห์สารห้ามใช้เบื้องต้นในตัวอย่างเครื่องสำอาง ขนาดเส้นผ่านศูนย์กลางของเส้นใยอยู่ในช่วง 500 ถึง 730 นาโนเมตร นำมาทดสอบประสิทธิภาพการแยกสารสามชนิด คือ ไฮโดรควิโนน (เอชคิว) กรดเรทิโนอิก (อาร์เอ) และวิตามินซี (วีซี) โดยใช้วัตุภาคเคลื่อนที่ คือ เมทานอล/น้ำ/กรดอะซิติก อัตราส่วน 65:35:2.5 (ร้อยละ โดยปริมาตร) พบว่าแผ่นแบบเส้นใยจัดเรียงตัวแบบเป็นแนวเดียวและแบบไร้แบบแผนมีประสิทธิภาพในการแยกสารดีที่เวลา 6 และ 4 ชั่วโมง ตามลำดับ เมื่อสังเกตด้วยตาเปล่าจะเห็นว่า สเปกตรัมเริ่มต้นของตัวอย่างบนแผ่นแบบแนวเดียวมีลักษณะเป็นรูปไข่มากกว่าแผ่นแบบไร้แบบแผน หลังจากทำการแยกแล้ว พบว่าสเปกตรัมของสารบนแผ่นแบบแนวเดียวมีขนาดเล็กกว่าและสีเข้มกว่าเมื่อเปรียบเทียบกับแผ่นแบบไร้แบบแผน เมื่อวัดขนาดสเปกตรัมพบว่าขนาดบนแผ่นแบบไร้แบบแผนมีขนาดใหญ่กว่าบนแผ่นแบบแนวเดียวสองเท่า ปริมาณของเอชคิวและอาร์เอ ที่สามารถตรวจพบบนแผ่นแบบแนวเดียวต่ำกว่าบนแผ่นแบบไร้แบบแผน ถึงสองเท่า และปริมาณของทั้งเอชคิว และอาร์เอที่สามารถตรวจพบบนแผ่นแบบแนวเดียวต่ำกว่าบนแผ่นชนิดที่ทำตามวิธีของอาเซียนถึงห้าเท่า ตัวทำละลายเคลื่อนที่ไปบนแผ่นแบบแนวเดียวได้เร็วกว่าแผ่นแบบไร้แบบแผน ในการศึกษาก่อนหน้านี้ เมื่อใช้วัตุภาคเคลื่อนที่เหมือนกัน การใช้แผ่นแบบแนวเดียว ในการแยกสารนั้นใช้เวลาน้อยกว่าแผ่นแบบไร้แบบแผน 2-3 เท่า นอกจากนี้สามารถใช้แผ่นแบบแนวเดียววิเคราะห์ตัวอย่างเครื่องสำอางที่สุ่มเก็บจากท้องตลาด สารเอชคิว และ อาร์เอ สามารถแยกออกจากสารอื่นๆ ที่สามารถเคลื่อนที่กับกรดฟอสโฟโมลลิค สรุปได้ว่าการศึกษาตรวจสอบเบื้องต้นด้วยแผ่นเส้นใยแบบแนวเดียวนั้นให้ผลการวิเคราะห์ที่สอดคล้องกับวิธี เอชทีแอลซี ตามวิธีที่อาเซียนกำหนด

สาขาวิชาเทคโนโลยีเกษตรกรรม

บัณฑิตวิทยาลัย มหาวิทยาลัยศิลปากร

ลายมือชื่อนักศึกษา.....

ปีการศึกษา 2558

ลายมือชื่ออาจารย์ที่ปรึกษาวิทยานิพนธ์ 1.....2.....

ACKNOWLEDGEMENTS

I wish to express sincere appreciation to every people who contributed in diverse ways to the success of my research. I am heartily thankful to my thesis advisor, Associate Professor Dr. Praneet Opanasopit and Associate Professor Dr. Theerasak Rojanarata whose encouragement, guidance and support from the initial to the final level enabled me to develop an understanding of the dissertation. I also would like to appreciate Ms. Areerut Sripattanaporn for her helpful support and supplying me in laboratory instruments.

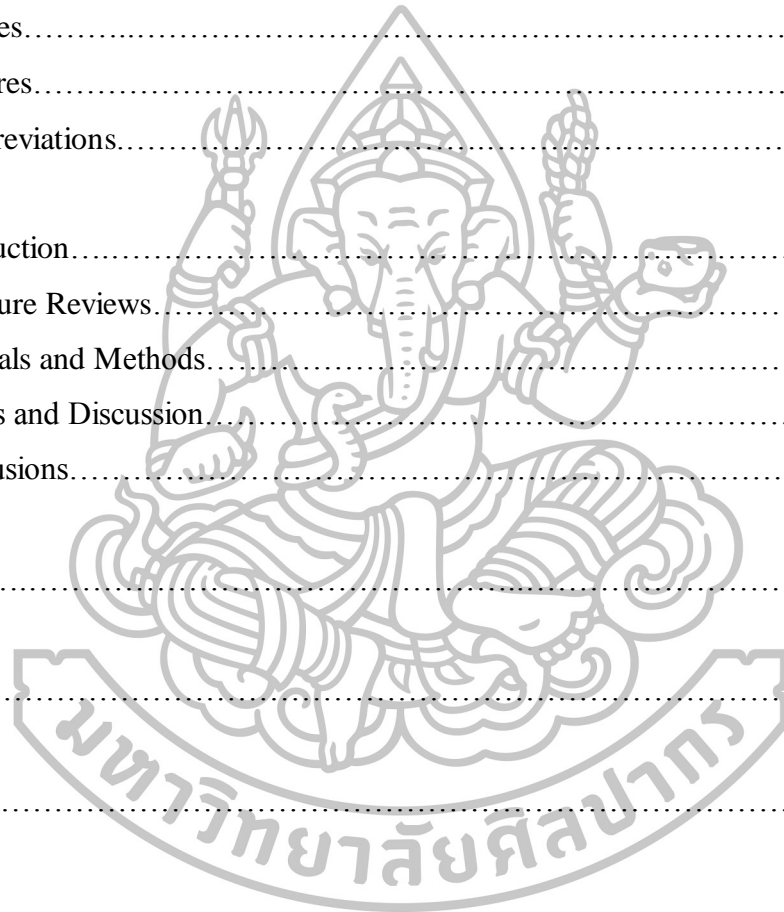
I would like to sincere thanks to all teachers, follow graduate students, researchers and the staff in Faculty of pharmacy, Silpakorn University, for giving me the place, equipments, knowledge and friendship.

My next appreciation goes to the graduate school of Silpakorn University for financial support. The Silpakorn Research and Development Institute for facility support. I also would like to pass my heartfelt thanks to all my friends and members of the Pharmaceutical Development of Green Innovation Group (PDGIG) for caring, friendship and generous support.

Finally, I would like to show my greatest appreciation to my family and Mr. Anon Chumphonanan for everything especially love, caring, understanding, encouragement, and believing in me.

TABLE OF CONTENTS

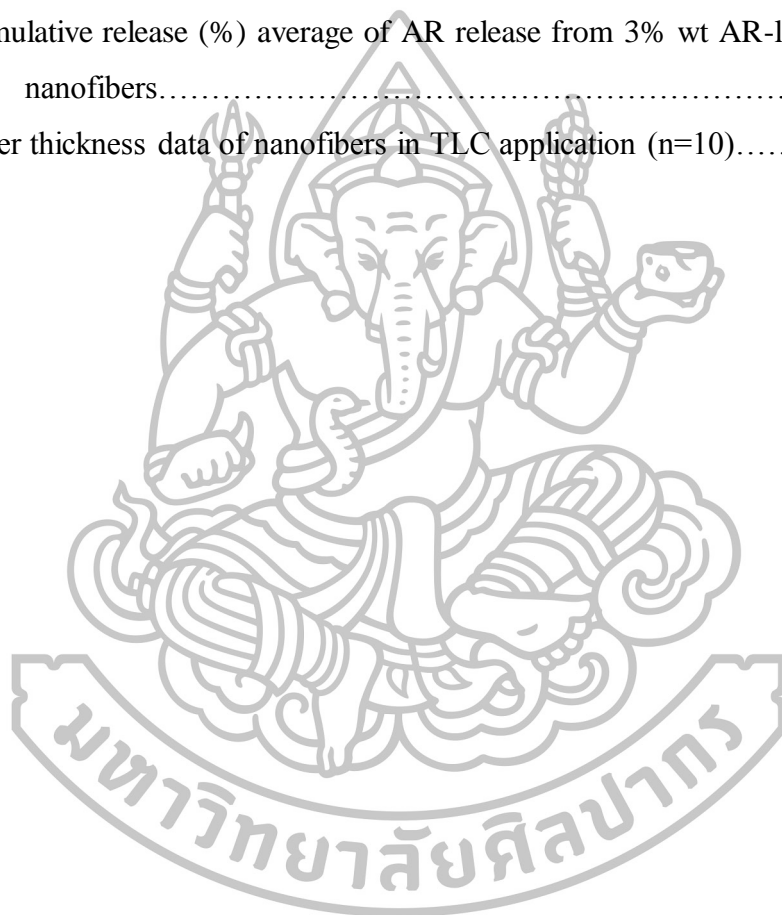
	Page
English Abstract.....	iv
Thai Abstract.....	v
Acknowledgements.....	vi
List of Tables.....	viii
List of Figures.....	x
List of Abbreviations.....	xiii
Chapter	
1 Introduction.....	1
2 Literature Reviews.....	5
3 Materials and Methods.....	43
4 Results and Discussion.....	56
5 Conclusions.....	82
References.....	84
Appendix.....	94
Biography.....	116



LIST OF TABLES

Table	Page
2.1 Different polymers used in electrospinning, characterization methods and their applications.....	12
2.2 Electrospinning parameters and their assumed effects on fiber morphology	19
2.3 Chromatographic adsorbents.....	36
2.4 Eluting solvents for chromatography.....	38
2.5 Adsorbability of organic compounds by functional group	39
3.1 Physicochemical properties of some chemicals used in this study	45
4.1 Shear viscosity and electrical conductivity of CA solution with and without AR (n=5).....	58
4.2 Effect of collector rotation speed on fiber morphology, alignment, diameters and layer thickness of AR-loaded nanofibers	60
4.3 Tensile strength (N/mm ²) of AR-loaded nanofiber mats (n=5).....	63
4.4 Loading efficiency of AR in CA nanofibers (n=3).....	69
4.5 Effect of drum-rotation speed on fiber morphology and alignment of CA nanofibers	74
4.6 Effect of spin time on TLC separation of HQ, RA and VC	76
4.7 Area of analyte spots on mostly aligned and random CA nanofibers (n=4).....	78
4.8 Masses of HQ and RA which could be visualized on different types of TLC plates	79
A.1 The diameter data of AR-loaded nanofibers (n = 50).....	96
A.2 Layer thickness data of AR-loaded nanofibers (n = 10).....	98
A.3 Tensile strength (N/mm ²) data of AR-loaded nanofibers (n = 5).....	99
A.4 The % degree of swelling data in first 10 min of AR-loaded nanofibers	101
A.5 The % degree of swelling and % weight loss data in 24 h of AR-loaded nanofibers.....	101

Table	Page
A.6 Cumulative release (%) of AR release from 3% wt AR-loaded random nanofibers.....	102
A.7 Cumulative release (%) of AR release from 3% wt AR-loaded semi-aligned nanofibers.....	103
A.8 Cumulative release (%) of AR release from 3% wt AR-loaded aligned nanofibers.....	104
A.9 Cumulative release (%) average of AR release from 3% wt AR-loaded nanofibers.....	105
A.10 Layer thickness data of nanofibers in TLC application (n=10).....	107



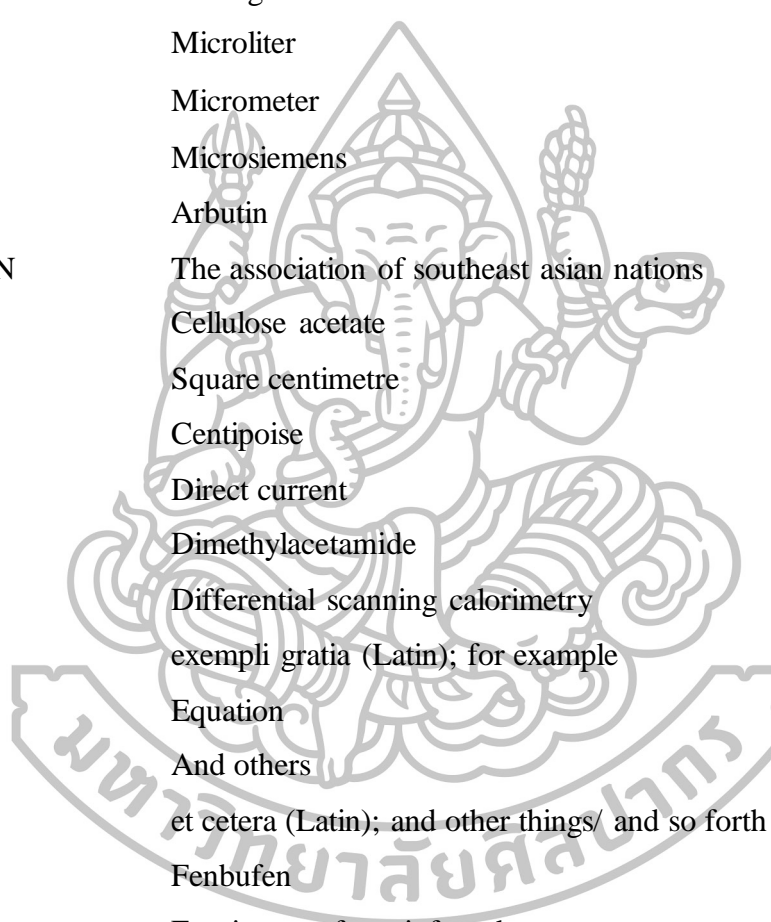
LIST OF FIGURES

Figure	Page
2.1 Schematic illustrating the electrospinning setup	8
2.2 Schematic diagram of set up of electrospinning apparatus (a) typical vertical setup and (b) horizontal setup of electrospinning apparatus	9
2.3 Illustration of Taylor cone formation: (A) Surface charges are induced in the polymer solution due to the electric field. (B) Elongation of the pendant drop. (C) Deformation of the pendant drop to the form the Taylor cone and jet initiation.....	10
2.4 Schematic illustrating the inverted conical path the jet travels before being collected as randomly oriented fibers. The inset shows a SEM image of randomly deposited electrospun nylon 6,6 fibers.....	11
2.5 Schematic illustration of the effect of the concentration, flow rate, and voltage on electrospayed/electrospun nano/microstructure	21
2.6 Different applications of electrospun nanofibers	23
2.7 A rotating cylinder collector to obtain unidirectional nanofiber alignment along the rotation direction	26
2.8 Influence of conducting wire placed below a glass slide on the deposition of the electrospun fibers. (A) Grounded electrode placed under a glass cover slip. (B) Electrospun fibers deposited on the glass cover slip	27
2.9 Controlled deposition area using a single auxiliary ring	28
2.10 (a) Schematic illustration of a gap method setup used generate uniaxially aligned nanofibers. The collector contained two pieces of conductive silicon stripes separated by a gap. (b) Calculated electric field strength vectors in the region between the the needle and the collector. The arrows denote the direction of the electrostatic field	

Figure	Page
(c) Electrostatic force analysis of a charged nanofiber spanning across the gap. The electrostatic force (F_1) resulted from the electric field and the Coulomb interactions (F_2) between the positive charges on the nanofiber and the negative image charges on the two grounded electrodes	29
2.11 Magnetic forces through the use of a pair of permanent magnets (The yellow plates are grounded conductive electrodes).....	31
2.12 Scheme presenting the possibilities drug loading in/on nanofibers.....	32
2.13 Different mechanism of drug release	34
2.14 Position of the spot on a thin layer plate	40
2.15 TLC plate showing distances traveled by the spot and the solvent after solvent front nearly reached the top of the adsorbent	40
3.1 Schematic representation of the electrospinning apparatus setup.....	48
3.2 HPLC chromatogram of AR.....	51
3.3 Standard curve for the quantitation of AR using HPLC-UV detector...	52
4.1 FT-IR spectra of the AR, CA and three types of CA nanofibers	61
4.2 Proposed illustrations of differently aligned nanofibers upon being stretched in parallel or perpendicular directions; (a) and (b) mostly aligned, (c) random nanofibers	63
4.3 Powder X-ray diffractograms of the AR, CA and three types of CA nanofibers	64
4.4 DSC thermograms of the AR, CA and three types of CA nanofibers.....	65
4.5 Degree of swelling of AR loaded nanofibers within the first 10 min; (▼) mostly aligned (o) semi-aligned (●) random nanofibers (n=3).....	67
4.6 Degree of swelling and weight loss of the AR loaded nanofibers at 24 h (n=3).....	67

Figure	Page
4.7 Images of nanofibers in swelling experiments at 1 min, 10 min and 24 h	68
4.8 Percent cumulative release of AR from nanofibers; (▼) mostly aligned, (o) semi-aligned, (●) random nanofibers (n=3).....	70
4.9 Model of drug release in mostly aligned and random nanofibers.....	72
4.10 Thickness of mostly aligned (●) and random (o) nanofiber layers as a function of spin time (n=10).....	75
4.11 The separation of hydroquinone and retinoic acid on the (a) silica plates (upper spot: RA and lower spot: HQ) and (b) C18 silica plates (upper spot: HQ and lower spot: RA) using mobile phases containing different percentages of methanol to water in the presence of 2.5% acetic acid.....	77
4.12 Results of interference study for the proposed TLC screening method. The masses of HQ, RA, VC, AR and RS are 62, 335, 500, 500 and 50 ng per spot, respectively.....	81
4.13 TLC results for the analysis of three different samples on mostly aligned CA nanofiber plates. S1 contained neither HQ nor RA whereas S2 and S3 were adulterated with HQ and RA, respectively. Standard (STD) RA, VC and HQ are in the right lane.....	81
A.1 Layer thickness of (a) random nanofibers, (b) semi-aligned nanofibers and (c) Aligned nanofibers.....	98
A.2 Percent cumulative release of AR from nanofibers; (▼) mostly aligned, (o) semi-aligned, (●) random nanofibers (n = 3) in 90 min.....	106
A.3 Percent cumulative release of AR from nanofibers; (▼) mostly aligned, (o) semi-aligned, (●) random nanofibers (n = 3) in 10 min.....	106

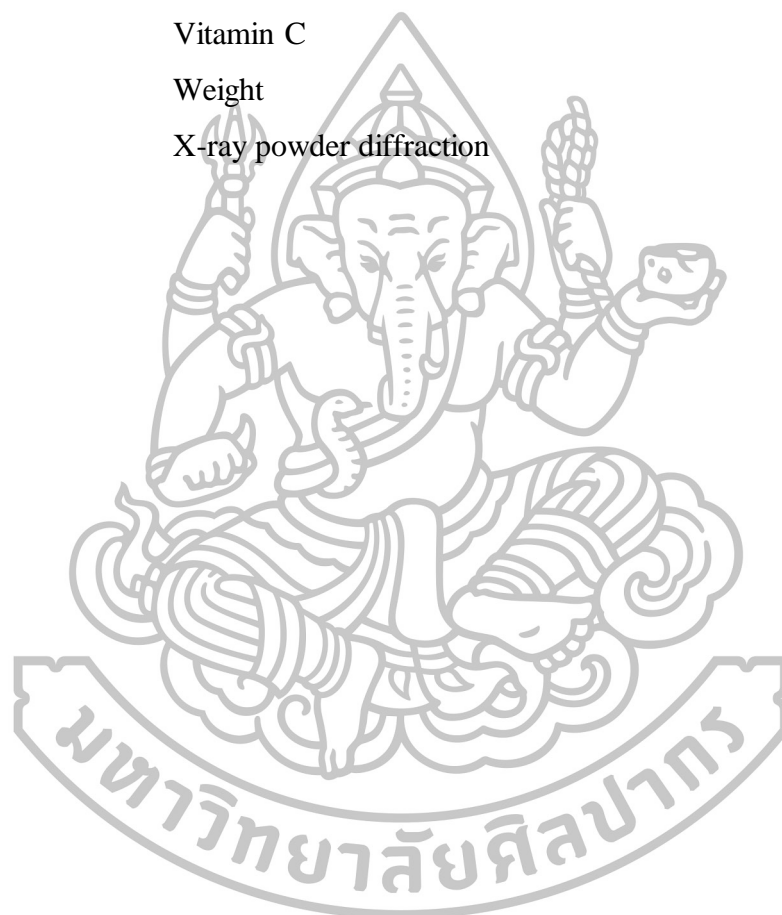
LIST OF ABBREVIATIONS



®	Registered trademark
% w/v	Percent weight by volume
% v/v	Percent volume by volume
°C	Degree Celsius
µg	Microgram
µL	Microliter
µm	Micrometer
µs	Microsiemens
AR	Arbutin
ASEAN	The association of southeast asian nations
CA	Cellulose acetate
cm ²	Square centimetre
cP	Centipoise
DC	Direct current
DMAc	Dimethylacetamide
DSC	Differential scanning calorimetry
e.g.	exempli gratia (Latin); for example
Eq	Equation
et al.	And others
etc.	et cetera (Latin); and other things/ and so forth
FBF	Fenbufen
FT-IR	Fourier transform infrared spectroscopy
g	Gram
h	Hour
H-NMR	Proton nuclear magnetic resonance
HCl	Hydrochloride
HPLC	High performance liquid chromatography
HPTLC	High performance thin layer chromatography
HQ	Hydroquinone

i.e.	id est (Latin); that is
IBU	Ibuprofen
IND	Indomethacin
IR	Infrared
KBr	Potassium bromide
kV	Kilovolt
L.O.D.	Limit of detection
mg	Milligram
min	Minute
mL	Milliliter
mm	Millimeter
mm ²	Square metre
MW	Molecular weight
N	Newton
NAP	Naproxen
ng	Nanogram
nm	Nanometer
OH	Hydroxide
PAN	Polyacrylonitrile
PBS	Phosphate buffer saline
pH	Potentia hydrogenii (latin); power of hydrogen
pKa	$-\log_{10}K_a$
PLGA	Poly(lactide-co-glycolide)
PVA	Polyvinyl alcohol
q	Coulomb
RA	Retinoic acid
R _f	Retardation factor
rpm	Round per minute
RS	Resorcinol
s	Second
SD	Standard deviation

SEM	Scanning electron microscopy
STD	Standard
SUL	Sulindac
TLC	Thin layer chromatography
UPS	Uninterruptible power supply
UV	Ultraviolet
V	Volume
VC	Vitamin C
wt	Weight
XRD	X-ray powder diffraction



CHAPTER 1

INTRODUCTION

1.1 Statement and significance of the research problem

Electrospinning is used to produce nanofibers because it is a simple and easy way to control the morphology of ultrafine fibers. In electrospinning process, high voltage is applied to a capillary containing a polymer solution. A droplet of the polymer solution then forms at the tip of the capillary, creating a point known as the “Taylor cone.” As electrostatic forces overcome the surface tension of the polymer solution, the solution is ejected from the nozzle tip towards the grounded collector, solvent rapidly evaporates and nonwoven fiber mat is collected [1, 2]. This phenomenon results in the formation of extremely small fibers with high surface area, high porosity and controllable compositions and size. Because there are many advantages, electrospun nanofibers are popular in a variety of fields, for example, medical wound dressings, tissue engineering, thin layer chromatography (TLC) and drug loading into nanofibers for delivery to the drug target [3] e.g. Wei Quin et al. prepared core-shell nanofibers that provided *in vitro* dual drug release profiles of acetaminophen [4] and Nagy et al. prepared Donepezil HCl loaded nanofibers as a potential orally dissolving dosage form for producing acceptable and effective dosage forms for children, older people and patients with dysphagia [5]. From the examples of research mentioned above, displays the advantages of nanofibers for drug delivery. Our particular interest is to study how do the nanofibers with different arrangement affect the drug release.

Electrospinning technique has become a new technique to prepare the stationary phase for TLC. There have been some reports about the fabrication and use of electrospun nanofibers as TLC stationary phase for the separation of amino acids, laser dyes, steroidal compounds and food preservatives. However, the polymers used for the fabrication are limited to glassy carbon [6], silica [7], polyacrylonitrile (PAN) [8-10], polyvinyl alcohol (PVA) [11] and cellulose acetate (CA) [12]. Nanofibers are

prepared by conventional method, nonwoven layers can be oriented with randomly aligned structures. Later, uniaxially aligned electrospun nanofibers have increasingly attracted attention. The method used to control the alignment of fibers is divided into three major categories i.e. mechanical, electrostatic, and magnetic methods [13]. Furthermore, uniaxially aligned nanofibrous mats can be applied in a variety of fields e.g. cell scaffolds because fiber orientation imitates the parallel structure of fibrous tissues, so it can direct the migration and extension of cells [14, 15]. In addition, uniaxially aligned electrospun nanofibers have been currently applied to analytical chemistry e.g. electrochemical/optical based detection systems, solid phase extraction and membrane separation [14]. In the recent times, Olesik and co-workers reported the potential of aligned PAN electrospun nanofibers as an alternative membrane material to separate a mixture of β -blockers and steroidal compounds. Compared to those with random orientation, the aligned nanofibers improved reproducibility and separation efficiency as well as shortened run time [9]. After that, Kampalanonwat et al. firstly optimized the rotation speeds of drum collector to control the alignment of PAN nanofibers [10]. From these researches, it shows the performance enhancements motivated further pursuit of new electrospun TLC materials. It is hypothesized that TLC with uniaxially aligned electrospun nanofibers may increase chromatographic performance when compared with randomly aligned electrospun TLC plates.

CA is an environmentally degradable material made from cellulose that is the most abundant biopolymer on earth [15]. It is much cheaper than some synthetic polymers such as PAN, and nanofibers made from CA can be readily used for TLC after the electrospinning process without additional steps such as pyrolysis or chemical crosslinking. Lately, TLC plates made from randomly aligned CA nanofibers have been prepared for screening of steroidal adulterants in traditional medicines and nutraceutical products and have been used with eco-friendlier hydro-alcoholic mobile phases [10].

The purpose of this study is to prepare randomly and uniaxially aligned electrospun nanofibers and to compare them in 2 aspects i.e. drug release and TLC performance. In this study, we optimized the parameters of the electrospinning process to find the optimal point of each of the factors used to produce uniaxially

aligned CA nanofibers, including drum collector rotation speed and spin time. The effects of each parameter on the morphology of CA nanofiber mats were evaluated. The morphology of nanofibers was characterized by Scanning electron microscopy (SEM). To evaluate TLC performance of nanofibers, uniaxially aligned fibers were compared to that randomly aligned ones for the ability to separate hydroquinone (HQ), retinoic acid (RA) and vitamin C (VC). To date, there are many studies about drug release from nanofibers. Drug-incorporated electrospun nanofibers have been used for treatment of various diseases. The nanofiber mats are applied as topical, implanted drug delivery systems or oral administration. Some of the unique features of electrospun fibers as drug delivery vehicles relate to their ability to incorporate a wide range of drugs, their high surface area leading to an efficient drug release, their interconnecting porous structure with high permeability and the ease of fabricating the delivery vehicle in the required form. But the study to compare release of the drug from the nanofibers with different arrangement does not appear. So in the present study, Arbutin was loaded into CA electrospun nanofibers with 3 different types of nanofibers including randomly aligned, semi-aligned and uniaxially aligned. The release behavior in the aqueous medium was investigated.

1.2 Objective of this research

1. To prepare uniaxially aligned and randomly aligned CA electrospun nanofibers and optimize the electrospinning parameters.
2. To compare the drug release behaviors between uniaxially aligned versus randomly aligned CA electrospun nanofibers.
3. To compare the TLC performances between uniaxially aligned versus randomly aligned CA electrospun nanofibers.

1.3 The research of hypothesis

1. Speed rotating mandrel influences on the arrangement of CA electrospun nanofibers.
2. The release of arbutin from uniaxially aligned CA electrospun nanofibers is different from that of randomly aligned CA electrospun nanofibers.

3. Uniaxially aligned CA electrospun nanofibers can be potentially used as a stationary phase for TLC with shorter run time than randomly aligned CA electrospun nanofibers.



CHAPTER 2

LITERATURE REVIEWS

- 2.1 Electrospinning of nanofibers
 - 2.1.1 History
 - 2.1.2 The electrospinning setup
 - 2.1.3 The electrospinning process
 - 2.1.4 Polymer Selection in Electrospinning
 - 2.1.5 Working principle of an electrospinning machine
 - 2.1.6 Electrospinning process parameters
 - 2.1.7 Electrospinning process parameter summary
- 2.2 Recent developments in electrospun nanofibers and their applications
- 2.3 Controlling electrospun nanofiber alignment
 - 2.3.1 Alignment caused by mechanical forces
 - 2.3.2 Alignment caused by electrostatic forces
 - 2.3.3 Alignment caused by magnetic forces
- 2.4 Cellulose acetate (CA)
- 2.5 Electrospinning of CA
- 2.6 Drug loading in/on nanofibers
- 2.7 Drug release
- 2.8 Thin layer chromatography (TLC)
 - 2.8.1 Theory of TLC

2.1 Electrospinning of nanofibers

2.1.1 History

Electrospinning is a remarkably simple and versatile method for generating ultrathin fibers from a rich variety of materials that include polymers, composites and ceramics. To date it has been successfully applied to more than 200 different types of polymers from both natural and synthetic origins [3, 18-20]. Although the term electrospinning (derived from “electrostatic” and “spinning”) has come into use relatively recently (since around 1994), its fundamental idea dates back more than 60 years earlier. The crucial patent in which the electrospinning of plastics was described for the first time appeared in 1934 by Anton Formhals. From 1934 to 1944, Formhals published a series of patents describing an experimental setup for the production of polymer filaments using an electrostatic force [21]. The polymer filaments were formed from a CA solution introduced into an electric field between two electrodes bearing electrical charges of opposite polarity. One of the electrodes was placed into the solution and the other onto a collector. Once ejected out of a metal spinneret with a small hole, the charged solution jets evaporated to become fibers which were collected on an electrically grounded collector. Despite its early discovery, the procedure was not utilized commercially and was overshadowed by other fiber producing techniques. In 1971, Baumgarten made an apparatus to electrospin acrylic fibers with diameters in the range of 0.05–1.1 μm [22]. In this process, a polymer solution droplet was suspended from a stainless steel capillary tube and maintained constant in size by adjusting the feed rate by an infusion pump. A high-voltage DC current was connected to the capillary tube whereas the fibers were collected on a grounded metal screen at a specified distance. However, this work which was followed by other patents also remained fairly unnoticed. Since the 1990s and especially in recent years, the electrospinning process essentially similar to that described by Baumgarten has regained considerably more attention. Probably due in part to a surging interest in nanotechnology, as ultrafine fibers or fibrous structures of various polymers can be easily fabricated with a rudimentary setup in the laboratory and have viable industrial scale application.

Recent articles found on electrospinning focused on various spinnable polymeric materials, processing techniques for fabricating nanofiber assemblies, effects of processing parameters on fiber diameter and morphology and characteristics of the fibers and their applications. Some of the many reviews published on the many developments of electrospinning are cited in references [1, 23-29]. Also a good summary of the various studies on electrospinning, its nanofibers and their references can be found in the book by Ramakrishna et al. (2005) [18].

2.1.2 The electrospinning setup

At first glance, electrospinning gives the impression of being a very simple and, therefore, easily controlled technique for the production of nanofibers. A typical modern apparatus for electrospinning is shown in Figure 2.1, which consists of three major components: a high-voltage power supply, a spinneret, and an electrically conductive collector [30, 31]. An ordinary hypodermic needle and a piece of aluminum foil serve well as the spinneret and collector respectively. The polymer to be electrospun may be in the form of a solution or melt that is typically loaded in a syringe and fed into the spinneret at a specific rate by a modulating syringe pump. The high voltage source is utilized to inject electric charge of a certain polarity into the polymer solution or melt, which is then accelerated towards the collector which is grounded or of opposite polarity and is used for the collection of both random and aligned fibers [32, 33]. Electrospinning is generally conducted at room temperature with atmosphere conditions but in some cases a well-controlled environment (e.g. with suitable humidity, temperature and atmosphere) may be required in which case the electrospinning region is enclosed in a transparent encasing.

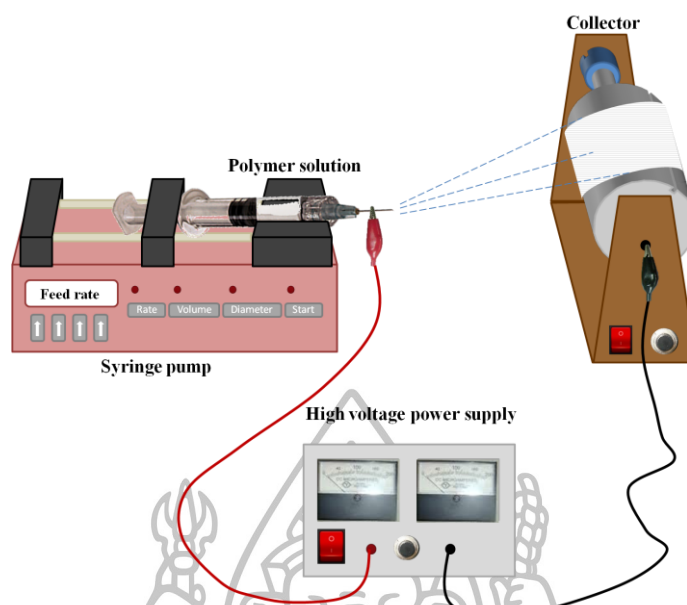


Figure 2.1 Schematic illustrating the electrospinning setup.

Currently there are two standard electrospinning setups, vertical and horizontal, as can be seen in the sketches of Figure 2.2. The various groups working on electrospinning have adopted different methods for the polymer feed. Some have simply opted for placing the syringe perpendicularly (vertical setup), letting the polymer solution drip with the help of gravitation and laying the collector underneath. Sometimes the syringe can be tilted at a defined angle to control the flow. In the second most common case, the syringe is horizontal and a pump is used to initiate the droplet, the pump being also often used in the case of vertical feeding. The electrode can be inserted either directly into the polymer fluid or placed onto the metallic tip of the capillary if a syringe with a metal needle is used. With the expansion of this technology, several research groups have developed more sophisticated systems that can fabricate more complex nanofibrous structures and assemblies in a more controlled and efficient manner which shall be the topic of a later section.

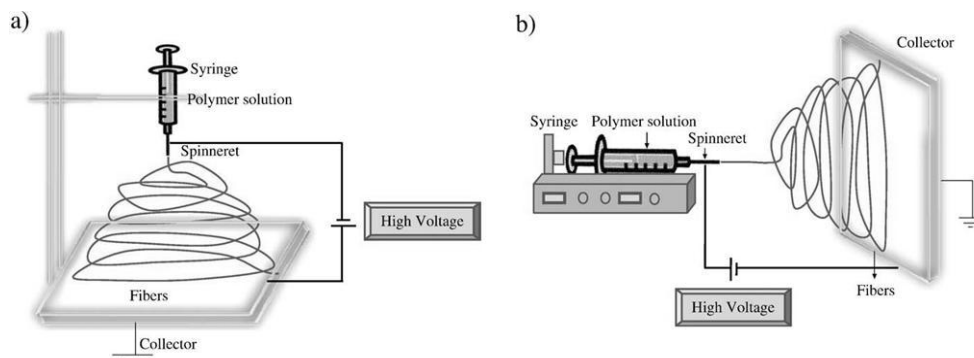


Figure 2.2 Schematic diagram of set up of electrospinning apparatus (a) typical vertical setup and (b) horizontal setup of electrospinning apparatus.

Source: Bhardwaj, N., and S. C. Kundu. (2010). "Electrospinning: a fascinating fiber fabrication technique." *Biotechnology Advances* 28, 3 (May-June): 325–347.

2.1.3 The electrospinning process

In contrast to the simplicity of setup, the detailed mechanisms of electrospinning are much more complicated and the modeling of the fiber formation process has been the topic of extensive research [34]. The formation of the nanofibers is based on a uniaxial stretching of the viscoelastic solution by an electrostatic force. More specifically, a polymer solution droplet held by its surface tension at the spinneret opening (the capillary tip) is subjected to an electric field by applying a high voltage. An electric charge is induced on the liquid surface due to this electric field. As the intensity of the electric field is increased, the repulsive electrical forces gradually offset the droplets surface tension forces and the droplets hemispherical surface elongates into a conical structure known as a Taylor cone. Under an increasing electric field, a critical voltage is attained whereby the repulsive electrostatic force totally overcomes the solutions surface tension, allowing charged fluid jets to be ejected from the tip of the Taylor cone. An illustration of the process is shown in Figure 2.3. The discharged polymer solution jets undergo an unstable and rapid whipping motion in the space between the capillary tip and collector wherein the solvent evaporates, leaving behind an electrically charged polymer fiber which is highly stretched and reduced in diameter as it travels towards the collector [35, 36].

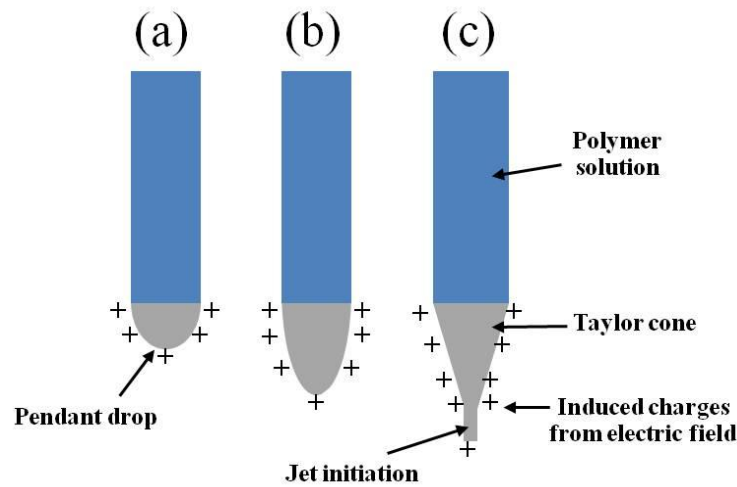


Figure 2.3 Illustration of Taylor cone formation: (A) Surface charges are induced in the polymer solution due to the electric field. (B) Elongation of the pendant drop. (C) Deformation of the pendant drop to the form the Taylor cone and jet initiation.

During its travel, the jet only follows a direct path towards the counter electrode for a certain distance but then changes its appearance significantly by moving laterally and forming a series of coils, the envelope of which has the form of a cone opening towards the counter electrode. A schematic illustrating the inverted conical path is given in Figure 2.4. It is now known that the small diameter of electrospun fibers is the result of the rapid whipping motion that exerts a strong axial force rather than the splaying of jet (the splitting of the main jet into minor jets), as was previously believed [2, 35, 37]. It is because of this continuous acceleration and stretching of the jet that electrospun nanofibers are typically several orders of magnitude thinner than those produced using conventional spinning techniques that draw the fibers in a uniform direction. The inset in Figure 2.4 shows a snapshot of the violent jet, which was captured with the aid of a high-speed camera. The whipping instability is thought to originate mainly from the electrostatic interactions between the external electric field and the charges immobilized on the surface of the jet. Naturally, the polymer solution utilized in the electrospinning must possess the appropriate viscoelastic properties in order to survive the whipping process that can break the jet into individual droplets.

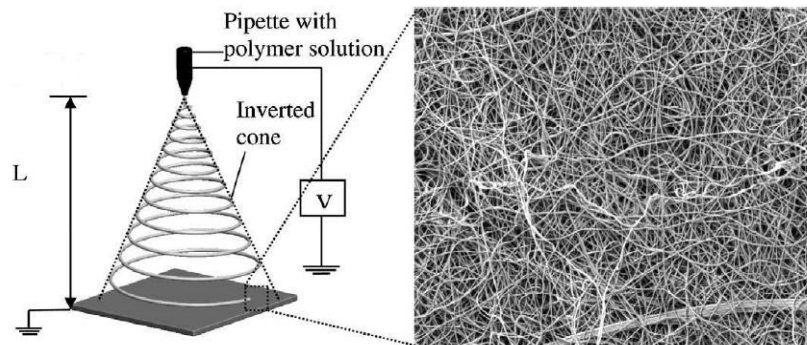


Figure 2.4 Schematic illustrating the inverted conical path the jet travels before being collected as randomly oriented fibers. The inset shows a SEM image of randomly deposited electrospun nylon 6,6 fibers.

Source: Baji, A., et al. (2010). “Electrospinning of polymer nanofibers: Effects on oriented morphology, structure and tensile properties.” **Composites Science and Technology** 70, 5 (May): 703-718.

2.1.4 Polymer Selection in Electrospinning

Hundreds of polymers have been electrospun to produce nanofibers for various applications. Table 2.1 lists a few polymer solvent systems that are widely used in electrospinning [38]. Polymers such as polyvinyl alcohol (PVA) are widely used in tissue engineering and drug delivery. There are many more polymers that have not been successfully electrospun based on their properties and the parameters involved in electrospinning. Properties of the polymer in solution are very important in both the electrospinning process and the end application of the electrospun nanofibers.

Concentration and solvent type directly impact the properties of the solution. Highly concentrated polymer solutions are very difficult to electrospin as viscosity is an essential parameter in electrospinning. Polymer solvent is also pertinent to electrospinning as the polymer must be dissolved in a suitable solvent and spun from solution. Solvent type is also important when generating nanofibers. Nanofibers in the range of 10 to 2000 nm diameter can be achieved by choosing the appropriate

polymer solvent system [39]. Table 2.1 lists some polymer solvent systems used in electrospinning. Depending on the system, applications may vary.

Table 2.1 Different polymers used in electrospinning, characterization methods and their applications.

Polymers	Applications
Poly(glycolide) (PGA)	Nonwoven tissue engineering scaffolds
Poly(lactide-co-glycolide) (PLGA)	Biomedical applications, wound healing
Poly(ϵ -caprolactone) (PCL)	Bone tissue engineering
Poly(L-lactide) (PLLA)	3D cell substrate
Polyurethane (PU)	Nonwoven tissue template wound healing
Poly(ethylene-co-vinyl alcohol) (PEVA)	Nonwoven tissue engineering scaffolds
Polystyrene (PS)	Skin tissue engineering
Syndiotactic 1,2-polybutadiene	Tissue engineering applications
Fibrinogen	Wound healing
Poly(vinyl alcohol)/cellulose acetate (PVA/CA)	Biomaterials
Cellulose acetate (CA)	Adsorptive membranes/felts
Poly(vinyl alcohol) (PVA)	Wound dressings
Silk fibroin, silk/PEO	Nanofibrous tissue engineering scaffolds
Silk	Biomedical applications
Silk fibroin	Nanofibrous scaffolds for wound healing
Silk/chitosan	Wound dressings
Chitosan/PEO	Tissue engineering scaffolds, drug delivery, wound healing
Gelatin	Scaffold for wound healing
Hyaluronic acid (HA)	Medical implant
Cellulose	Affinity membrane
Gelatin/polyaniline	Tissue engineering scaffolds

Table 2.1 Different polymers used in electrospinning, characterization methods and their applications (continued).

Polymers	Applications
Collagen/chitosan	Biomaterials

Source: Bhardwaj, N., and S. C. Kundu. (2010). "Electrospinning: a fascinating fiber fabrication technique." **Biotechnology Advances** 28, 3 (May-June): 325–347.

2.1.5 Working principle of an electrospinning machine

Electrospinning process can be explained in 5 steps, such as:

- a. Charging of the polymer fluid
- b. Formation of the cone jet (Taylor cone)
- c. Thinning of the jet in the presence of an electric field
- d. Instability of the jet
- e. Collection of the jet

a. Charging of the polymer fluid

The syringe is filled with a polymer solution, the polymer solution is charged with a very high potential around i.e. 10-30 kV. The nature of the fluid and polarity of the applied potential free electrons, ions or ion-pairs are generated as the charge carriers form an electrical double layer. This charging induction is suitable for conducting fluid, but for non-conducting fluid charge directly injected into the fluid by the application of electrostatic field.

b. Formation of the cone jet (Taylor cone)

The polarity of the fluid depends upon the voltage generator. The repulsion between the similar charges at the free electrical double layer works against the surface tension and fluid elasticity in the polymer solution to deform the droplet into a conical shaped structure i.e. known as Taylor-cone. Beyond a critical charge density Taylor-cone becomes unstable and a jet of fluid is ejected from the tip of the cone [1].

c. Thinning of the jet in the presence of an electric field

The jet travels a path to the ground, this fluid jet forms a slender continuous liquid filament. The charged fluid is accelerated in the presence of electrical field. This region of fluid is generally linear and thin.

d. Instability of the jet

Fluid elements accelerated under electric field and thus stretched and succumbed to one or more fluid instabilities which distort as they grow following many spiral and distort path before collected on the collector electrode. This region of instability is also known as whipping region.

e. Collection of the jet

Charged electrospun fibers travel downfield until it impact with a lower potential collector plate. Orientation of the collector affects the alignment of the fibers. Different type of collector also affects the morphology and the properties of produced nanofiber. Different type of collectors are used : Rotating drum collector, moving belt collector, rotating wheel with bevelled edge, multifilament thread, parallel bars, simple mesh collector etc.

2.1.6 Electrospinning process parameters

In principal, nearly all soluble or fusible polymers can be processed into fibers by electrospinning, provided that the solution parameters and the operational parameters are optimized [19, 20]. The main parameters can be divided into three categories:

1. The intrinsic properties and parameters of the electrospun solution:

1.1. Viscosity, volatility, elasticity, conductivity, polarity and surface tension of the solution.

1.2. Molecular weight, conformation and polymer chain entanglement of the polymer

2. The operational parameters:

2.1. Strength and distribution of the applied electric field e.g. voltage

- 2.2. Setup geometry e.g. Tip-to-collector distance
 - 2.3. The feeding rate of the solution and spinneret (needle) diameter
 - 2.4. Effect and design of collector
3. The environmental parameters:
 - 3.1. Temperature and humidity in electrospinning chamber
 - 3.2. Pressure and air velocity patterns in the electrospinning chamber

The different parameters must coincide to yield a successful electrospinning with the desired nanofiber qualities as they can act either synergistically or counterproductively with each other. For instance, the polymer solution must have a concentration high enough to enable sufficient polymer chain entanglement during fiber formation yet not so high that its viscosity prevents polymer motion induced by the electric field. The solution must also have a surface tension low enough to allow Taylor cone formation as well as be able to carry a charge high enough to allow stretching. Morphological changes also occur upon changing the operational parameters like decreasing the distance or changing the electric field strength between the spinneret and the substrate. Obviously, it is not possible to make general recommendations for particular concentrations, viscosities, electrical conductivities, surface tensions, etc. because the values of these parameters vary considerably with the polymer–solvent system. As long as a polymer can be electrospun into nanofibers, ideal targets would be in that:

- a. The diameters of the fibers be consistent and controllable
- b. The fiber surface be defect-free or defect-controllable
- c. Continuous single nanofibers to be collectable.

Research so far has shown that controlling the fiber diameter and morphology is by no means easily achievable. As mentioned earlier, the numerous correlations between the parameters makes this difficult and system specific boundary conditions for each parameter must be set to achieve successful electrospinning. An often occurring problem is that the parameters adjusted to achieve a certain goal such as a lower diameter can also lead to an adverse effect on another parameter thereby offsetting the initial adjustment. A simple example is the increasing of the voltage to

obtain a higher degree of electrostatic stretching (by increased whipping motion) and assuming it will yield a reduced fiber diameter. This choice of action can be counteracted by the reduced fiber flight time due to increased acceleration toward the collector (leading to less stretching), and an increase in polymer solution supply in the fibers drawn out by the electric field which ultimately can yield thicker fibers. Extensive summaries regarding the effects of the parameters can be found in the following review articles and in the book by Ramakrishna et al. [3, 18, 40-42]. Here will only be discussed the most basic parameters relevant to an understanding of the electrospinning process and to this work.

Since nanofibers are resulted from evaporation or solidification of polymer fluid jets, the fiber diameters will depend primarily on the jet sizes as well as on the polymer contents in the jets. The traveling solution jet from the pipette onto the collector may or may not split into multiple jets, resulting in different fiber diameters. As long as no splitting is involved, the major factors that control the diameter of the fibers are deemed to be:

- a. Concentration and viscosity of the solution
- b. Type of solvent used
- c. Conductivity of the solution
- d. Feeding rate of the solution
- e. Applied electric voltage
- f. Tip-to-collector distance

Viscosity, concentration and molecular weight

According to prior investigations, a higher viscosity results in a larger fiber diameter due in part to the higher polymer supply [43]. The solution viscosity is proportional to the polymer concentration and its solubility in solvent. Thus it is natural to conclude that lowering the polymer concentration should also result in a reduction in nanofiber diameters. But for fiber formation to occur a minimum solution concentration is required as polymer chain interaction and entanglements are required for fiber formation. It has also been found that at very low solution concentrations a mixture of beads and fibers may be obtained. For a solution of low viscosity, surface tension is the dominant factor and just beads or beaded fibers are formed while above

a critical concentration a continuous fibrous structure is obtained. There is also a need for a certain polymer molecular weight, weight distribution, and chain architecture (e.g. linear, branched etc.) that can ensure sufficient entanglement. It has been observed that a high molecular weight is not always essential, if sufficient intermolecular interactions can provide a substitute for the interchain connectivity obtained through chain entanglements. To summarize, the concentration parameter is highly dependent on the polymer-solvent system. There is an optimum solution concentration, as at low concentrations beads are formed instead of fibers, and at too high of a concentration the formation of continuous fibers is prohibited because of the inability to maintain a stable flow of the solution to the tip of the needle [44].

Surface tension

It's also been reported that by reducing the surface tension of a polymer solution, fibers could be obtained without beads [45]. Naturally, different solvents contribute to different resultant surface tensions. Generally a high surface tension of a solution inhibits the electrospinning process because of an arising instability of the jets and the generation of sprayed droplets [46]. However, not necessarily will a lower surface tension of a solvent be more suitable for electrospinning and it may yield undesired morphological or fiber diameter change. Many papers promote the use of solvent mixtures as opposed to just a single solvent to adjust the surface tension or by the extra addition of a surfactant [45].

Conductivity

Increasing the solution conductivity with e.g. salts can result in fibers free of beads and with smaller diameters [41]. The argument is that the addition of salts yields a higher charge density on the surface of the solution jet during the electrospinning, bringing more electric charges to the jet. As the charges carried by the jet increase, stronger elongation forces are imposed on the jet under the electrical field, resulting in less beading and thinner smoother fiber diameters. It has been found that with the increase of electrical conductivity of the solution there is a significant decrease in the diameter of the electrospun nanofibers whereas with low conductivity of the solution there results insufficient elongation. However, the highly conductive

solutions are extremely unstable in the presence of strong electric fields, which results in a dramatic bending instability as well as a broad diameter distribution [47].

Feed-rate

An increased feed-rate will increase the amount of polymer available and will consequently lead to an increase in the fiber diameter but must be set to match the applied voltage to avoid instability of the Taylor cone. A lower feed rate is usually more desirable as the solvent will get enough time for evaporation but reduces the output of fibers in a given time frame. High flow rates may also result in beaded fibers due to unavailability of proper stretching and drying time prior to reaching the collector [41, 48].

Voltage

A parameter which affects the fiber diameter to a remarkable extent is the applied electrical voltage. In general, a higher applied voltage ejects more fluid in a jet, resulting in a larger fiber diameter and only after attainment of a threshold voltage does fiber formation actually occur [41]. This threshold voltage induces the necessary charges on the solution and initiates the electrospinning process. Other authors have reported that an increase in the applied voltage increases the electrostatic repulsive force on the fluid jet which ultimately favors the narrowing of fiber diameter. The higher voltage causes greater stretching of the jet, due to the greater columbic forces present in the jet as and provides a stronger electric field. These combined effects lead to reduction in the fiber diameter and also a more rapid evaporation of solvent from the fibers [49].

Tip-to-collector distance

The distance between the spinneret tip and the collector has often been examined as another approach to control the fiber diameters and morphology. Varying the distance will have a direct influence on the flight time and the electric field strength. A longer flight time enables the fibers to be stretched for longer periods of time before they are deposited but weakens the strength of the electric field. It has been found that a minimum distance is required to give the fibers sufficient time to dry before reaching the collector, otherwise with distances that are too close wet

fibers, beads or intermeshed fibers have been observed [41, 42]. An excessively far distance will lessen the deposited amount of fibers on the collector. There should be an optimum distance between the tip and collector at an applied voltage which yields the optimal electric field strength for the evaporation of solvent from the nanofibers and stretching of the fibers.

Temperature

At high temperature, viscosity of the solution is decreases and there is increase in higher evaporation rate which allows greater stretching of the solution and a uniform fiber is formed.

Diameter of pipette orifice

Orifice with small diameter reduces the clogging effect due to less exposure of solution to the atmosphere and leads to the formation of fibers with smaller diameter. However, very small orifice has the disadvantage that it creates problem in extruding droplet of solution from the tip of the orifice.

2.1.7 Electrospinning process parameter summary

A summary of the discussed parameters and their general assumed effect withholding the above discussed intricacies is given in Table 2.2 and Figure 2.5.

Table 2.2 Electrospinning parameters and their assumed effects on fiber morphology.

Parameter	Effect on fiber morphology
Applied voltage	Minimum voltage needed to induce electrospinning. Probable increase in fiber diameter with increase in voltage with lesser probability of beading.
Concentration	Increase in fiber diameter with increase of concentration.
Conductivity	Decrease in fiber diameter with increase in conductivity but also increases bending instability and diameter distribution

Table 2.2 Electrospinning parameters and their assumed effects on fiber morphology (continued).

Parameter	Effect on fiber morphology
Diameter of pipette orifice	Orifice with small diameter reduces the clogging effect due to less exposure of solution to the atmosphere and leads to the formation of fibers with smaller diameter. However, very small orifice creates problem in extruding droplet of solution from the tip of the orifice.
Feed-rate	Low feed-rate: Decrease in fiber diameter High feed-rate: Increase in bead generation and Taylor cone instability
Surface tension	Reduction in surface tension minimizes beads, high surface tension results in instability of jets
Temperature	At high temperature, viscosity of the solution is decreases and there is increase in higher evaporation rate which allows greater stretching of the solution and a uniform fiber is formed.
Tip-to-collector distance	Minimum distance required for dry fibers. Excessively far distance will lessen the deposited amount of fibers on the collector
Viscosity	Low viscosity: Increase in bead generation High viscosity: Increase in fiber diameter, disappearance of beads.

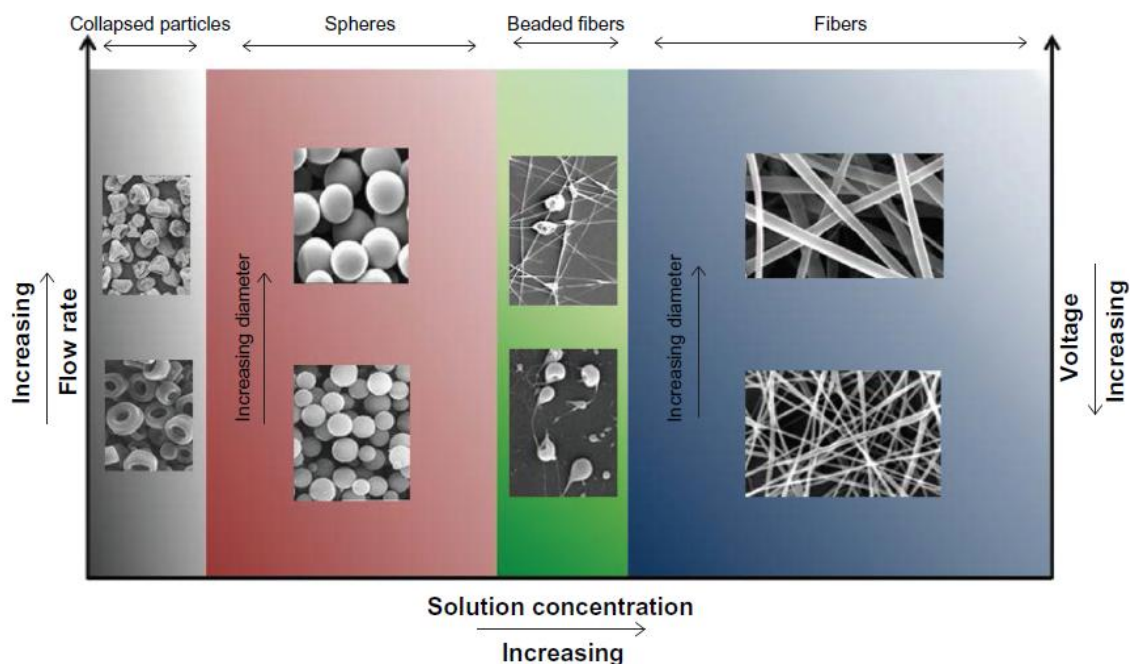


Figure 2.5 Schematic illustration of the effect of the concentration, flow rate, and voltage on electrospayed/electrospun nano/microstructures.

Source: Zamani, M., et al. (2013). "Advances in drug delivery via electrospun and electrospayed nanomaterials." **International Journal of Nanomedicine** 28, 3: 325-347.

Notes: At very low concentrations, fabricated particles collapse into rings, discs, etc, by varying the electrospaying condition. By increasing the concentration, spherical particles can be formed with different sizes by changing the flow rate and applied voltage. Further increase in concentration results in formation of particle-tail structures or beaded fibers depending on the processing condition. When a critical concentration is reached, uniform fibers are produced. Although these general principles are applicable for most electrospinning/electrospaying conditions, solutions with specific properties such as high conductivity may behave differently.

2.2 Recent developments in electrospun nanofibers and their applications

Many different methodologies have been employed to modify the electrospinning process, yielding a variety of pathways for controlling the final composition of electrospun nanofibers. In addition to just varying the fundamental operational parameters, further advanced developments have been made by altering the design of the electrospinning setup or the final makeup of the electrospun material. Examples of such developments, excluding to just those inherent to the process operational parameters, are the co-processing of different polymer mixtures, chemical cross-linking of the formed nanofibers and the production of various hierarchical nanofiber assemblies [1, 19, 28, 42]. The electrospinning technique also provides the capacity to lace together a variety of types of nanofillers to be encapsulated into an electrospun nanofiber matrix. Carbon nanotubes, ceramic nanoparticles, etc. may be dispersed in polymer solutions, which are then electrospun to form nanoscale composites. Another interesting aspect of using nanofibers is that it is possible to modify not only their morphology and internal bulk content but also their surface structure to carry various functionalities [50, 51].

As mentioned earlier, the main advantage of the electrospinning process is not only its versatility, but also its easy setup and relatively low cost compared to that of other nanofiber producing methods. The resulting nanofibers samples are often uniform and continuous and in most cases do not require further purification. Hence, electrospun polymer nanofibers are considered for use in a variety of applications such as nonwoven fabrics, filtration, reinforcement in composite systems, drug delivery systems, tissue engineering, fuel cells, photonics, sensorics, wound dressings, nanocatalyst supports and fiber templates for the preparation of nanotubes or porous materials, to name just a few [3, 18, 41, 52, 53]. Some applications in the different sectors are given in Figure 2.6.

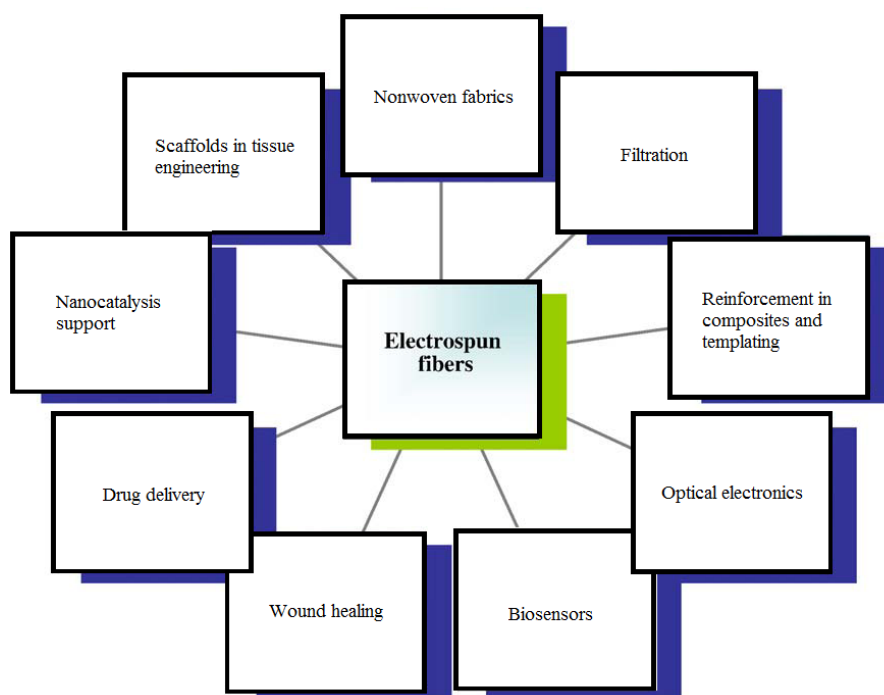


Figure 2.6 Different applications of electrospun nanofibers.

Source: Bhardwaj, N., and S. C. Kundu. (2010). "Electrospinning: a fascinating fiber fabrication technique." *Biotechnology Advances* 28, 3 (May-June): 325–347.

2.3 Cellulose acetate (CA)

Cellulose acetate was first developed by Schutzenberger in 1865 by heating cotton with acetic anhydride. Cellulose acetate fibers were first manufactured commercially in Great Britain in 1919 (Celanese[®]). Cellulose acetate is prepared from cotton linters and/or purified wood pulp that is acidified, usually with sulfuric acid, then acetylated with acetic acid and acetic anhydride. This produces cellulose triacetate; cellulose diacetate is obtained by partial hydrolysis to replace some of the acetyl groups with hydroxyl groups. Cellulose diacetate (Degree of substitution about 2.45) is commonly called acetate while the cellulose triacetate (Degree of substitution approaching 3) is called triacetate.

Acetate fiber is the generic name of a fiber that is partially acetylated cellulose. They are also known as cellulose acetate and triacetate fibers. While acetate and triacetate differ only moderately in the degree of acetylation, this small difference

accounts for differences in the physical and chemical behavior for these two fiber materials.

2.4 Electrospinning of CA

Electrospinning of polysaccharides is not an easy task to accomplish because of their poor solubility and the high surface tension of solutions [54]. Cellulose gives a vivid example of it. Solvents that can dissolve this polysaccharide have low volatility and high melting temperature, which makes it hard to remove them completely from the fibers and requires electrospinning to be performed at relatively high temperatures [55-59].

CA is a cellulose derivative that is much easier to handle which makes it favorable in electrospinning processes. In order to choose a good solvent several factors should be taken into consideration. First of all, the solvent must have a high enough boiling point and dipole moment in order to evaporate during the stretching of the fibers towards the collector and not before. Otherwise clogging of the needle tip is observed. Secondly, the resulting solution should not be too viscous, but it should have high conductivity and low surface tension [60-62]. That is why the presence of solvents with a high dielectric constant and boiling point like dimethylacetamide, methanol, dimethylformamide or water improves the spinnability of CA solutions. Usually they are mixed with low-boiling solvents (acetone, chloroform, dichloromethane) in different weight ratios to obtain the best suitable solvent for a particular molecular weight of CA and a target structure. After getting CA fibers they are regenerated to cellulose by aqueous or ethanolic hydrolysis [54].

2.5 Controlling electrospun nanofiber alignment

In a typical situation, electrospun nanofibers are deposited on the collector as a nonwoven mat, with no preferential orientation of the fibers. Yet, electrospinning is far from limited to the production of nonwovens as various assemblies of nanofibers can be constructed by alteration of the electrospinning process and apparatus. The orientation of nanofibers along a preferred direction is of particular interest for many applications e.g. for structural reinforcement in composites or in tissue engineering to give cultivated cells a preferred growth direction. As was mentioned in a previous

section, the nanofibers are typically deposited on the surface of a flat collector (a piece of conductive substrate) as a randomly oriented mess due to the chaotic bending instability of the highly charged jet. This inability to predict the final fiber placement and orientation has been the limiting factor in producing aligned fiber mats and numerous methods have been investigated to resolve this issue. There are generally two main methods utilized and many other developed variants which can be considered as combinations of these basic methods. One method is to use a dynamic (most often rotating) collection device as oppose to just a static collector hence introducing an element of mechanical handling to the fiber collection process. The other is to control the flight of the electrospinning jet through the manipulation of the macro electrostatic field, mainly by altering the build and configuration of the collector and or the use of auxiliary directional electrodes.

2.5.1 Alignment caused by mechanical forces

It has been suggested that by rotating a cylindrical collector at a very high speed of up to thousands of rpm (rotations per minute), continuous electrospun nanofibers could be oriented circumferentially around the collector in an aligned fashion. Furthermore, the diameter of the fiber can be controlled and tailored based on the rotational speed of the drum [52, 63-65]. The mechanism behind the technique has not been fully explained in detail, yet some intuitive conjectures in the literature are given as follows. When the linear speed of the rotating cylinder surface, which serves as a fiber take-up device, matches that of evaporated jet depositions, the fibers are taken up on the surface of the cylinder tightly in a circumferential manner, resulting in a fair alignment. Such a speed can be called the alignment speed. If the surface speed of the cylinder is slower than the alignment speed, randomly deposited fibers will be collected, as it is the fast chaotic motions of jets that determine the final deposition manner. On the other hand, there must be a limit rotating speed above which continuous fibers cannot be collected since the overfast take-up speed will break the fiber jet. Another point of concern is the aerodynamic motion resultant from the high speed rotating drum that can ultimately repel the deposition of the fine fibers and lessen the deposited amounts as well as their orientation.

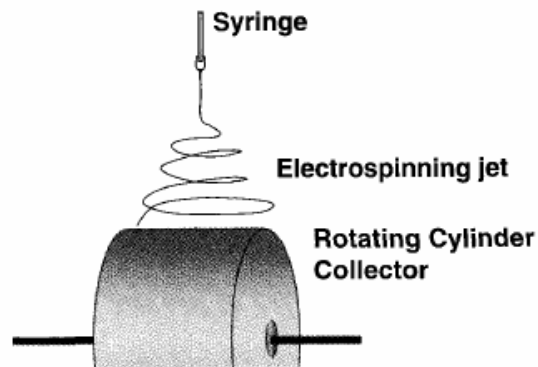


Figure 2.7 A rotating cylinder collector to obtain unidirectional nanofiber alignment along the rotation direction.

Source: Ramakrishna, S., et al. (2005). “An Introduction to Electrospinning and Nanofibers.”, Singapore: World Scientific Publishing Co. Pte. Ltd.

2.5.2 Alignment caused by electrostatic forces

The force that stretches the solution into a fine strand is the electrostatic charge applied and given to it by the high voltage power supply. Since the electrostatic charges are distributed along the electrospinning jet and the electrospun fibers are charged in flight, an external electric field can be used to control their travel patterns until final impact with the lower potential electrode or collector. Simply put, the fibers may be guided by altering the electric field and their travel patterns roughly visualized by the electric field lines [18, 52, 65, 66]. Even with a slight variation in the electric field profile, its effect on the deposition of the electrospun fibers can be seen. When a grounded wire was placed below a non-conducting substrate such as a glass slide, it induced the electrospun fibers to deposit preferentially on the areas on the glass slide just above the grounded wire as shown in Figure 2.8

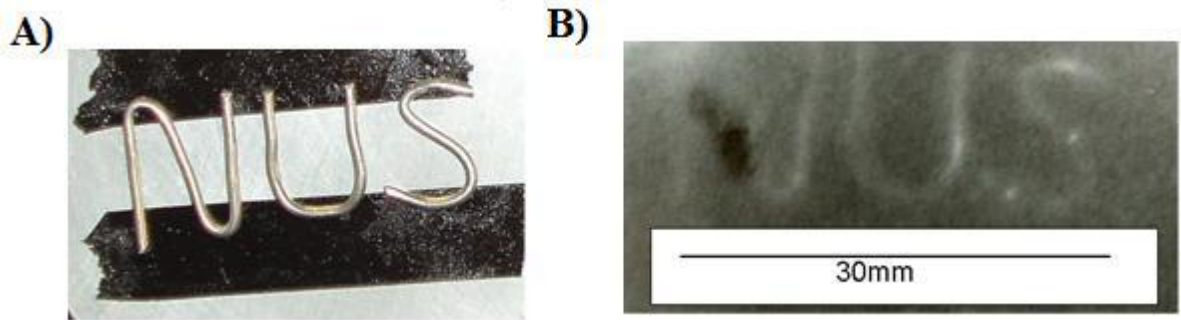


Figure 2.8 Influence of conducting wire placed below a glass slide on the deposition of the electrospun fibers. (A) Grounded electrode placed under a glass cover slip. (B) Electrospun fibers deposited on the glass cover slip.

Source: Teo, W. E. (2006). "A review on electrospinning design and nanofibre assemblies." *Nanotechnology* 17, 14 (June 30): R89.

Many other similar attempts that utilize auxiliary electrode ring(s) for controlled deposition can also be found. Jaeger et al. installed a single charged ring of like voltage and polarity concentrically about the syringe needle to stop the chaotic motion of the electrospinning jet as is shown in Figure 2.9 [67]. Similarly, Kim and co-workers used a single cylindrical auxiliary electrode around the nozzle tip to stabilize the spinning jet [68]. In both works, the electrospinning process was studied with different experimental lay-outs, electrostatic fields were simulated and the voltage - current characteristics of the electrospinning process were recorded. The advantages of this relatively simple set-up was that the deposition of the fibers could be controlled over an area which is despite still being quite large was confined within a ring area. Also worth mentioning are the works of Buttafoco et al., wherein a guiding electrode ring was used in conjunction with a rotating uptake device to obtain aligned fibers. A single charged ring was used to designate and reduce the deposition area such that most of the fibers would be directed on a rotating 3.1 mm diameter tube [69].

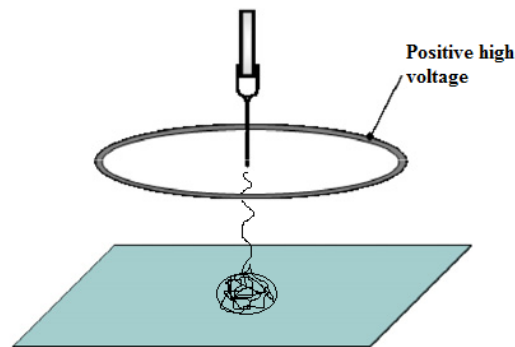


Figure 2.9 Controlled deposition area using a single auxiliary ring.

Source: Park, S., et al. (2007). “Apparatus for preparing electrospun nanofibers: designing an electrospinning process for nanofiber fabrication.”, **Polymer International** 56, 11 (November): 1361-1366.

It has been shown that a static electric field which has been properly designed can be used to obtain aligned or patterned fibers without the use of a mechanical element to the collector. As early as 1938, Formhals patented an electrospinning set-up where bars were placed in parallel with gaps between them as collectors to collect aligned fibers. The setups that utilize this so called “gap” method are basically the same as the conventional electrospinning method but use collectors consisting of pieces of electrically conductive substrates separated by non conductive gaps in which the deposited fibers would span. In a more recent work, Li et al. demonstrated that two electrodes placed in parallel were able to collect aligned fibers in the gap as shown in Figure 2.10 (A) [70, 71]. The electric-field lines in the gap near to the electrodes are drawn towards the electrode edges as seen in the electric field profile in Figure 2.10 (B). The jet would stretch itself across the gap as the field lines are attracted towards the electrodes. This results in electrospun fibers aligning themselves across the gap between the electrodes. Due to the presence of charges on the electrospun fibers, mutual repulsion between the deposited fibers will enhance the parallel and relatively even distribution of the fibers. This process could be repeated and arrays of uniaxially aligned nanofibers could be collected over large areas. By using this method, nanofibers with the length from hundreds of micrometers to several centimeters and diameters ranging from tens of nanometers to several

micrometers could be prepared as uniaxially aligned arrays. Their study showed that the degree of alignment of the nanofibers increased with collection time but the effects of width of gap and applied voltage were not studied. Other many works however have studied the effects of residual charge in fibers and gap width analysis on the degree of alignment [66, 72, 73]. One clear advantage of this setup over the previous conventional setup with a flat substrate or one that utilizes a mechanical drum is that the aligned fibers can be easily removed from the collector making it easy to transfer the fibers onto other solid substrates for further processing steps and applications.

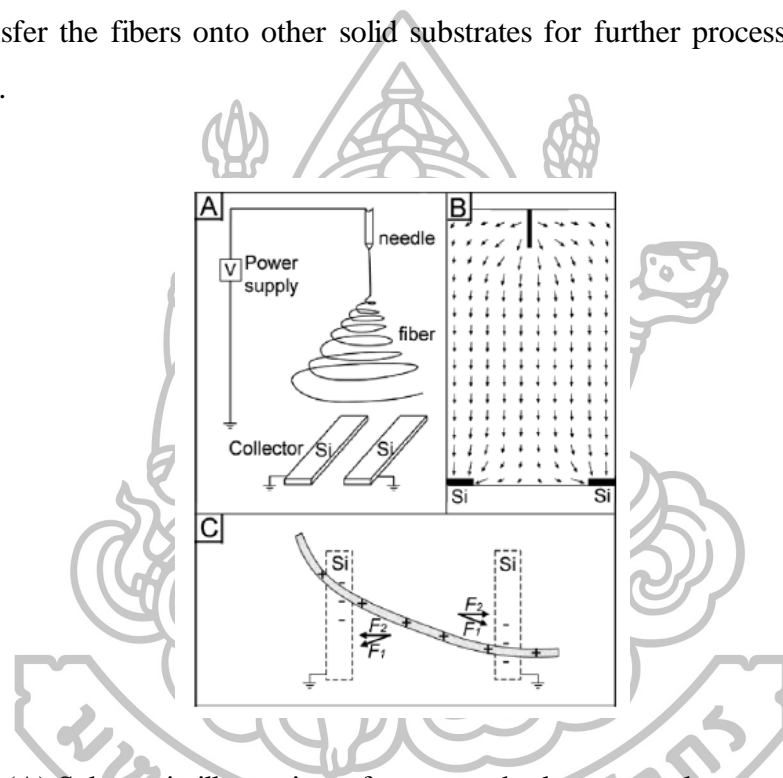


Figure 2.10 (A) Schematic illustration of a gap method setup used generate uniaxially aligned nanofibers. The collector contained two pieces of conductive silicon stripes separated by a gap. (B) Calculated electric field strength vectors in the region between the needle and the collector. The arrows denote the direction of the electrostatic field lines. (C) Electrostatic force analysis of a charged nanofiber spanning across the gap. The electrostatic force (F_1) resulted from the electric field and the Coulomb interactions (F_2) between the positive charges on the nanofiber and the negative image charges on the two grounded electrodes.

Source: Dan Li, Yuliang Wang, and Younan Xia. (2004). "Electrospinning Nanofibers as Uniaxially Aligned Arrays and Layer-by-Layer Stacked Films." *Advance Materials* 16, 4 (February): 361-366.

2.5.3 Alignment caused by magnetic forces

Alignment of electrospun nanofibers can also be achieved by applying an external magnetic field (Figure 2.11). Magnetized poly(vinyl alcohol) (PVA) fibers could be stretched into parallel fibers over large areas (more than $5 \times 5 \text{ cm}^2$) using a magnetic field by Jiang et al. [74]. The polymer solution was magnetized by adding a small amount (less than 0.5 %w/w) of magnetic nanoparticles. The solution was electrospun into nanofibers in the presence of a magnetic field generated by two parallel-positioned permanent magnets. The magnetic field stretched the fibers across the gap to form a uniaxially aligned array as they landed onto the magnets. Nanofibers of PVA were also electrospun without magnetic nanoparticles in a magnetic field, and they were randomly distributed without any alignment. The magnetic field could assist alignment of electrospun nanofibers, but only when electrospinning a magnetizable solution in a magnetic field [74]. Yang and coworkers also demonstrated that by increasing the flow rate of the electrospun jet, the morphology of resultant nanofibers would change from uniaxially aligned to wavy [75]. In this case, both PLGA and poly(vinyl pyrrolidone) (PVP) were electrospun at different flow rates in a magnetic field. At a flow rate of 0.5 mL/h, the PLGA and PVP fibers were straight and uniaxially aligned, while at a flow rate of 3.0 mL/h, the fibers became wavy in morphology without losing the overall alignment. The generation of aligned polymer fibers (both straight and wavy) by magnetic field-assisted electrospinning was independent of the solution and solvent used and did not require the solution to be magnetically active [75]. Further efforts are needed to investigate the mechanism of alignment for nanofibers electrospun in a magnetic field.

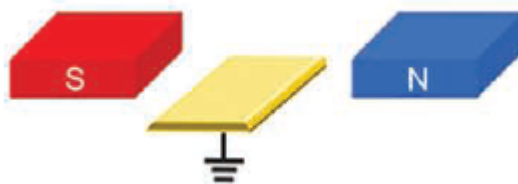


Figure 2.11 Magnetic forces through the use of a pair of permanent magnets (The yellow plates are grounded conductive electrodes).

Source: Wenying Liu, S. Thomopoulos, and Younan Xia. (2012). “Electrospun nanofibers for regenerative medicine.” **Advanced Healthcare Materials** 1, 1 (January 11): 10–25.

2.6 Drug loading in/on nanofibers

Active substances can be incorporated inside the nanofibers, physically adsorbed or chemically bound to the surface (Figure 2.12). However, knowledge of the drug’s behavior during its incorporation in the nanofibers and its subsequent release from the nanofibers is much more limited, compared to the knowledge available for drug incorporation and release from, for example, solid lipid nanoparticles. The loading of many different drugs and their localization in the lipid matrix have been systematically investigated. The results showed that the drug incorporation, localization and release depend on the physicochemical properties of the drug and the carrier matrix. Therefore, it is also expected that for nanofibers the loading mechanism will be governed by the drug solubility in the polymer solution and the drug–polymer interactions in the solid state [76].

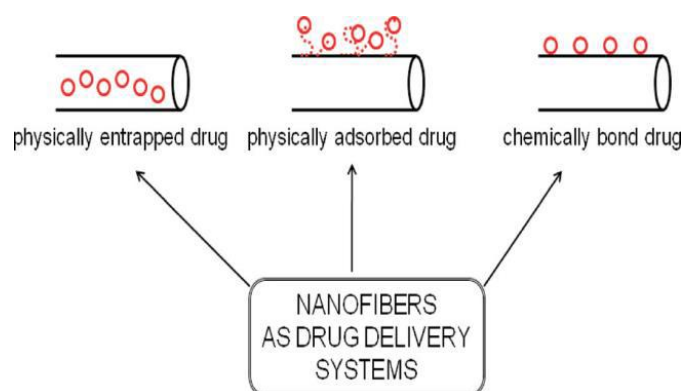


Figure 2.12 Scheme presenting the possibilities drug loading in/on nanofibers.

Source: Ashjaran, A., and A. Namayi. (2014). "Survey on Nanofiber Material as Drug Delivery Systems." **Research Journal of Pharmaceutical, Biological and Chemical Sciences** 5, 3: 1262-1274.

The various loading possibilities, physical entrapment are currently the most widespread, since the drug in the nanofibers is protected against unfavourable environmental conditions and it offers good control over the drug's release. A typically observed release profile from such nanofibers exhibits an initial burst effect followed by an almost linear, sustained release. Furthermore, the preparation of core-shell nanofibers provides a drug-reservoir system with a shell barrier protecting the incorporated drug and controlling the drug diffusion rate. The burst effect from such nanofibers is small and the entire release profile is more sustained [76]. The incorporation of a drug in nanofibers, either in the form of a matrix or as a core-shell system, is relatively easy to perform, since the drug is simply dissolved in the polymer solution prior to electrospinning. The formation of an amorphous drug, which shows a higher solubility with respect to the crystalline form, is favoured, due to a very limited time being available for the drug's recrystallization during the electrospinning process. Furthermore, a reasonable question can be raised concerning the preservation of the chemical and biological integrity of the incorporated drug due to the application of a high voltage during the electrospinning. Various studies using H-NMR, DSC, XRD and IR spectroscopy have proven that the electrospinning process does not affect the structural integrity of the incorporated drug [77]. The physical adsorption of a drug on the surface of the preformed nanofibers is achieved by dipping the

nanofibers into a solution of the drug, which associates with the nanofibrillar surface via electrostatic interactions. However, this technique is seldom used due to poor control over the drug's release and an undesirable competitive displacement of the drug with the components of biological fluids. The third approach to drug loading is the covalent immobilization of the drug on the nanofibrillar surface via the formation of chemical bonds. The latter is predominately used for the modification on the surface properties of nanofibers, since the technique is technically complex. However, there are some reports dealing with this approach for the delivery of active substances. The drug is released after the enzymatic or environmental degradation of the chemical bond [76]. However, the burst release may also be indicative of the drug being attached only on the surface. As the drug and carrier materials can be mixed together for electrospinning of nanofibers, the likely modes of the drug in the resulting nanostructured products are:

- a. Drug as particles attached to the surface of the carrier which is in the form of nanofibers,
- b. Both drug and carrier are nanofiber form; hence the end product will be the two kinds of nanofibers interlaced together,
- c. The blend of drug and carrier materials integrated into one kind of fibers containing both components, and
- d. The carrier material is electrospun into a tubular form in which the drug particles are encapsulated [78].

2.7 Drug release

Drug release from nanofibers can be described through three mechanisms: desorption from fiber surface, solid-state diffusion through fibers, and in vivo fiber degradation. Drug release tests from nanofibers are commonly conducted in phosphate-buffered saline (PBS) solutions. When the nanofiber drug carrier is subjected to PBS, the fibers will be surrounded by the solution. The solution will also penetrate the space in between individual nanofibers. When the nanofiber drug carrier is swollen by the aqueous phase, drugs or proteins attached to the fiber surfaces can be released. Drug release from nanofiber surface is a two-step mechanism, starting

from desorption of drugs from the fiber surface, followed by fast diffusion into the aqueous phase. The desorption mechanism is not limited to the outer surface of the nanofibers but also includes drugs on the surfaces of the nanopores inside the nanofibers. Considering the nanometer size scale of the inner pores, and that the nanopores are most likely interconnected to some degree, the surface area would be much larger than the fiber outer surface area [77].

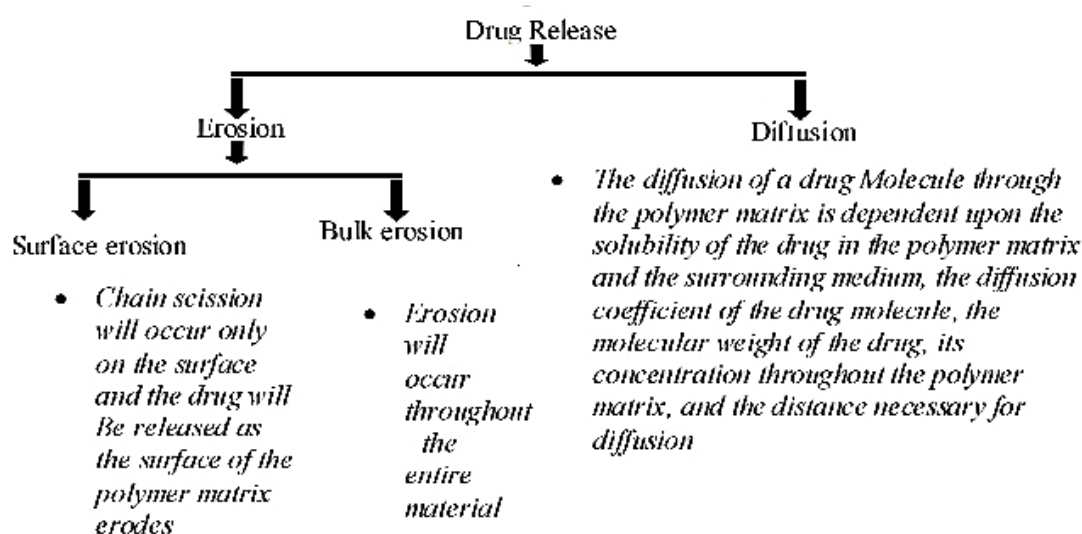


Figure 2.13 Different mechanism of drug release.

Source: Ashjaran, A., and A. Namayi. (2014). "Survey on Nanofiber Material as Drug Delivery Systems." **Research Journal of Pharmaceutical, Biological and Chemical Sciences** 5, 3: 1262-1274.

There have been some reports about the fabrication and use of electrospun nanofibers as carriers for the drug delivery. Taeaiboon and colleagues (2007) reported the use of mats of electrospun CA nanofibers and cast films as carriers for delivery of the model vitamins. In most cases, the vitamin loaded fiber mats exhibited a gradual and monotonous increase in the cumulative release of the vitamins over the test periods, while the corresponding cast films exhibited a burst release of the vitamins [79]. Suwantong et al. (2007) subsequently reported the fabricated ultra fine CA fiber mats containing curcumin use for transdermal delivery. In the total immersion method, almost all of the curcumin loaded in the curcumin loaded CA fiber mat

specimens was released into the medium (≈ 90 to $\approx 95\%$), while considerably lower values were obtained when the curcumin loaded CA fiber mats were placed on top of a piece of pig skin [80]. Tungprapa et al. (2007) showed the release characteristics of four model drugs, i.e., naproxen (NAP), indomethacin (IND), ibuprofen (IBU) and sulindac (SUL) loaded ultra fine fiber mats and cast films of CA. At any given immersion time point, the release of the drugs from the drug loaded e-spun CA fiber mats was greater than that from the corresponding as-cast films. The maximum release of the drugs from both the drug loaded fiber mats and films could be ranked as follows: $NAP > IBU > IND > SUL$ [81].

After so much study about production of random and aligned nanofiber with electrospinning technique, it was found that not so much work has done on to see the relationship between the arrangement of fibers with drug release.

In 2011, Meng and co-workers reported the release rate of fenbufen (FBF) in aligned PLGA and PLGA/gelatin nanofibrous scaffold was lower than that of randomly oriented scaffold [82]. Later, Meng et al. studied with PLGA/chitosan, it was found that the aligned PLGA/chitosan nanofibrous scaffold the release rate of FBF was lower than that of randomly oriented PLGA/chitosan nanofibrous scaffold, which indicated that the nanofiber arrangement would influence the release behavior [83].

2.8 Thin layer chromatography (TLC)

2.8.1 Theory of TLC

Chromatographic separations take advantage of the fact that different substances are partitioned differently between two phases, a mobile phase and a stationary phase. In thin layer chromatography, or TLC, the mobile phase is a liquid and the stationary phase is a solid absorbent.

In this method, a solid phase, the adsorbent, is coated onto a solid support as a thin layer (about 0.25 mm thick). In many cases, a small amount of a binder such as plaster of Paris is mixed with the absorbent to facilitate the coating. Many different solid supports are employed, including thin sheets of glass, plastic, and aluminum. The mixture (A plus B) to be separated is dissolved in a solvent and the resulting solution is spotted onto the thin layer plate near the bottom. A solvent, or mixture of

solvents, called the eluant, is allowed to flow up the plate by capillary action. At all times, the solid will adsorb a certain fraction of each component of the mixture and the remainder will be in solution. Any one molecule will spend part of the time sitting still on the adsorbent with the remainder moving up the plate with the solvent. A substance that is strongly adsorbed (say, A) will have a greater fraction of its molecules adsorbed at any one time, and thus any one molecule of A will spend more time sitting still and less time moving. In contrast, a weakly adsorbed substance (B) will have a smaller fraction of its molecules adsorbed at any one time, and hence any one molecule of B will spend less time sitting and more time moving. Thus, the more weakly a substance is adsorbed, the farther up the plate it will move. The more strongly a substance is adsorbed, the closer it will stay near the origin. Several factors determine the efficiency of a chromatographic separation. The adsorbent should show a maximum of selectivity toward the substances being separated so that the differences in rate of elution will be large. For the separation of any given mixture, some adsorbents may be too strongly adsorbing or too weakly adsorbing [84]. Table 2.3 lists a number of adsorbents in order of adsorptive power.

Table 2.3 Chromatographic adsorbents. The order in the table is approximate, since it depends upon the substance being adsorbed, and the solvent used for elution.

Most strongly adsorbent	Alumina (Al_2O_3)
	Charcoal (C)
	Florisil (MgO/SiO_2 ; anhydrous)
Least strongly adsorbent	Silica gel (SiO_2)

The eluting solvent should also show a maximum of selectivity in its ability to dissolve or desorb the substances being separated. The fact that one substance is relatively soluble in a solvent can result in its being eluted faster than another substance. However, a more important property of the solvent is its ability to be itself adsorbed on the adsorbent. If the solvent is more strongly adsorbed than the substances being separated, it can take their place on the adsorbent and all the substances will flow together. If the solvent is less strongly adsorbed than any of the components of the mixture, its contribution to different rates of elution will be only through its difference in solvent power toward them. If, however, it is more, strongly adsorbed than some components of the mixture and less strongly than others, it will greatly speed the elution of those substances that it can replace on the adsorbent, without speeding the elution of the others. Table 2.4 lists a number of common solvents in approximate order of increasing adsorbability, and hence in order of increasing eluting power. The order is only approximate since it depends upon the nature of the adsorbent. Mixtures of solvents can be used, and, since increasing eluting power results mostly from preferential adsorption of the solvent, addition of only a little (0.5-2%v/v) of a more strongly adsorbed solvent will result in a large increase in the eluting power. Because water is among the most strongly adsorbed solvents, the presence of a little water in a solvent can greatly increase its eluting power [84].

For this reason, solvents to be used in chromatography should be quite dry. The particular combination of adsorbent and eluting solvent that will result in the acceptable separation of a particular mixture can be determined only by trial.

Table 2.4 Eluting solvents for chromatography.

Least eluting power (alumina as adsorbent)	Petroleum ether
	Cyclohexane
	Carbon tetrachloride
	Benzene
	Dichloromethane
	Chloroform
	Ether (anhydrous)
	Ethyl acetate (anhydrous)
	Acetone (anhydrous)
	Ethanol
	Methanol
	Water
	Pyridine
Greatest eluting power (alumina as adsorbent)	Organic acids

If the substances in the mixture differ greatly in adsorbability, it will be much easier to separate them. Often, when this is so, a succession of solvents of increasing eluting power is used. One substance may be eluted easily while the other stays at the top of the column, and then the other can be eluted with a solvent of greater eluting power. Table 2.5 indicates an approximate order of adsorbability by functional group.

Table 2.5 Adsorbability of organic compounds by functional group.

Least strongly adsorbed	Saturated hydrocarbons; alkyl halides
	Unsaturated hydrocarbons; alkenyl halides
	Aromatic hydrocarbons; aryl halides
	Polyhalogenated hydrocarbons
	Ethers
	Esters
	Aldehydes and ketones
	Alcohols
Most strongly adsorbed	Acids and bases (amines)

Technique of Thin-layer Chromatography The sample is applied to the layer of adsorbent, near one edge, as a small spot of a solution. After the solvent has evaporated, the adsorbent-coated sheet is propped more or less vertically in a closed container, with the edge to which the spot was applied down. The spot on the thin layer plate must be positioned above the level of the solvent in the container (Figure 2.14). If it is below the level of the solvent, the spot will be washed off the plate into the developing solvent. The solvent, which is in the bottom of the container, creeps up the layer of adsorbent, passes over the spot, and, as it continues up, effects a separation of the materials in the spot ("develops" the chromatogram). When the solvent front has nearly reached nearly the top of the adsorbent, the thin layer plate is removed from the container (Figure 2.15).

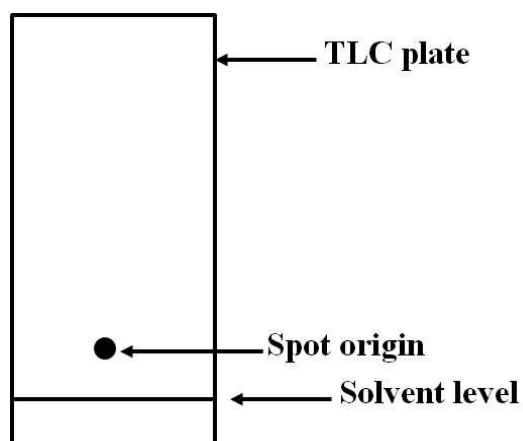


Figure 2.14 Position of the spot on a thin layer plate.

Since the amount of adsorbent involved is relatively small, and the ratio of adsorbent to sample must be high, the amount of sample must be very small, usually much less than a milligram. For this reason, thin-layer chromatography (TLC) is usually used as an analytical technique rather than a preparative method. With thicker layers (about 2 mm) and large plates with a number of spots or a stripe of sample, it can be used as a preparative method. The separated substances are recovered by scraping the adsorbent off the plate (or cutting out the spots if the supporting material can be cut) and extracting the substance from the adsorbent.

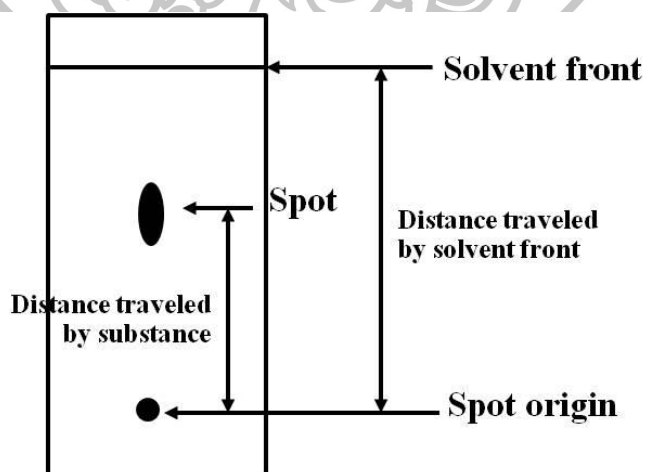


Figure 2.15 TLC plate showing distances traveled by the spot and the solvent after solvent front nearly reached the top of the adsorbent.

Because the distance traveled by a substance relative to the distance traveled by the solvent front depends upon the molecular structure of the substance, TLC can be used to identify substances as well as to separate them. The relationship between the distance traveled by the solvent front and the substance is usually expressed as the R_f value:

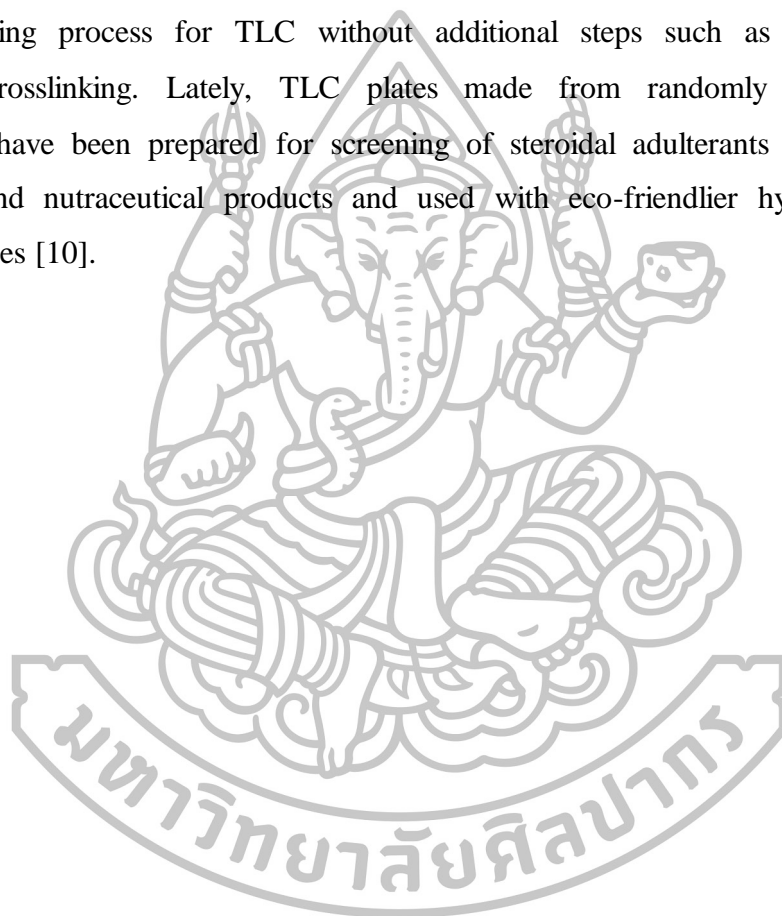
$$R_f \text{ value} = \frac{\text{distance traveled by substance}}{\text{distance traveled by solvent front}}$$

The R_f values are strongly dependent upon the nature of the adsorbent and solvent. Therefore, experimental R_f values and literature values do not often agree very well. In order to determine whether an unknown substance is the same as a substance of known structure, it is necessary to run the two substances side by side in the same chromatogram, preferably at the same concentration [84].

There have been some reports about the fabrication and use of electrospun nanofibers as TLC stationary phase for the separation of amino acids, laser dyes, steroidal compounds and food preservatives. However, the polymers used for the fabrication are limited to glassy carbon [6], silica [7], PAN [8-10], PVA [11] and CA [12]. Nanofibers are prepared by conventional method, nonwoven layers can be oriented with randomly aligned structures. Later, uniaxially aligned electrospun nanofibers have increasingly attracted attention. Furthermore, uniaxially aligned nanofibrous mats can be applied in a variety of fields e.g. cell scaffolds because fiber orientation imitates the parallel structure of fibrous tissues, so it can direct the migration and extension of cells [14-15]. In addition, uniaxially aligned electrospun nanofibers have been currently applied to analytical chemistry e.g. electrochemical/optical based detection systems, solid phase extraction and membrane separation [14]. In the recent, Olesik and co-workers reported the potential of aligned PAN electrospun nanofibers as alternative membrane material to separate a mixture of β -blockers and steroidal compounds. Compared to those with random orientation, the aligned nanofibers improved reproducibility and separation efficiency as well as shortened run time [9]. After that, Kampalanonwat et al. examined the investigation aimed to control the alignment of PAN nanofibers such as the optimization of rotating speed of drum collector has not been conducted yet [10]. From these researches, it

shows performance enhancements motivate further pursuit of new electrospun TLC materials. It is hypothesized that TLC with uniaxially aligned electrospun nanofibers may increase in chromatographic performance when compared with randomly aligned electrospun TLC plates.

CA is an environmentally degradable material made from cellulose that is the most abundant biopolymer on earth [15]. It is much cheaper than some synthetic polymers such as PAN and nanofibers made from CA can be readily used after electrospinning process for TLC without additional steps such as pyrolysis or chemical crosslinking. Lately, TLC plates made from randomly aligned CA nanofibers have been prepared for screening of steroidal adulterants in traditional medicine and nutraceutical products and used with eco-friendlier hydro-alcoholic mobile phases [10].



CHAPTER 3

MATERIALS AND METHODS

3.1 Materials

3.2 Equipments

3.3 Methods

3.3.1 Study of drug release from nanofibers with different degrees of alignment

3.3.1.1 Electrospinning of arbutin (AR)-loaded cellulose acetate (CA) nanofibers

3.3.1.2 Characterizations of AR-loaded CA nanofibers

3.3.1.2.1 Morphological characterizations

3.3.1.2.2 Chemical characterizations

3.3.1.2.3 Mechanical characterizations

3.3.1.2.4 Physical state of AR

3.3.1.3 Study of degree of swelling and weight loss

3.3.1.4 AR content analysis

3.3.1.5 Drug release study

3.3.2 Study of TLC performance of nanofibers with different degree of alignment

3.3.2.1 Electrospinning of CA nanofibers and preparation of TLC plates

3.3.2.2 Characterizations of CA nanofibers

3.3.2.3 TLC procedures

3.3.2.4 Evaluation of TLC performance

3.3.3 Statistical analysis

3.1 Materials

Acetone (Carlo, Italy; purity $\geq 99.5\%$)

Arbutin (AR; purity $\geq 98.0\%$) (Sigma Aldrich®, St. Louis, MO, USA)

Cellulose acetate (CA; Mw= 30 kDa; degree of acetylation ≈ 2.4) (Sigma Aldrich®, St. Louis, MO, USA)

Dimethylacetamide (DMAc, 99.5%) (Sigma Aldrich®, St. Louis, MO, USA)

Distilled water

Ethanol (Merck, Germany; purity $\geq 99.9\%$)

Glacial acetic acid (Merck, Germany; purity $\geq 99.8\%$)

Hydrochloric acid (Scharlau Chemie S.A., Spain; purity $\geq 99.8\%$)

Hydroquinone (HQ; purity $\geq 99.0\%$) (Sigma Aldrich®, St. Louis, MO, USA)

Methanol (Merck, Germany; purity $\geq 99.9\%$)

Phosphomolybdic acid (Sigma Aldrich®, St. Louis, MO, USA)

Resorcinol (purity $\geq 99.0\%$) (Sigma Aldrich®, St. Louis, MO, USA)

Retinoic acid (RA; purity $\geq 98.0\%$) (Sigma Aldrich®, St. Louis, MO, USA)

Sodium metabisulphite (purity $\geq 99.0\%$) (Sigma Aldrich®, St. Louis, MO, USA)

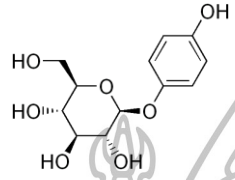

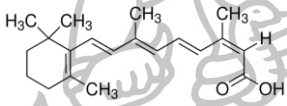
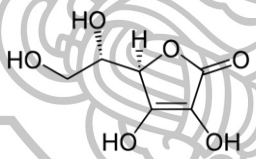
Vitamin C (VC; purity $\geq 99.0\%$) (Sigma Aldrich®, St. Louis, MO, USA)

Vitamin E (purity $\geq 95.5\%$) (Sigma Aldrich®, St. Louis, MO, USA)



The chemical structures and physicochemical properties of some chemicals are shown in Table 3.1.

Table 3.1 Physicochemical properties of some chemicals used in this study.

Drug	Structure	MW (g/mol)	pK _a	Log P
Arbutin (AR)		272.25	9	-1.35
Hydroquinone (HQ)		110.11	9.9	0.59
Retinoic acid (RA)		300.44	4.79	4.65
Vitamin C (VC)		176.12	4.17, 11.57	-2.05

3.2 Equipments

Analytical balance (Sartorius CP224S; Scientific Promotion Co., Ltd., Bangkok, Thailand)

Aluminium foil

Beaker (Pyrex, USA)

Brookfield viscometer (Model DV-III ultra, Brookfield Engineering Laboratories, Inc., MA, USA)

Centrifuge tube (Biologix Research Company, KS, USA)

Conductivity meter (Eutech Instruments Pte Ltd, Ayer Rajah Crescent, Singapore)

Duran bottle 50, 100, 250, 500, 1,000 mL

Differential scanning calorimetry (DSC, Pyris Sapphire DSC, PerkinElmer instrument, USA)

Electrospinning apparatus (Bangkok cryptography, Model rotating mandrel collector, Thailand)

Fourier transform infrared spectrophotometer (FT-IR, Nicolet 4700, Becthai, USA)

Glass syringe 5 mL

Hair dryer

Hot air oven (WTB Binder, Germany)

High performance liquid chromatography (HPLC) instrument (Agilent 1100 series, Agilent Technologies, USA)

HPLC column (Ascentis[®] C18, 5 μ m, 15 cm x 4.6 mm)

High voltage power supply (Model: Gamma High Voltage Research, USA)

Incubated shaker (Model: KBLee 1001, Daiki sciences, Bio-Active, Bangkok, Thailand)

Magnetic stirrer (Framo, Germany) and magnetic bar

Micropipette 0.1-2.5 μ L, 2-20 μ L, 20-200 μ L, 100-1000 μ L, 1-5 mL, and micropipette tip

Microcentrifuge (Microfuge 16[®], Model: A46473, Beckman Coulter Inc., Germany)

Microcentrifuge tube (Eppendorf[®], Corning Incorporated, NY, USA)

Needle 20G (Nipro, Japan)

Nylon membrane filter (diameter 47 mm, pore size 0.45 μ m)

Plain glass microscope slide (Sail brand, China)

Powder X-ray diffractometer (X-ray diffraction apparatus, Rigaku, model miniflex II, Japan)

Reagent spray bottle

Scanning electron microscope (SEM, Camscan Mx2000, England)

Sonicate Bath

Solvent filtration kit (all glass membrane filter holder, borosilicate glass (47mm))

with sintered disc for membrane support, aluminum (duck) clamp, vacuum pump)

Syringe pump (Model: NE-300, New Era Pump Systems Inc., NY, USA)

Texture analyzer (TA.XT plus, Stable Micro Systems UK)

Thickness tester (Minitest, model 600 B, Germany)

Thin-layer chromatography (TLC) developing tank

Uninterruptible power supply (UPS)

Vortex mixer (VX100, Model: Labnet, NJ, USA)

3.3 Methods

3.3.1 Study of drug release from nanofibers with different degrees of alignment

3.3.1.1 Electrospinning of arbutin (AR)-loaded cellulose acetate (CA) nanofibers

CA nanofibers with different degrees of alignment which contained AR were fabricated by electrospinning process. Initially, drug-polymer solution was prepared by dissolving CA (17 % w/v) and AR (3 % wt to polymer) in the solvent mixture of acetone and *N,N*-dimethylacetamide (2:1, v/v). Before electrospinning process, the electrospinning solution viscosity and conductivity were measured using a Brookfield viscometer and a EUTECH ECtestr11+ conductivity meter. The electrospinning process was conducted as previously described [80]. Briefly, the solution was then subjected to electrospinning at room temperature (Figure 3.1) by loading into 5 mL glass syringe equipped with a flat tip of stainless steel needle (20G, inner diameter of 0.9 mm) and connected to the positive electrode of a high voltage power supply. The feeding rate of the CA solution into the tip was controlled at 0.4 mL/h using a syringe pump. The applied voltage and the distance between the needle tip and the collector were fixed at 17.5 kV and 15 cm, respectively. The electrospun nanofibers were collected on an aluminium foil covering the grounded collector (diameter \approx 19 cm) of which the rotating speeds were varied at 350, 2000 and 6000 rpm in order to produce the nanofibers with different degrees of uniaxial alignment. When using the collector at higher speed, it had partial loss of polymer that should be deposited onto the target aluminium foil since the rotation of collector at high speed

resulted in undesirable dispersion of polymer jets into the air during travelling towards the collector. Thus, to obtain the nanofiber mats with comparable weight per area for subsequent studies, the spin times were varied to 5, 8 and 12 h for the fabrication of nanofibers collected by using drum speed of 350, 2000 and 6000 rpm, respectively.

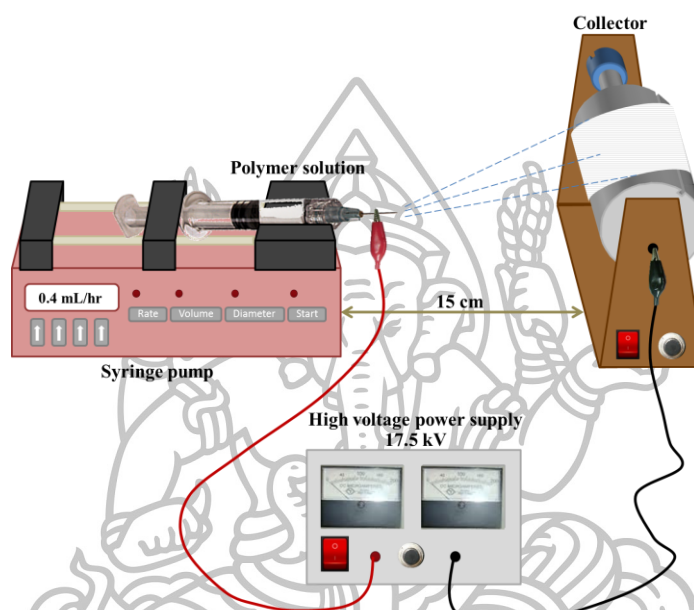


Figure 3.1 Schematic representation of the electrospinning apparatus setup.

3.3.1.2 Characterizations of AR-loaded CA nanofibers

AR-loaded CA nanofibers were characterized as follows;

Morphological characterizations

The morphologies, fiber orientation, diameters of CA electrospun nanofibers and thickness of layers were investigated using a scanning electron microscope (SEM, Camscan Mx2000, England). For this process, a small section of each fiber was prepared by cutting an aluminum foil covered with the CA electrospun nanofibers and then sputtered with a thin layer of gold prior to the SEM observation. Image analysis software (JMicroVision V.1.2.7, Switzerland) was used to measure 50 randomly chosen nanofibers to determine each diameter of these nanofibers and the thickness of layers from the SEM image.

The alignment of nanofibers was assessed as the number of fibers oriented in a determine direction with respect to a vertical reference line (0° angles). The angles from which individual fibers were deviated from this line are determined ($n = 50$) by using image analysis software (JMicroVision V.1.2.7, Switzerland) and then plotted as a function of frequency in a histogram [85]. The narrow distribution of nanofiber angles indicates more alignment.

Chemical characterizations

The chemical structure of the nanofibers was characterized by using a Fourier transform infrared spectrophotometer (FT-IR) with a wave number range of $400\text{-}4000\text{ cm}^{-1}$, compared with AR and neat CA. Samples were mixed and ground with potassium bromide and punched to the disc with 1.2 mm diameter.

Mechanical characterizations

The tensile strength of nanofibers were spun at different speed of collector was evaluated by using a texture analyzer with 5 kg load cell equipped with tensile grips holder ($n = 5$). For this purpose, the nanofiber mats with comparable weight per area were used. The size of each specimen was 6 x 35 mm in rectangular shape. For all type of nanofibers, the stretch was applied in pararell and perpendicular direction.

Physical state of AR

The powder X-ray pattern of AR, CA and AR-loaded nanofibers spun at different speeds of collector were recorded by using X-ray powder diffractometer. Samples were irradiated with monochromatized CuK α radiation after passing through Nickel filters and then were analyzed between 5° and 50° (2theta). The voltage and current applied were 30 kV and 15mA, respectively.

The thermal behavior of AR, CA and AR-loaded nanofibers spun at different speeds of collector were determined by Differential scanning calorimetry (DSC). Samples (3-5 mg) were placed in a seal aluminium pan and crimped with its cover to provide hermetically sealed samples. The heating rate was $10\text{ }^\circ\text{C}/\text{min}$. All measurements were obtained over $50\text{ - }350^\circ\text{C}$ under nitrogen flow at $20\text{ mL}/\text{min}$.

3.3.1.3 Study of degree of swelling and weight loss

The swelling degree and weight loss of the AR-loaded nanofibers spun at different speeds of collector were determined in deionized water at room temperature. The initial weight of AR-loaded nanofibers (≈ 10 mg) was recorded. Then, the AR-loaded nanofiber mats are placed in 50 mL of the deionized water that was incubated at $30 \pm 1^\circ\text{C}$ under shaking at 200 rpm for 10 min and 24 h. The swollen nanofiber mats were weighed and recorded as the wet weight. After that the swollen AR-loaded nanofiber mats were dry in the hot air oven at 65°C for 48 h. The dry nanofiber mats were weighed and recorded as the dry weight [90]. The swollen processes were recorded using a digital camera (Cannon, Japan). The degree of swelling and weight loss of each AR-loaded nanofiber mats were calculated according to equations (1) and (2), respectively:

$$\text{Degree of swelling (\%)} = \frac{M_w - M_d}{M_d} \times 100 \quad (1)$$

$$\text{Weight loss (\%)} = \frac{M_0 - M_d}{M_d} \times 100 \quad (2)$$

where M_w and M_d are the wet and dry weights of each AR-loaded nanofiber mats after submersion in the medium and M_0 is the initial weight of the samples in dry state.

3.3.1.4 AR content analysis

The AR-loaded nanofiber mats were cut into the area of $2 \times 2 \text{ cm}^2$ and weighed to determine the exact weights. The drug amount contained in CA nanofibers was determined by placing the nanofibers in 5 mL of deionized water and sonicated at 50°C . After 1 h, the extraction medium was centrifuged and the supernate was collected. The sedimented nanofibers were repeatedly extracted for another 2 rounds in the same manner to ensure the complete release of drug and all the supernate were pooled. By this manner, 97% of drug was extracted in the first two rounds and no peak of AR was observed in the third round of extraction, indicating

the acceptable extraction efficiency. The amount of drug dissolved in water was determined by HPLC consisting of C18 column (150 x 4.60 mm, 5 μ m), a mobile phase composed of (89:10:1) water:methanol:0.1 M hydrochloric acid flowing at 1.0 mL/min and UV detector set at 222 nm. The sample injection volume was 100 μ L. The assays were run in triplicates. AR was eluted at 1.51 min (Figure 3.2). The actual drug amount contained in the nanofiber mats were back calculated from the obtained data against a predetermined standard curve of drugs (Figure 3.3) where the relationship between peak area (y) and concentration of AR (x) was $y = 151.7x + 100.03$ ($r^2 = 0.9999$). Then, the percentage of drug loading efficiency and loading capacity were calculated according to equations (3) and (4), respectively:

$$\text{Loading efficiency (\%)} = \frac{\text{Real AR content (\mu g of AR/gm of nanofibers)}}{\text{Theoretical AR content (\mu g of AR/gm of nanofibers)}} \times 100 \quad (3)$$

$$\text{Loading capacity (\%)} = \frac{P_t}{M_t} \times 100 \quad (4)$$

where P_t is the amount of AR embedded in the nanofiber mats and M_t is the weight of nanofiber mats.

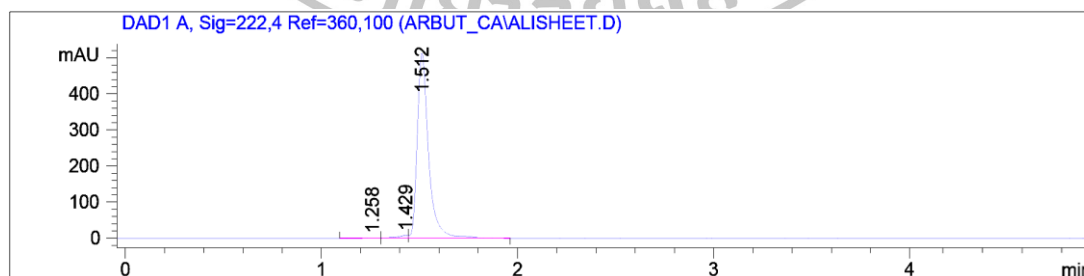


Figure 3.2 HPLC chromatogram of AR.

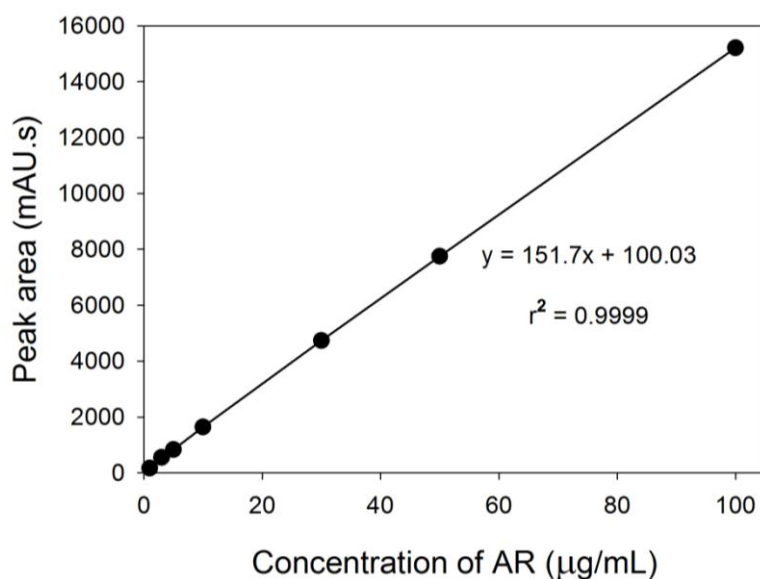


Figure 3.3 Standard curve for the quantitation of AR using HPLC-UV detector.

3.3.1.5 Drug release study

The AR-loaded nanofiber mats used for drug release test require the comparable weight per area. Therefore, the nanofiber mats were cut into square shape ($2 \times 2 \text{ cm}^2$), removed from the backing foil and then weighed to determine the exact weights. After statistically testing the differences between means of weights obtained from each type of nanofibers (ANOVA at the 95% confidence intervals), the mats with a comparable weight per area were used for drug release comparison.

The AR-loaded nanofiber mats ($2 \times 2 \text{ cm}^2$) were weighed and placed into the bottle containing 25 mL of deionized water as a release medium that was incubated at $30 \pm 1 \text{ }^\circ\text{C}$ under shaking at 200 rpm. At a given time (0.25, 0.5, 0.75, 1, 3, 5, 10, 20, 30, 45, 60 and 90 min), an aliquot of 500 μl samples were withdrawn from the medium and fresh deionized water with equal volume was added into the medium to maintain sink conditions. The taken medium was subjected to the assay of the amounts of AR released from the nanofibers by using HPLC. All the measurements were conducted in triplicate.

The AR release profiles from nanofibers with different alignment were studied by plotting the graphs of cumulative concentrations of drug released (Y-

axis) versus times (X-axis). From the graph, the times to reach 80% of drug release were determined and used for the comparison among different types of nanofibers.

3.3.2 Study of TLC performance of nanofibers with different degree of alignment

3.3.2.1 Electrospinning of CA nanofibers and preparation of TLC plates

CA nanofibers used for the study of TLC performance were prepared in the similar manner as previously described in 3.3.1.1, except that no AR was added into the polymer solution. The drum collector was set to rotate at different speeds (350, 4,500, 6,000 and 7,500 rpm) to obtain the nanofibers with different alignment. To investigate the appropriate nanofiber mat thickness for satisfactory TLC separation, different spin times (1, 2, 4, 6, and 8 h) were used. After electrospinning, the aluminum foil covered with CA nanofiber layer was carefully taken off from the collector and cut into rectangular shape ($7.5 \times 2.5 \text{ cm}^2$) by selecting the area with the uniform thickness. For use as TLC plates, the cut foil was then fixed onto the glass backing using double sided adhesive tape to produce CA nanofiber plate which was ready to use for TLC separation.

3.3.2.2 Characterizations of CA nanofibers

CA nanofibers were characterized for the morphologies and diameters of nanofibers, thickness of layers and degree of alignment by using the similar methods mentioned in 3.3.1.2.

3.3.2.3 TLC procedures

The separation of HQ, RA and VC on electrospun nanofiber plates was carried out by manually spotting 0.5 μL of standard solutions, prepared in absolute ethanol, of HQ (0.125 mg/mL), RA (0.67 mg/mL) and VC (1 mg/mL) side by side, 1 cm from the bottom edge with the aid of calibrated micropipette and tips. The plate was then developed vertically in a closed chamber containing mobile phase (methanol/water/acetic acid) which was previously saturated at 30°C for 30 min. The

mobile phase was allowed to migrate for a distance of 5 cm from the starting point. Subsequently, the plate was removed from the chamber and air dried. The spots of HQ, RA and VC were detected by spraying the plate with 5% (w/v) phosphomolybdic acid solution in ethanol following the ASEAN guidelines and blowing with hot air (95°C) from hairdryer at 5 cm distance from the plate for 2.5 min. HQ, RA and VC were directly visualized as grey spots under visible light.

3.3.2.4 Evaluation of TLC performance

The performance to separate HQ, RA and VC of aligned versus randomly aligned nanofibers were compared in the following aspects.

Run time

The time in which the mobile phase used to migrate on different types of CA nanofibers for a distance of 5 cm to finish TLC analysis were measured and calculated as the migration constant.

$$\text{Migration constant} = \frac{\text{Migration distance}^2}{\text{Time}}$$

(4)

Spot shape and size

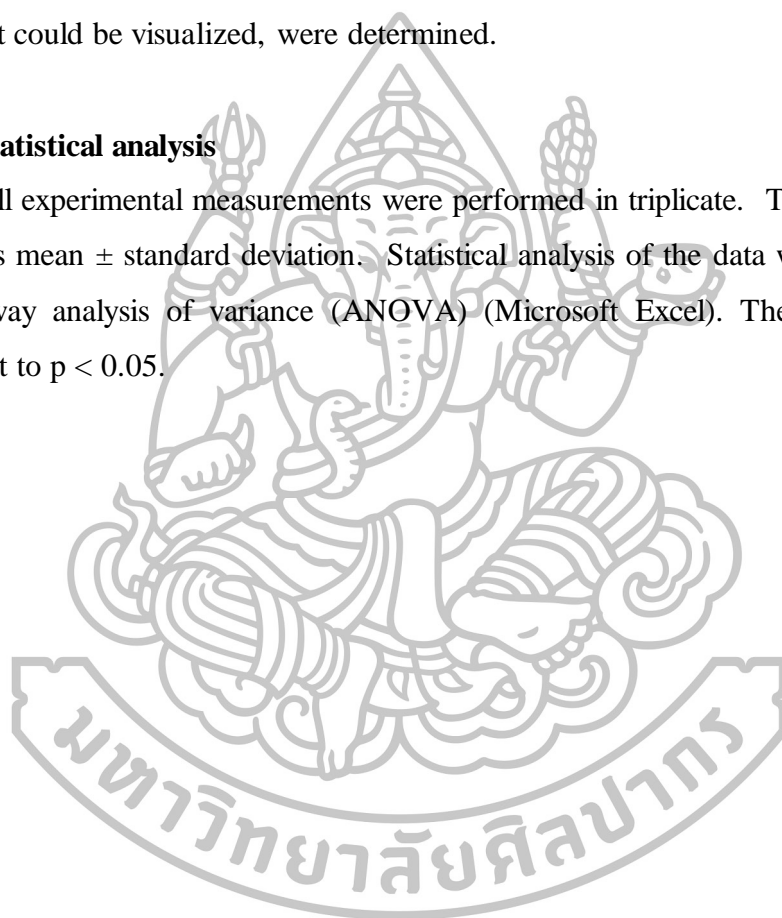
The shape and tailing of spots were observed directly as appeared on the sprayed plates. To measure the spot size, the images of the TLC plates (n = 4) were captured by a scanner (HP Deskjet 1050, Hewlett Packard, China) at a resolution of 300 dpi and saved as TIF files. The image was then opened with Photoshop CS2 software (Adobe System, Mountain View, CA, USA). The mode of color was changed to grayscale and the threshold level was adjusted to 220. The area of spot was measured as pixels by using Magic Wand Tool and Histogram of Photoshop CS2 software (Adobe System, Mountain View, CA, USA).

Limit of detection

Since the spot intensity may affect the ability to visualize the spots on the plate, limit of detection (L.O.D.) for HQ and RA spots was determined and compared among iniaxially aligned and randomly aligned CA nanofiber as well as commercial silica gel plates. For this purpose, series of standard solutions of HQ and RA were spotted on the different types of plates to obtain 5, 10, 20, 40, 80 ng of HQ and 25, 50, 100, 200, 400 ng of RA. After TLC run, L.O.D., defined as the lowest quantity that could be visualized, were determined.

3.3.3 Statistical analysis

All experimental measurements were performed in triplicate. The results are expressed as mean \pm standard deviation. Statistical analysis of the data was evaluated using one-way analysis of variance (ANOVA) (Microsoft Excel). The significance level was set to $p < 0.05$.



CHAPTER 4

RESULTS AND DISCUSSION

- 4.1 Drug release from nanofibers with different degrees of alignment
 - 4.1.1 Characteristics of AR-loaded nanofibers
 - 4.1.1.1 Morphological characteristics
 - 4.1.1.2 Chemical characteristics
 - 4.1.1.3 Mechanical characteristics
 - 4.1.1.4 Physical state of AR in nanofibers
 - 4.1.2 Degree of swelling and weight loss
 - 4.1.3 Drug loading efficiency in nanofibers
 - 4.1.4 Drug release
- 4.2 TLC performance of nanofibers with different degree of alignment
 - 4.2.1 Characteristics of CA nanofibers
 - 4.2.2 Chromatographic separation ability of CA nanofibers
 - 4.2.3 Appearance and detectability level of spots on CA nanofibers
 - 4.2.4 Migration rate of solutes on CA nanofibers
 - 4.2.5 Application of CA nanofibers to TLC screening of adulterated substances in cosmetic samples

4.1 Drug release from nanofibers with different degrees of alignment

4.1.1 Characteristics of AR-loaded nanofibers

In the electrospinning process, there are many of parameters that affect fiber formation and structure. The parameter can be classified to solution parameter, process parameter and environment parameter. The factors affecting the nanofibers morphology were the viscosity, conductivity and surface tension of electrospinning solution [3]. The concentration and molecular weight of polymer influence the viscosity of solution. If the concentration of polymer increases the solution viscosity will increase. Another way to increase the solution viscosity is using the higher molecular weight polymer. One of the important condition necessary of electrospinning to occur where fibers are formed is that the solution must provide the sufficient molecular weight or concentration and the solution must be of sufficient viscosity. When the viscosity is increased which mean that there is the higher amount of polymer chain entanglement in the solution, the charges on the electrospinning jet will be able to fully stretch the solution with the solvent molecule distributed among the polymer chains. With increased viscosity, the diameter of the fiber also increases. However, when the viscosity is too high, the solution may dry at the tip of the needle before electrospinning can be initialed [87]. In the case of conductivity, it has been found that with the increase of electrical conductivity of the solution, there is a significant decrease in the diameter of the electrospun nanofibers whereas with low conductivity of the solution, it results in insufficient elongation of a jet by electrical force to produce uniform fiber, and beads may also be observed [88]. Therefore prior to electrospinning, shear viscosity and electrical conductivity of CA solutions with and without AR were measured. As summarized in Table 4.1, both properties were not significantly different between the solutions, indicating that the drug at the concentration used (3% w/w) did not considerably affect the viscosity and electrical

conductivity of neat CA solution. Therefore, the AR was favorably incorporated into the CA nanofiber mats and prepared as AR-loaded nanofiber mats.

Table 4.1 Shear viscosity and electrical conductivity of CA solution with and without AR (n=5).

Type of CA solution	Shear viscosity (cP s)	Electrical conductivity ($\mu\text{S cm}^{-1}$)
Without AR	865.1 ± 39.6	4.8 ± 0.1
With 3% wt AR	860.7 ± 16.7	4.7 ± 0.2

Aligned nanofibers can be used in many applications such as skeletal tissue regeneration, neural cell seeding in scaffold, fuel cell electrolytes, electrochemical sensing, bone and blood vessel engineering [89]. Resultant fiber diameter, porosity, and other characteristics can be controlled by modifying the solution flow rate, composition, electric field potential, and distance between the needle and target. Additionally, fiber arrangement can be altered by modifying the deposition target geometry [52]. Among different ways of producing aligned electrospun nanofibers, the simplicity of fast moving drum has made it attractive and widespread. The speed of rotating drum is usually known as the main cause of alignment [90]. In the present study different drum speeds have been used to see their effect on the alignment of the fiber. In the preliminary study where the electrospinning was carried out in within fixed 5 h, the nanofiber mats deposited on the collector rotating at the drum speed of 6000 and the mats collected at 2000 rpm were found to be obviously thinner and had smaller weights than those collected at 350 rpm. This effect was caused by the partial loss of polymer that should be deposited onto the target aluminum foil since the rotation of collector at high speed resulted in undesirable dispersion of polymer jets into the air during travelling towards the collector. Thus, to obtain the nanofiber mats with comparable weight per area for subsequent studies, the spin times were varied to 5, 8 and 12 h for the fabrication of nanofibers collected by using drum speed of 350,

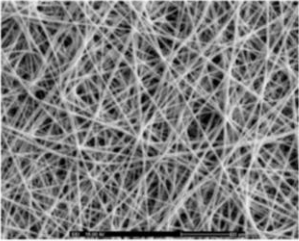
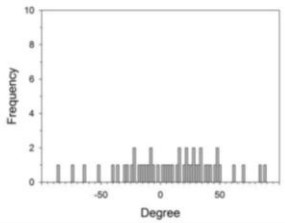
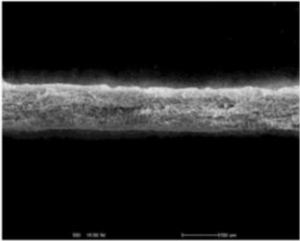
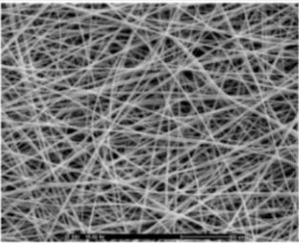
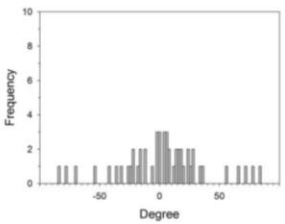
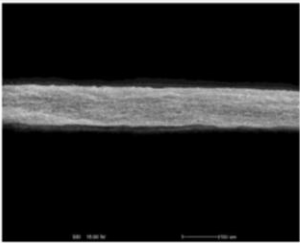
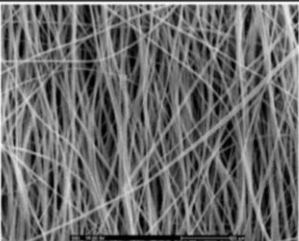
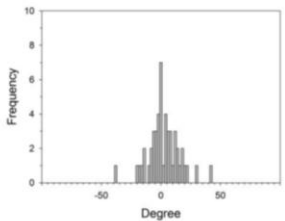
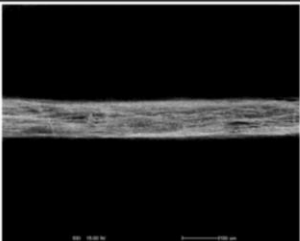
2000 and 6000 rpm, respectively. After electrospinning was done, the nanofibers were characterized in the following aspects.

Morphological characteristics

Table 4.2 shows SEM images, alignment, diameters and layer thickness of AR-loaded nanofibers. Overall, all types of them showed smooth, uniform and bead-free morphologies. The increasing rotation speed of drum collector from 350 to 2000 and 6000 rpm resulted in the nanofibers with random, semi-aligned and mostly aligned orientation, respectively. This is in accordance with early discovery on cellulose nanofibers electrospun using a high speed rotating drum of 300 m/min as the collector [91]. The average diameters ranged from 616 - 624 nm which were not statistically different among the different types of nanofibers. By using the different spin times as described earlier, the random, semi-aligned and mostly aligned nanofibers had comparable weight per area of about 0.0025 g/cm². Nevertheless, their layer thickness was slightly different. In the case of mostly aligned nanofibers which had the thinnest layers, it was possible that they were deposited tightly onto the collector and arranged themselves in the highly ordered pattern inside the layers as a result of high stretching force generated by high speed drum rotation.



Table 4.2 Effect of collector rotation speed on fiber morphology, alignment, diameters and layer thickness of AR-loaded nanofibers.

Speed of collector (rpm)	Characteristics of nanofibers				
	SEM (Top view)	Alignment	Diameter (nm)	SEM (Cross section)	Layer thickness (μm)
350			624 ± 40		54 ± 1
2000			616 ± 38		48 ± 1
6000			620 ± 43		42 ± 4

Chemical characteristics

The FTIR spectra of AR, CA and three types of AR-loaded nanofibers are shown in Figure 4.1. The spectrum of CA exhibited the characteristic peaks at 3500 cm^{-1} for $-\text{OH}$ stretching, 2960 cm^{-1} for $-\text{C}-\text{H}$ stretching, 1750 cm^{-1} for $-\text{C}=\text{O}$ stretching and 1250 and 1040 cm^{-1} for $-\text{C}-\text{O}-$ stretching. The AR showed a broad band at $3500\text{-}3000\text{ cm}^{-1}$ for $-\text{OH}$ stretching, $2900\text{-}3000\text{ cm}^{-1}$ for $-\text{C}-\text{H}$ asymmetrical stretching, and $1400\text{-}1600\text{ cm}^{-1}$ for $-\text{C}-\text{C}-$ stretching in aromatic ring. When AR was incorporated into CA nanofibers, the prominent sharp peak at 1500 cm^{-1} corresponding to $-\text{C}-\text{C}-$ stretching in aromatic ring was observed. This chemical functionality is present in only AR, but absent in CA [92].

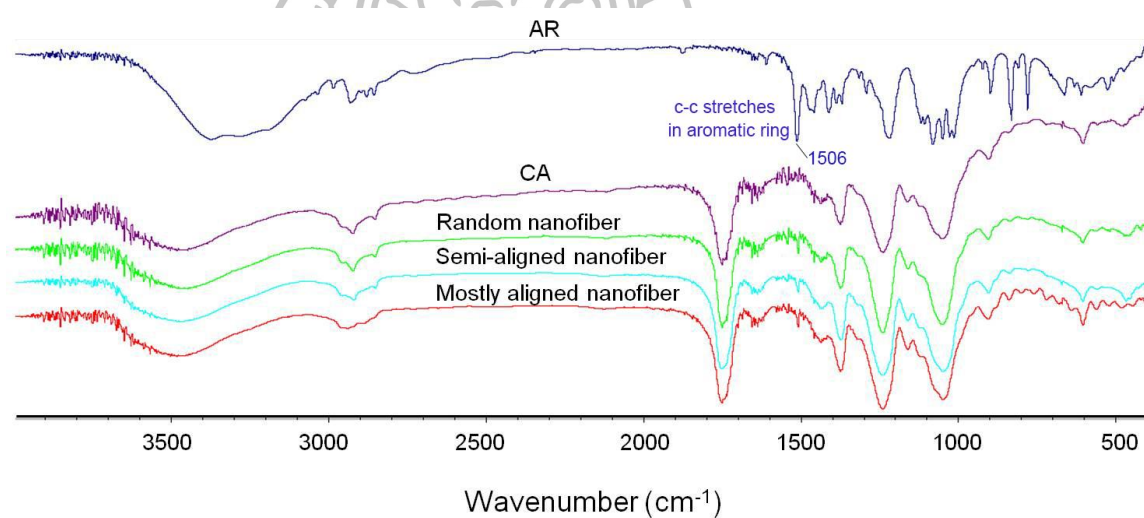


Figure 4.1 FT-IR spectra of the AR, CA and three types of CA nanofibers.

Mechanical characteristics

To compare the tensile property of the differently aligned AR-loaded nanofibers, the nanofiber mats with comparable weight per area were used in the study and the results are shown in Table 4.3. It was found that different types of nanofibers possessed different tensile strengths depending on their fiber alignment as well as the direction of pulling force applied in the experiments. Clearly, the mostly aligned nanofiber mats had the lowest tensile strengths when they were stretched in the direction perpendicular to the fiber alignment since the force simply separated fibers apart from each other without tearing (Figure 4.2). In contrast, if the mats were pulled along the fiber alignment direction, the assembly of parallel nanofibers as bundles provided the efficient resistance to the stretch and showed the highest tensile strength value, before the intra-fibrous breakage occurred. No difference of tensile strength was observed for the randomly aligned nanofibers even they were pulled in the different directions. For semi-aligned nanofibers, this mechanical behavior was in between those of the random and mostly aligned nanofibers. This result was in accordance with previous study by He et al. [91]. This result revealed that pulling in the different directions largely affected the tensile strengths of aligned and semi-aligned nanofiber mats. Subramanian and coworkers fabricated 2D random and 3D longitudinally oriented nanofibers of poly(lactide-co-glycolide) (PLGA) by the modified electrospinning process and revealed that the tensile strength and Young's modulus of random PLGA fibers were significantly higher than those of the aligned PLGA nanofibers ($p < 0.05$) [93]. This difference might be caused from that they did not concern about the direction of pulling force applied in their experiments.

Table 4.3 Tensile strength (N/mm²) of AR-loaded nanofiber mats (n=5).

Random		Semi-aligned		Mostly aligned	
parallel	perpendicular	parallel	perpendicular	parallel	perpendicular
19.0 ± 3.2	18.2 ± 2.6	70.1 ± 9.5	14.4 ± 3.7	226.6 ± 18.0	8.3 ± 1.0

* Stretching force was applied in the direction parallel or perpendicular to the fiber alignment direction.

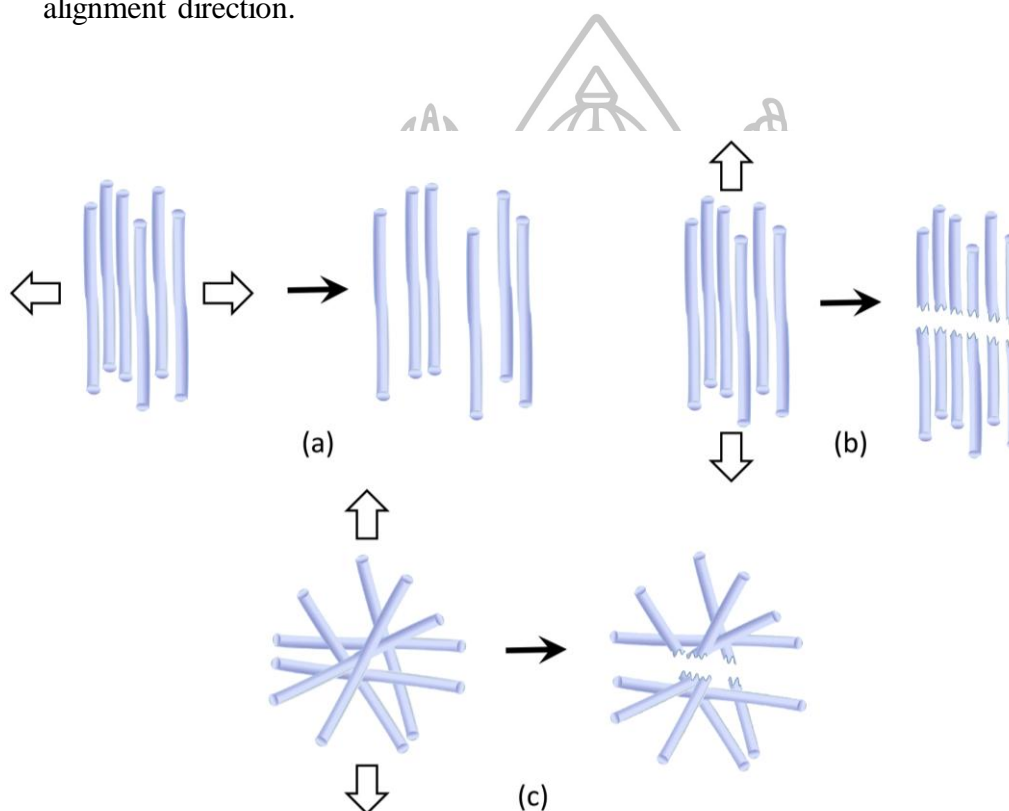


Figure 4.2 Proposed illustrations of differently aligned nanofibers upon being stretched in parallel or perpendicular directions; (a) and (b) mostly aligned, (c) random nanofibers.

Physical state of AR in nanofibers

Since the physical state of drug may influence on its solubility, XRD and DSC measurements were undertaken to reveal whether AR in the nanofibers was present in crystalline or amorphous state. The XRD patterns of the AR, CA and three types of AR loaded nanofibers are presented in Figure 4.3. The diffractogram of the

AR displayed strong crystalline peaks, indicating its high degree of crystallinity. However, no such peak was found in the diffractograms of all types of AR loaded nanofibers, indicating that AR was incorporated into CA nanofibers in an amorphous state.

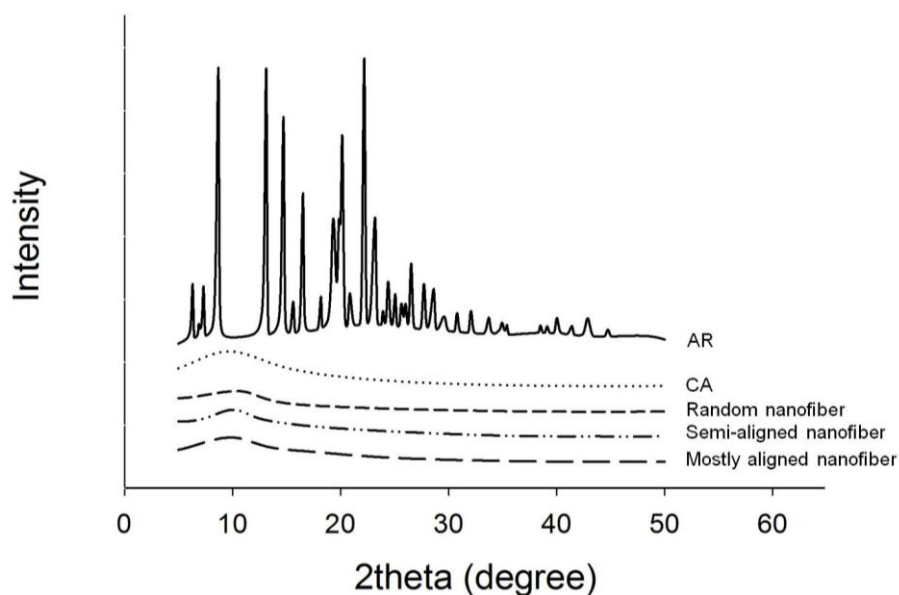


Figure 4.3 Powder X-ray diffractograms of the AR, CA and three types of CA nanofibers.

Additionally, thermograms obtained from the DSC studies (Figure 4.4) revealed that AR exhibited an endothermic sharp peak at 197.11 °C corresponding to its melting temperature. However, AR melting was not observed in all types of drug loaded nanofibers, confirming that AR in the nanofibers changed from crystalline to amorphous state. These results were corresponding to the data from X-ray pattern of the AR in the nanofibers.

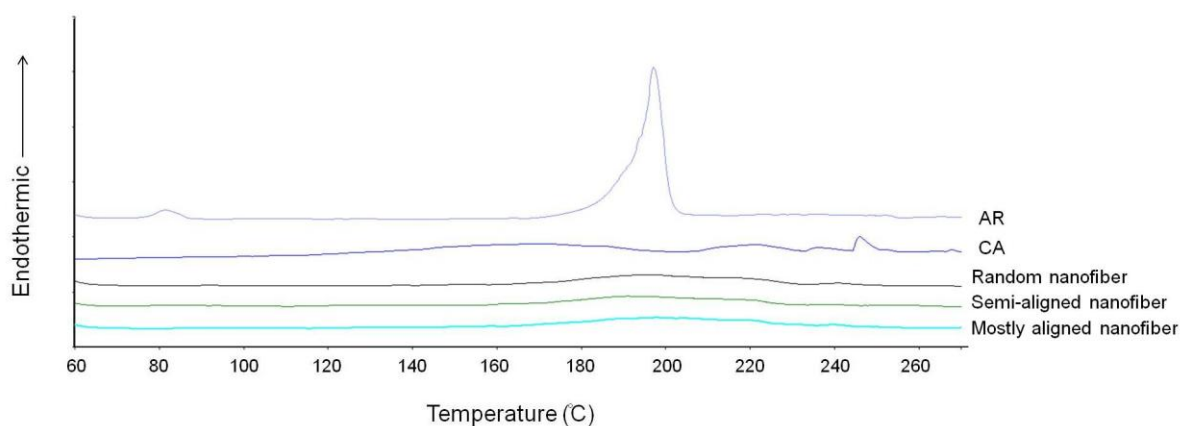


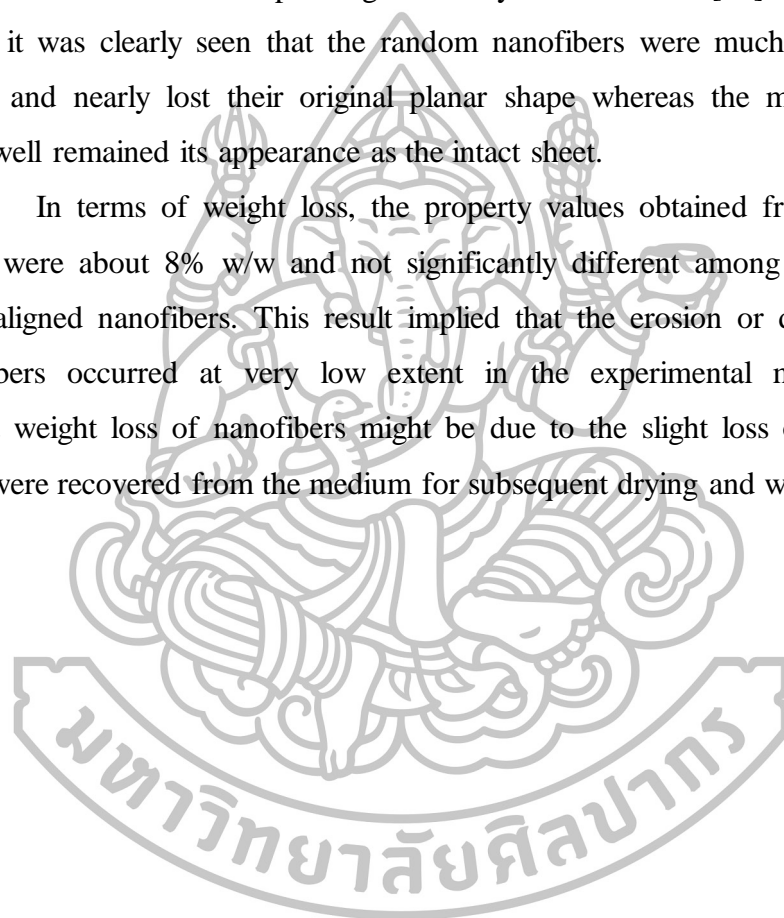
Figure 4.4 DSC thermograms of the AR, CA and three types of CA nanofibers.

4.1.2 Degree of swelling and weight loss

The swelling behavior of the AR loaded nanofibers was investigated by immersing the nanofibers in water at 30°C for several time intervals. During the first 10 min, the uptake of water into the fiber mats was rapid to reach the degree of swelling of 251%, 188% and 153% for random, semi-aligned and mostly aligned nanofibers, respectively (Figure 4.5). The high amount of water uptake should attribute to the physical adsorption of water in the individual fibers and the retention of water by capillary action in the inter-fibrous pores. The highest swelling ability of the random nanofibers was probably due to the looser arrangement of nanofibers compared to other types, which facilitated the penetration of water into inter-fibrous space and provided the larger room for water retention. At this 10 min, however, the visual appearance of all types of nanofibers was not noticeably distinct (Figure 4.7). After the experiment was continued to 24 h, all types of nanofibers went on swelling to the higher degree of swelling. The degree of swelling of random, semi-aligned and mostly aligned nanofibers was 381%, 270% and 202%, respectively (Figure 4.6). This observation is in agreement with Suwantong et al., 2007, [80] who found that the swelling ratio of random neat CA nanofibers was ~370% (in acetate buffer solution containing 0.5% v/v polysorbate 80 and 3% v/v methanol at 37 °C for 48 h). Moreover, they found that the swelling ability of the fiber mats prepared from the CA solutions containing 5 and 10 %wt curcumin was slightly lower (340 and 355%,

respectively), while that of the spun fiber mats prepared from the CA solutions containing 15 and 20 %wt curcumin was essentially the same [80]. A much greater value of 715% (in acetate buffer at 37 °C for 24 h) was reported by Tungprapa et al. [81] (for the neat CA fiber mats that were 20-35 μm in thickness with the average diameter of the individual fibers being ~ 230 nm). Previously, Meng et al. reported that the swelling ratio of aligned PLGA and PLGA/gelatin (9/1) nanofibrous scaffolds were lower than those of corresponding randomly oriented ones [82]. As shown in Figure 4.7, it was clearly seen that the random nanofibers were much fluffier than other types and nearly lost their original planar shape whereas the mostly aligned nanofibers well remained its appearance as the intact sheet.

In terms of weight loss, the property values obtained from the 24 h experiment were about 8% w/w and not significantly different among the types of differently aligned nanofibers. This result implied that the erosion or dissolution of CA nanofibers occurred at very low extent in the experimental medium. The insignificant weight loss of nanofibers might be due to the slight loss of nanofibers when they were recovered from the medium for subsequent drying and weighing.



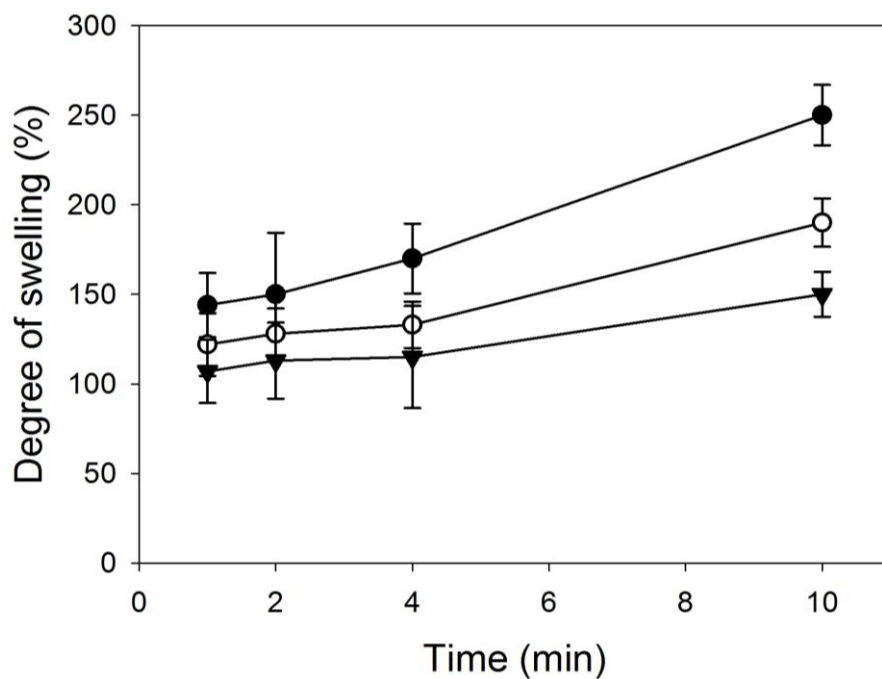


Figure 4.5 Degree of swelling of AR loaded nanofibers within the first 10 min; (▼) mostly aligned (○) semi-aligned (●) random nanofibers (n=3).

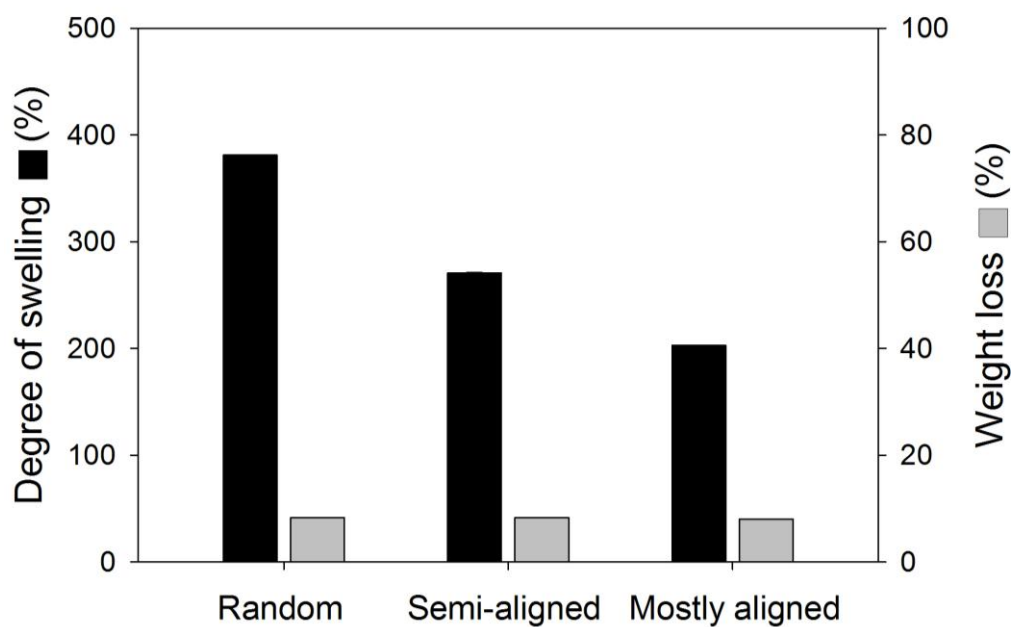


Figure 4.6 Degree of swelling and weight loss of the AR loaded nanofibers at 24 h (n=3).

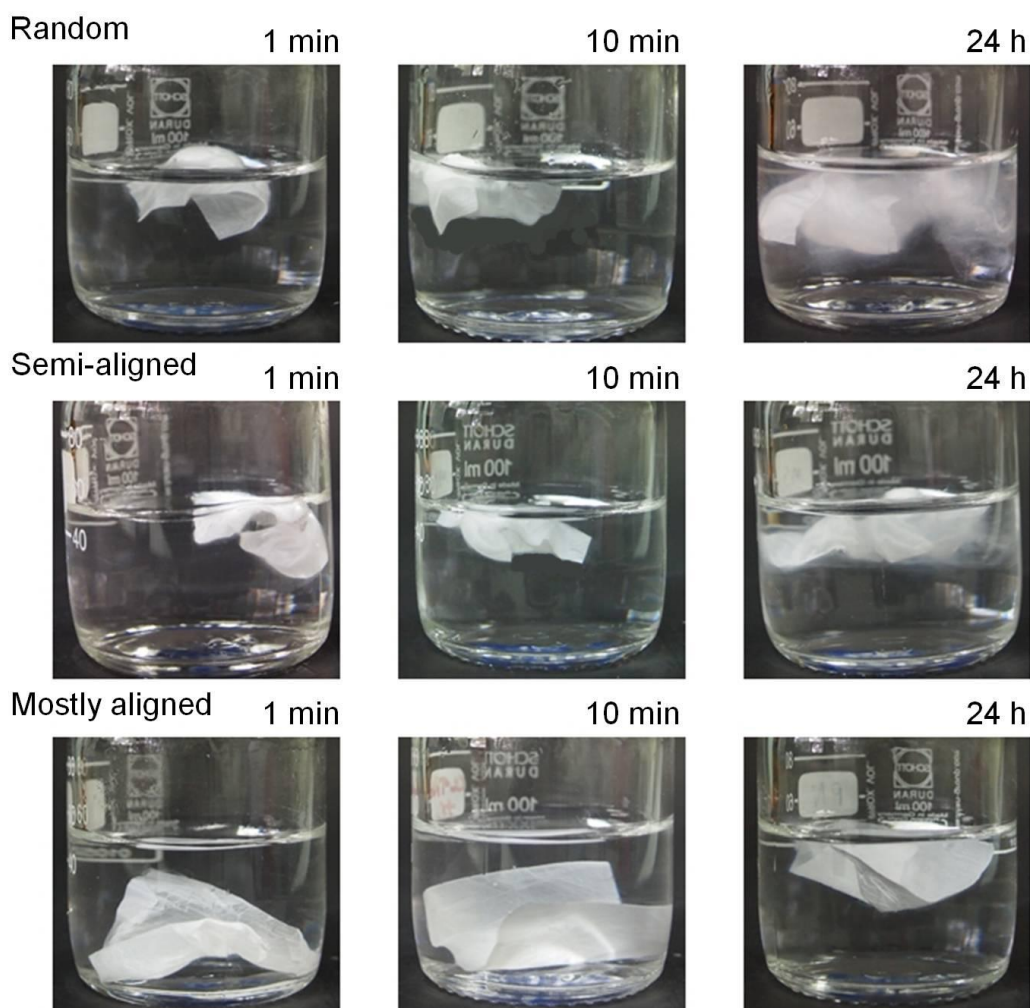


Figure 4.7 Images of nanofibers in swelling experiments at 1 min, 10 min and 24 h.

4.1.3 Drug loading efficiency in nanofibers

The amount of AR in each nanofiber mats determined as the percentage loading efficacy and loading capacity, are listed in Table 4.4. The actual amounts of AR incorporated in the nanofibers and loading efficiency were determined prior to the investigation of their release characteristics. In general, the amounts of AR in all types of samples were in the range of 2.7 – 2.8 % w/w (weight of drug to weight of nanofibers). Calculated based on the theoretical content of 3%w/w, the drug loading efficiencies were found to be more than 90 % (Table 4.4), demonstrating that most AR was successfully loaded into the nanofibers. In addition, the small S.D. values

implied the uniform dispersion of drug in the different areas of nanofibers. The discrepancy from the ideal value of 100% for the actual content could be due to the small amount of drug which was not extracted into the medium for HPLC assay and remained inside the fibers.

Table 4.4 Loading efficiency and loading capacity of AR in CA nanofibers (n = 3).

	Random	Semi-aligned	Mostly aligned
Loading efficiency (%)	91.6 ± 0.7	93.4 ± 0.8	95.9 ± 1.2
Loading capacity (%)	2.7 ± 1.1	2.7 ± 0.6	2.8 ± 1.4

4.1.4 Drug release

The drug release from nanofibers was investigated by using water as medium. The nanofiber mats with comparable weight and area were used as tested samples to ensure that the comparison was performed among the nanofibers with the same quantities of drug and polymer as well as surface area. It was revealed that for all types of nanofibers, the release of AR which is water soluble was rapid within 10 min (Figure 4.8) and reached the maximum cumulative amounts at about 84.0 - 86.1% (Figure 4.8). It was hypothesized that the fast release happened via the rapid dissolution of drug once water penetrated into the fiber layers, followed by the diffusion of drug from the matrix through the water-filled channels in the entangled network of nanofibers into the medium. However, the dissolution and/or erosion of CA nanofibers should not take part in the drug release since CA is water insoluble polymer and the nanofibers were found to erode at very low extent according to the weight loss determination results.

Interestingly, as can be seen in Figure 4.8, the fastest drug release over the first 10 min period was obtained from the mostly aligned nanofibers, followed by the semi-aligned and then the random ones. By the estimation, 80% of drug release was achieved in 1.7, 4.2 and 9.4 min for the mostly aligned, semi-aligned and random nanofibers, respectively. From these results, it can be concluded that the drug release

patterns during the initial burst period was significantly affected by the orientation of nanofibers. This conclusion can be explained that in the case of AR, the solubility of drug should not be an influencing factor on drug release since AR is freely soluble and similarly present in the amorphous state in all types of nanofibers. Also, the differences of drug release should not be the effect of different compactness of nanofiber layers and their swelling ability because even in the mostly aligned nanofibers with the least swelling degree and the most dense fiber arrangement, the drug release reached 75% within 1 min, compared with the random counterparts which released only 30% of drug over the same period. From this finding, it was assumed that the swelling in all types of nanofibers occurred at the high level which was sufficient for the formation of water-filled spaces within nanofiber mats, in regardless of their initial compactness, and eventually led to the free dissolution of drug.

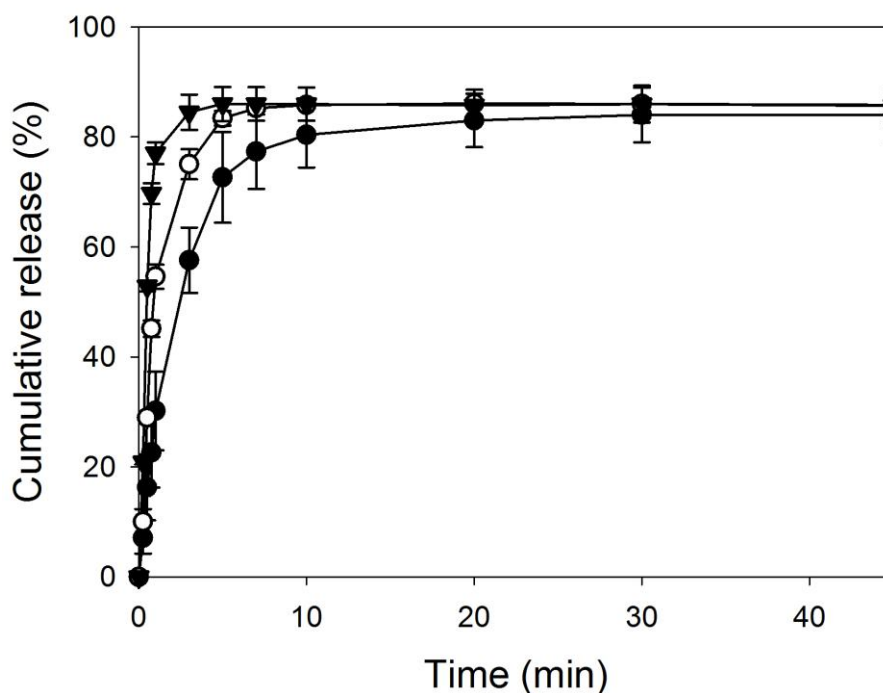


Figure 4.8 Percent cumulative release of AR from nanofibers; (▼) mostly aligned, (○) semi-aligned, (●) random nanofibers (n = 3).

The alignment of nanofibers is assumed to be the key reason underlying the distinct rate of drug release. In the nanofibers with random alignment, highly tangled network of fibers were formed. As a result, the drug diffusing in the water-filled inter-fibrous gaps were retarded by lengthy and tortuous paths and thereby took longer time to reach the external medium (Figure 4.9). On the contrary, the uniaxially aligned nanofibers arranged themselves in more ordered fashion and the entanglement was assumed to arise at the lower degree. Therefore, the drug would be allowed to transport to the boundary connected with the external medium at the faster rate. This phenomenon is alike to Eddy diffusion in chromatographic separation where the solutes that move along the more tangled paths generated by the packed beds of stationary phase are eluted out of the column in the longer retention time than those moving via the relatively straight shots.

In the aspect of drug release which is influenced by the fiber alignment, Meng et al. reported their investigation using PLGA, PLGA/gelatin and PLGA/chitosan nanofibers loaded with poorly water soluble fenbufen [82, 83]. They found that the release rate of drug from aligned nanofibrous scaffold to the aqueous medium was lower than that from randomly oriented nanofibers and proposed that the aligned nanofibers enhanced the density of nanofibers and decreased the pore size of scaffolds compared with the randomly oriented ones. Then, the outwards diffusion rate of the drug from the scaffold with aligned nanofibers was lower than that from the scaffold with random nanofibers. However, since PLGA is more hydrophobic than CA and fenbufen is much less water-soluble than AR, Meng's proposed explanation may not be applied to our case. In addition, in those works the release profiles of fenbufen were slow and sustained up to 25 h whereas AR was rapidly released in our experiments within 10 min. The mechanisms of drug release should be quite different between these two drugs from the different nanofibers.

From these results, it is concluded that the faster drug release profile may be achieved by the control of nanofiber alignment. However, whether random or aligned scaffolds will give the faster rate probably depends on the properties of drug and/or polymer used. At least from our study, it was found that very fast release of AR can be obtained from the fabrication of CA nanofibers in highly aligned

orientation. This finding indicates the feasibility to use highly aligned nanofibers the delivery of certain drugs in fast-releasing or fast-acting formulations.

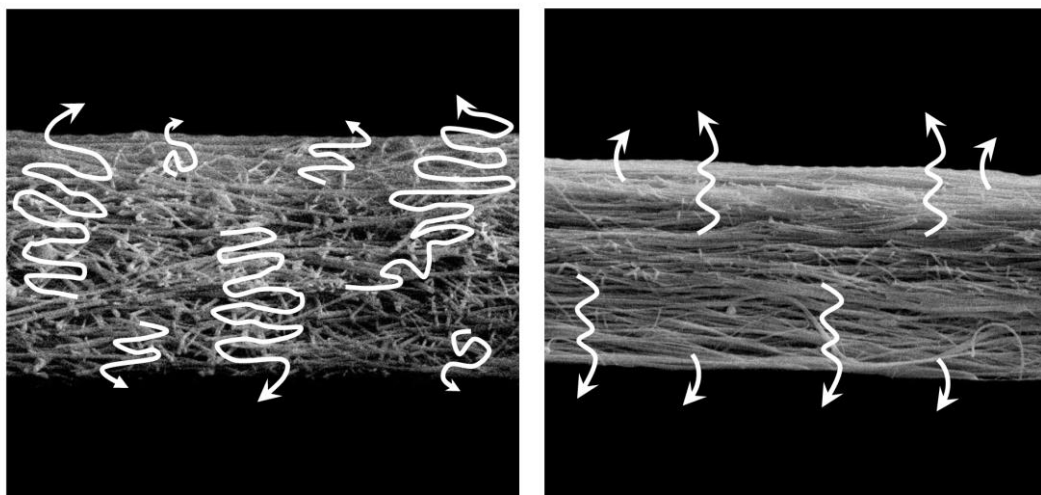


Figure 4.9 Model of drug release in mostly aligned (right) and random (left) nanofibers.

4.2 TLC performance of nanofibers with different degree of alignment

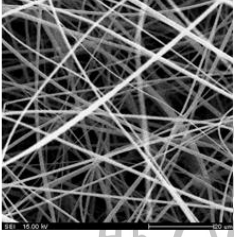
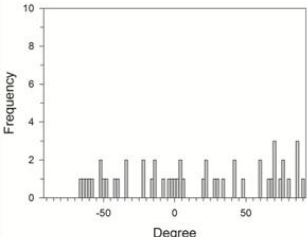
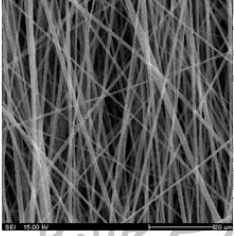
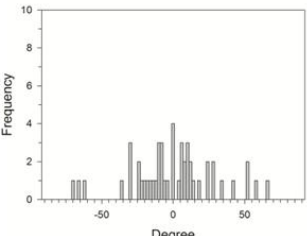
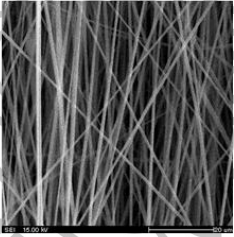
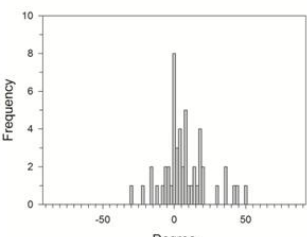
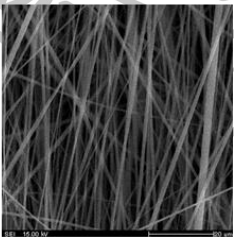
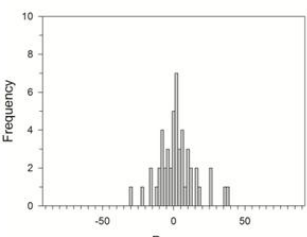
4.2.1 Characteristics of CA nanofibers

Of several means to control the alignment of electrospun nanofibers, a mechanical method through the use of a drum collector rotating at a high speed was employed in this study. CA nanofibers were characterized for the morphologies, degree of alignment, diameters of nanofibers and thickness of layers by using the similar methods mentioned in 4.1.1. As shown in Table 4.5, the drum rotation at 350 rpm was apparently too slow to orient the deposited fibers in the uniaxial direction. By raising the collector speeds, nanofibers were found to be more aligned as indicated by the narrower distribution of nanofiber angles. Along with the higher degree of alignment, the average diameter of nanofibers decreased with the increasing rotation speeds due to the higher stretch of the polymer jets wounded around the drum (Table 4.5). Compared with the AR-loaded nanofibers, the decrease of diameter of neat CA nanofibers was more obvious since no significant difference was found among the differently aligned nanofiber types of AR-loaded nanofibers. No evidence of fiber

breakage was observed at all tested rotation speeds as seen under SEM. Since the nanofibers collected at 6000 rpm showed satisfactory alignment and insignificant morphological difference from those collected at the higher rpm, this rotation speed was chosen for the subsequent study. To investigate the effect of spin time, the aligned nanofibers were electrospun at times of 1, 2, 4, 6, 8 and 10 h, maintaining the optimized collector rotation speed at 6000 rpm. Spin time is an important process parameter because the longer time generates more fibers on the collector and the electrical charge accumulated on the deposited fibers may interfere with the incoming ones resulting in the fibers with less alignment [52]. In another way, too short spin time produces insufficient thickness of fiber layers and may give rise to the poor chromatographic performance in terms of loading capacity of sample solution and separation quality. As shown in Figure 4.10, the thickness of mostly aligned nanofiber layers increased with the increasing spin time. Besides, the mostly aligned nanofiber mats were thinner than the random ones which were electrospun at 350 rpm using the equal spin time. This effect was probably caused by the partial loss of polymer that should be deposited onto the target aluminum foil and the more dense deposit of mostly aligned nanofibers with smaller diameter size on the aluminum backing when the high speed rotation of collector was used.



Table 4.5 Effect of drum-rotation speed on fiber morphology and alignment of CA nanofibers.

Speed of collector (rpm)	Characteristics of nanofibers		
	SEM	Diameter (nm)	Alignment
350		730 ± 60	
4500		650 ± 70	
6000		500 ± 40	
7500		500 ± 70	

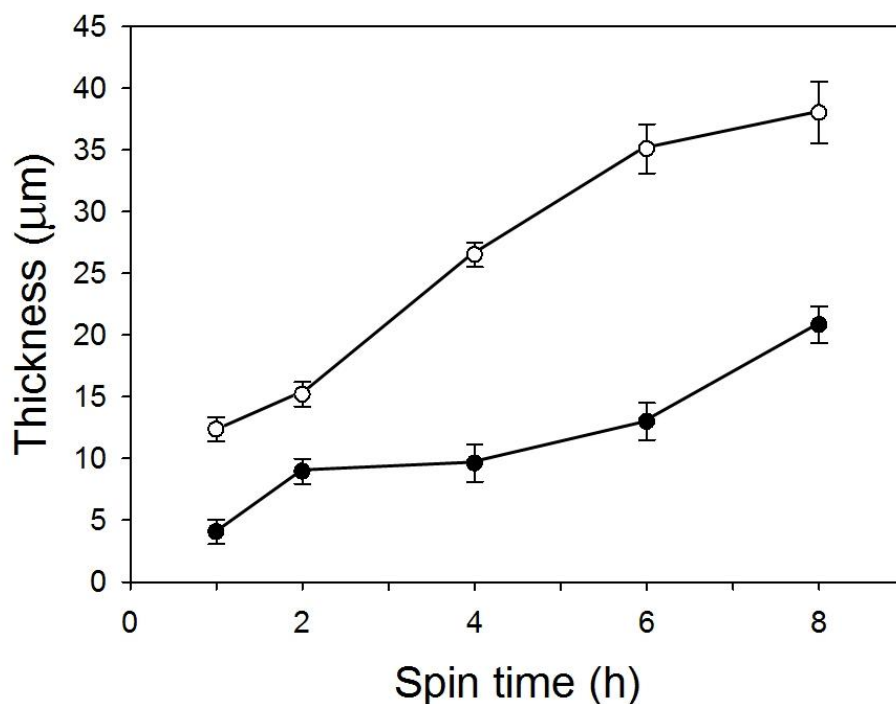
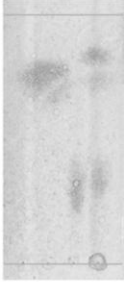
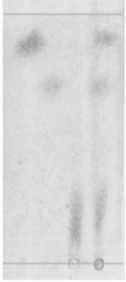





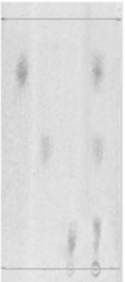
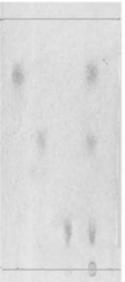
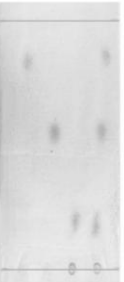


Figure 4.10 Thickness of mostly aligned (●) and random (○) nanofiber layers as a function of spin time (n=10).

4.2.2 Chromatographic separation ability of CA nanofibers

To select the electrospun CA nanofibers which were suitable for TLC, mostly aligned and random nanofibers produced at various spin times were evaluated using previously optimized 65:35:2.5 methanol/water/acetic acid as the mobile phase. Both mostly aligned and random CA nanofibers were able to separate HQ, RA and VC with good performance, as illustrated in Table 4.6, compared with the silica based plates which sometimes failed to separate the analytes and sometimes gave too high R_f values closed to 1 (Figure 4.11). Good resolution without the solutes remaining at the initial spots was obtained from mostly aligned and random nanofibers electrospun for at least 6 h and 4 h, respectively. The nanofibers collected at the shorter time than these periods were too thin for the efficient separation due to the inadequate chromatographic beds.

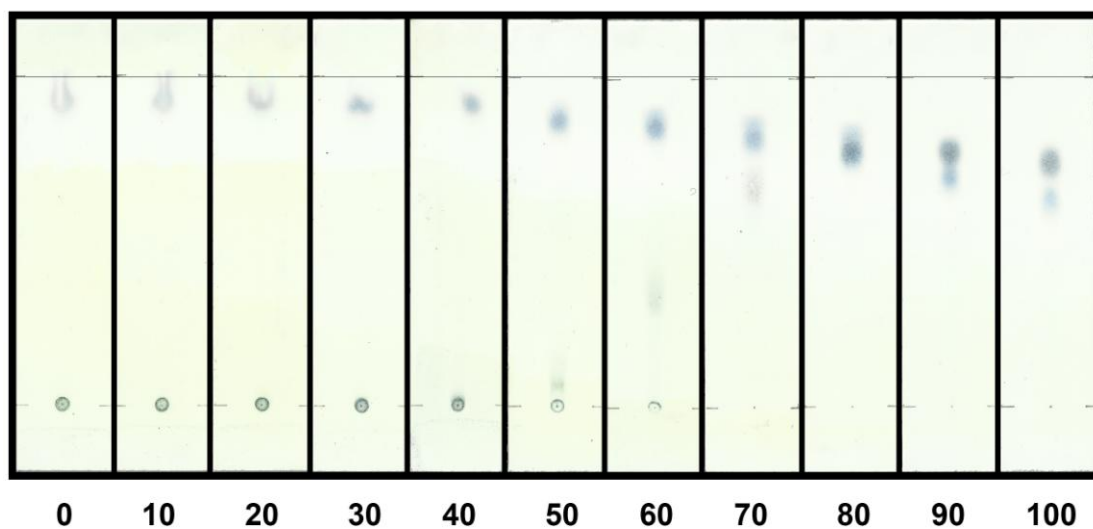
Table 4.6 Effect of spin time on TLC separation of HQ, RA and VC.

Type of nanofibers	Spin time (h)				
	1	2	4	6	8
Random					
Run time (min)	47 ± 3	40 ± 4	38 ± 3	37 ± 3	35 ± 2
Migration constant (cm ² /min)	0.53	0.63	0.66	0.68	0.71
Mostly aligned					
Run time (min)	34 ± 3	15 ± 2	13 ± 2	13 ± 2	16 ± 2
Migration constant (cm ² /min)	0.74	1.67	1.92	1.92	1.56

* The order of spots from bottom to top of plates was RA, HQ and VC

** Migration constant was calculated from $\text{Migration constant} = \frac{(\text{Migration distance})^2}{\text{time}}$

(a)



(b)

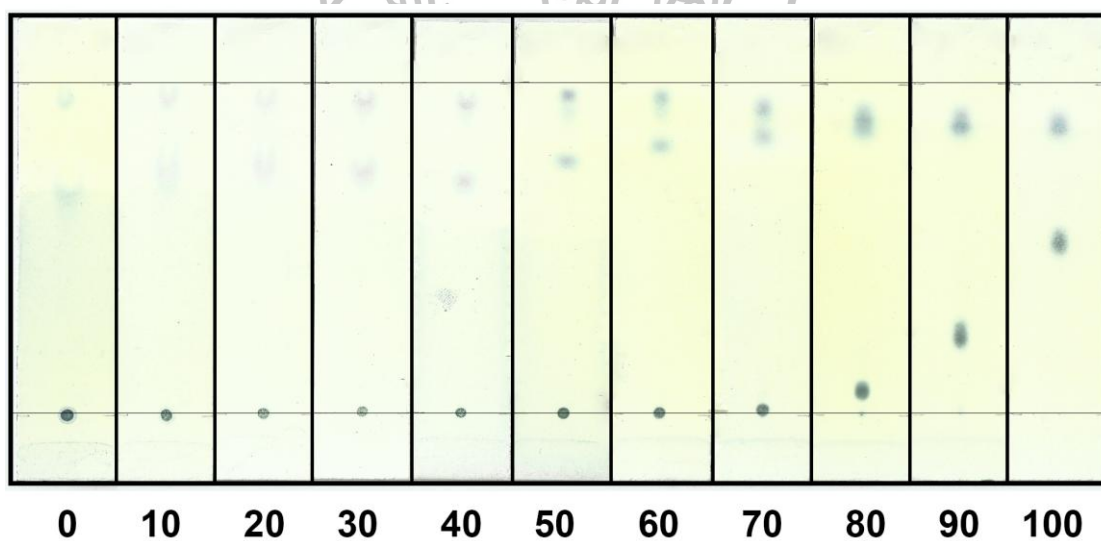


Figure 4.11 The separation of hydroquinone and retinoic acid on the (a) silica plates (upper spot: RA and lower spot: HQ) and (b) C18 silica plates (upper spot: HQ and lower spot: RA) using mobile phases containing different percentages of methanol to water in the presence of 2.5% acetic acid.

4.2.3 Appearance and detectability level of spots on CA nanofibers

In spite of the comparable separation ability, the mostly aligned and random nanofibers were found to be different in some aspects. By visual analysis, the initial spots of samples on the mostly aligned nanofibers were more elliptical than those on random ones due to the preferential diffusion along the vertical direction of nanofibers. After the separation, the spots on the mostly aligned nanofibers were generally smaller and appeared darker compared to those on the random ones which were more diffused in broad areas (Table 4.6). The measurement of spot dimension by digital imaging software revealed that the spots on the random nanofiber plates were almost twice as large as those on the mostly aligned ones in pixels (Table 4.7). This difference probably arose due to the fact that while the solutes were moving up in the flow of mobile phase on the random nanofibers, they were likely to disperse in all directions due to the random arrangement of nanofiber mesh. On the other hand, the solute migration on the mostly aligned nanofibers occurred preferentially along the vertical channels, giving rise to the lower extent of transverse (across-channel) diffusion. In addition, the reduced spot diffusion might associate with the lower thickness and higher density of the aligned media compared to the random one.

Table 4.7 Area of analyte spots on mostly aligned and random CA nanofibers (n = 4).

CA nanofibers	Area of spot (pixel)	
	HQ	RA
Mostly aligned	1260 + 130	1020 + 140
Random	2520 + 300	1770 + 330

For practical application, this feature offers the advantage of mostly aligned nanofibers over the random ones in the terms of the ease of spot visualization and the lower mass of the analyte which could be detected. Therefore, the masses of the analytes which could be visualized on different types of plates or the detectability

levels were investigated. Interestingly, the masses of HQ and RA which could be visually detected on the mostly aligned CA nanofiber plates were twice lower than those on the random nanofibers (Table 4.8) due to the darker spots on this type of fibers as previously discussed. Moreover, the masses of both compounds which could be detected on the mostly aligned CA nanofibers were five times lower than those on typical silica plates which were used in the ASEAN method using the same visualization reagent. It was probable that the thinner chromatographic bed of electrospun nanofibers (8.5 μm) compared to that of commercial silica gel plates (200-250 μm) contributed to the better ability to visualize the analyte at the lower mass. To the best literature review, this is the first report about the advantage of nanofibrous stationary phases, especially in the mostly aligned orientation, over conventional TLC plates in the aspect of the lower mass of the analyte which could be detected.

Table 4.8 Masses of HQ and RA which could be visualized on different types of TLC plates.

Stationary phase	Mobile phase	Mass (ng)	
		HQ	RA
Mostly aligned CA	65:35:2.5 methanol:water:acetic acid	10	25
Random CA	65:35:2.5 methanol:water:acetic acid	20	50

In all cases, 5% (w/v) phosphomolybdic acid in ethanol was used as a visualization reagent.

4.2.3 Migration rate of solutes on CA nanofibers

From Table 4.6, the thinner mats of nanofibers took longer run time, probably related to the low capillary action to draw the solvent up the plate. More interesting is the markedly faster separation ability of the mostly aligned nanofibers. From the results, about two to three times reduction of developing time could be

achieved by using the mostly aligned nanofibers instead of the random ones (Table 4.6). In addition, the solvent migration on the mostly aligned nanofibers used in this study (migration constant $\approx 1.9 \text{ cm}^2/\text{min}$) was more rapid than that on the random ones reported in the previous work (migration constant $\approx 1.0 \text{ cm}^2/\text{min}$), using the similar mobile phase [12]. It was hypothesized that the vertical channeling generated from the mostly aligned nanofibers facilitated the solvent to move straight up the plate and minimized the lengthy distracted traveling along the random paths. In another point of view, the faster run time also reduced the chance of solute diffusion happening in the flow of mobile phase, thereby promoting the compact size of spots. Since fast analysis is preferred for screening tasks, uniaxially aligned CA nanofibers with the adequate thickness were appropriate and practical for use.

4.2.3 Application of CA nanofibers to TLC screening of adulterated substances in cosmetic samples

The applicability of the mostly aligned CA nanofibers was evaluated by the analysis of cosmetic creams collected from the local markets. In terms of the specificity, CA nanofiber based TLC was free from the interference by the ingredients commonly found in cosmetic creams. As depicted in Figure 4.12, HQ and RA were efficiently separated from the substances which could form colored spots with phosphomolybdic acid i.e. VC, RS and AR. For vitamin E and sodium metabisulfite, they did not react with phosphomolybdic acid and thus did not interfere with the test.

Also, it was found that the screening performed by using the mostly aligned CA nanofibers gave results in agreement with the confirmatory HPLC method according to ASEAN guidelines [94, 95]. Figure 4.13 presents the TLC results of analysis of three different samples run on the mostly aligned CA nanofiber plates. It was found that the sample S1 contained neither HQ nor RA whereas S2 and S3 were adulterated with HQ and RA, respectively.

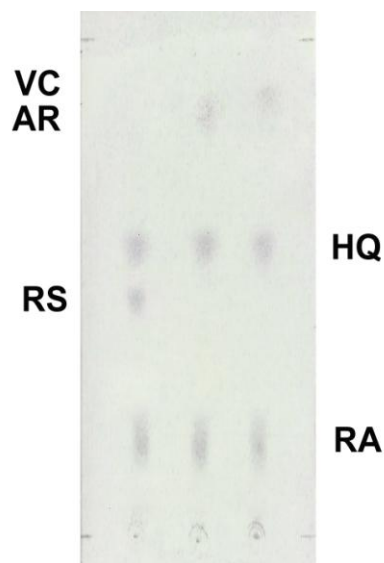


Figure 4.12 Results of interference study for the proposed TLC screening method.

The masses of HQ, RA, VC, AR and RS are 62, 335, 500, 500 and 50 ng per spot, respectively.

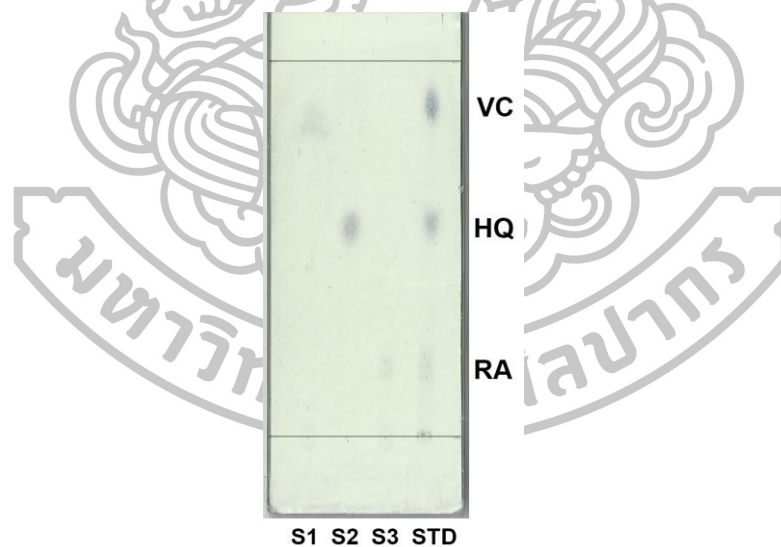


Figure 4.13 TLC results for the analysis of three different samples on mostly aligned CA nanofiber plates. S1 contained neither HQ nor RA whereas S2 and S3 were adulterated with HQ and RA, respectively. Standard (STD) RA, VC and HQ are in the right lane.

CHAPTER 5

CONCLUSIONS

In this study, three types of CA electrospun nanofibers arranged in random, semi-aligned and aligned nanofibers were fabricated and studied in two aspects i.e. drug release and TLC performance as follow:

5.1 Drug release from nanofibers with different degree of alignment

AR-loaded CA nanofibers were successfully prepared by electrospinning. An increasing rotation speed of drum collector resulted in the nanofibers with higher alignment. By using the different spin times at 5, 8 and 12 h, the random, semi-aligned and mostly aligned nanofibers had comparable weight per area of about 0.0025 g/cm^2 . The mechanical properties of three types of nanofibers were stretched in the perpendicular and parallel direction. The mostly aligned nanofiber mats had the lowest tensile strengths when they were stretched in the direction perpendicular to the fiber alignment, but they showed the highest tensile strength if they were pulled along the fiber alignment direction. No difference of tensile strength was observed for the randomly aligned nanofibers even they were pulled in the different directions. For semi-aligned nanofibers, this mechanical behavior was in between those of the random and mostly aligned nanofibers. In the first 10 min, the uptake of water into the fiber mats was rapid to reach the degree of swelling of 251%, 188% and 153% for random, semi-aligned and mostly aligned nanofibers, respectively. After 24 h, the random nanofibers were much fluffier than other types and nearly lost their original planar shape whereas the mostly aligned nanofibers well remained its appearance as the intact sheet. The amounts of AR in all types of samples were in the range of 2.7 – 2.8 % w/w, equivalent to the drug loading efficiencies of more than 90 %, demonstrating that most AR was successfully loaded into the nanofibers. The drug release from all types of nanofibers was revealed that the release of AR was rapid within 10 min and reached the maximum cumulative amounts at 84.0 - 86.1%. By the estimation, 80% of drug release was achieved in 1.7, 4.2 and 9.4 min for the mostly aligned, semi-aligned and random nanofibers, respectively. It can be concluded that

the drug release patterns during the initial burst period was significantly affected by the orientation of nanofibers.

5.2 TLC performance of nanofibers with different degree of alignment

Aligned CA electrospun nanofibers were successfully fabricated by using high speed rotating drum collector and applied to use as TLC media. Besides the efficient separation ability, the mostly aligned nanofibers with the appropriate layer thickness provided 2 – 3 times shorter run time than the randomly oriented ones. Furthermore, the masses of HQ and RA which could be detected on this material were 2 times lower than those on the random nanofibers and 5 times lower than those on typical silica gel plates as a result of more intense spots appearing on the nanofibers. In this work, the applicability of the mostly aligned CA nanofibers was also demonstrated in the screening of HQ and RA adulterated in cosmetics. Due to the satisfactory analytical performance as well as facile and inexpensive production process, mostly aligned CA electrospun nanofiber is promising stationary phase for use in planar chromatography.

It can be concluded that mostly aligned CA electrospun nanofiber is promising to use for the delivery of certain hydrophilic drugs in fast-release dosage forms. Moreover, it can also be applied to use as TLC stationary phase.



REFERENCES

- [1] Zheng-Ming Huang, et al. (2013). "A review on polymer nanofibers by electrospinning and their applications in nanocomposites." **Composites Science and Technology** 63, 15 (November): 2223-2253.
- [2] Rutledge, G. C., and S. V. Fridrikh. (2007). "Formation of fibers by electrospinning." **Advanced Drug Delivery Reviews** 59, 14 (December 10): 1384-1391.
- [3] Bhardwaj, N., and S. C. Kundu. (2010). "Electrospinning: a fascinating fiber fabrication technique." **Biotechnology Advances** 28, 3 (May-June): 325-347.
- [4] Wei Qian, et al. (2014). "Dual Drug Release Electrospun Core-Shell Nanofibers with Tunable Dose in the Second Phase." **International Journal of Molecular Sciences** 15, (January 8): 774-786.
- [5] Nagy, Zs. K., et al. (2010). "Electrospun water soluble polymer mat for ultrafast release of Donepezil HCl." **eXPRESS Polymer Letters** 4, 12: 763-772.
- [6] Clark, J. E., and S. V. Olesik. (2010). "Electrospun glassy carbon ultra-thin layer chromatography devices." **Journal of Chromatography A** 1217, 27 (July): 4655-4662.
- [7] Newsome, T. E., and S. V. Olesik. (2014). "Silica-based nanofibers for electrospun ultra-thin layer Chromatography." **Journal of Chromatography A** 1364, (October 17): 261-270.
- [8] Clark, J. E., and S. V. Olesik. (2009). "Technique for ultrathin layer chromatography using an electrospun, nanofibrous stationary phase." **Analytical Chemistry** 81, 10 (April 22): 4121-4129.
- [9] Beilke, M. C., et al. (2013). "Aligned electrospun nanofibers for ultra-thin layer chromatography." **Analytica Chimica Acta** 761, (January 25): 201-208.
- [10] Kampalanonwat, P., P. Supaphol, and G. E. Morlock. (2013). "Electrospun nanofiber layers with incorporated photoluminescence indicator for chromatography and detection of ultraviolet-active compounds." **Journal of Chromatography A** 1299, (July 19): 110-117.

- [11] Tian Lu, and S. V. Olesik. (2013). "Electrospun polyvinyl alcohol ultra-thin layer chromatography of amino acids." **Journal of Chromatography B** 912, (January 1): 98–104.
- [12] Rojanarata, T., et al. (2013). "Electrospun cellulose acetate nanofibers as thin layer chromatographic media for eco-friendly screening of steroids adulterated intraditional medicine and nutraceutical products." **Talanta** 115 (October 15): 208–213.
- [13] Xianfeng Wang, Bin Ding, and Bingyun Li. (2013). "Biomimetic electrospun nanofibrous structures for tissue engineering." **Materials Today** 16, 6 (June): 229-241.
- [14] Beason, D. P., et al. (2012). "Fiber-aligned polymer scaffolds for rotator cuff repair in a rat model." **Journal of Shoulder and Elbow Surgery** 21, 2 (February): 245-250.
- [15] Han Bing Wang, et al. (2010). "Varying the diameter of aligned electrospun fibers alters neurite outgrowth and Schwann cell migration." **Acta Biomaterialia** 6, 8 (August): 2970–2978.
- [16] Chigome, S., and N. Torto. (2011). "A review of opportunities for electrospun nanofibers in analytical chemistry." **Analytica Chimica Acta** 706, 1 (November 7): 25–36.
- [17] Puls, J., S. A. Wilson, and D. Holter. (2011). "Degradation of Cellulose Acetate-Based Materials: A Review." **Journal of Polymers and the Environment** 19, 1 (March): 152–165.
- [18] Ramakrishna, S., et al. (2005). "An Introduction to Electrospinning and Nanofibers.", **Singapore: World Scientific Publishing Co. Pte. Ltd.**
- [19] Dan Li, and Younan Xia. (2004). "Electrospinning of Nanofibers: Reinventing the Wheel?." **Advanced Materials** 16, 14 (July 19): 1151 - 1170.
- [20] Burger, C., B. S. Hsiao, and B. Chu. (2006). "Nanofibrous materials and their applications." **Annual Review of Materials Research** 36, (August): 333-368.
- [21] Anton, F., et al. (1934). "Process and apparatus for preparing artificial threads." **U.S. Patent** 1, 975, 504 Issue date: October 2.

- [22] Baumgarten, P. K. (1971). "Electrostatic spinning of acrylic microfibers." **Journal of Colloid and Interface Science** 36, 1 (May): 71-79.
- [23] Fong, H., and D. H. Reneker. (2001). "Electrospinning and formation of nanofibers." **Structure Formation in Polymeric Fibers**, Anonymous Munich: Carl Hanser, 225.
- [24] Reneker, D. H., and I. Chun. (1996). "Nanometre diameter fibres of polymer, produced by electrospinning." **Nanotechnology** 7, 3 (September): 216.
- [25] Dersch, R., A. Greiner, and J. H. Wendorff. (2009). "Polymer Nanofibers Prepared by Electrospinning." **Dekker Encyclopedia of Nanoscience and Nanotechnology**, (March 24): 3480.
- [26] Chronakis, I. S. (2005). "Novel nanocomposites and nanoceramics based on polymer nanofibers using electrospinning process - A review." **Journal of Materials Processing Technology** 167, 2-3 (August 30): 283-293.
- [27] Wan-Ju Li, R. L. Mauck, and R. S. Tuan. (2005). "Electrospun nanofibrous scaffolds: Production, characterization, and applications for tissue engineering and drug delivery." **Journal of Biomedical Nanotechnology** 1, 3 (August): 259-275.
- [28] Subbiah, T., et al. (2005). "Electrospinning of nanofibers." **Journal of Applied Polymer Science** 96, 557 - 569.
- [29] Jian Fang, et al. (2008). "Applications of electrospun nanofibers." **Chinese Science Bulletin** 53, 15 (August): 2265-2286.
- [30] Kumbar, S. G., et al. (2008). "Electrospun nanofiber scaffolds: engineering soft tissues." **Biomedical Materials** 3, 3 (September): 034002.
- [31] Tao Han, D. H. Reneker, and A. L. Yarin. (2007). "Buckling of jets in electrospinning." **Polymer** 48, 20 (September 21): 6064-6076.
- [32] Park, S., et al. (2007). "Apparatus for preparing electrospun nanofibers: designing an electrospinning process for nanofiber fabrication.", **Polymer International** 56, 11 (November): 1361-1366.
- [33] Baji, A., et al. (2010). "Electrospinning of polymer nanofibers: Effects on oriented morphology, structure and tensile properties." **Composites Science and Technology** 70, 5 (May): 703-718.

- [34] Reneker, D. H., and A. L. Yarin. (2008). "Electrospinning jets and polymer nanofibers." **Polymer** 49, 10 (May 13): 2387-2425.
- [35] Yarin, A. L., S. Koombhongse, and D. H. Reneker. (2001). "Bending instability in electrospinning of nanofibers." **Journal of Applied Physics** 89, 3018.
- [36] Taylor, G. (1969). "Electrically Driven Jets." **Proceedings of the Royal Society of London. A. Mathematical and Physical Sciences** 313, 1515 (December 2): 453-475.
- [37] Reneker, D. H., et al. (2000). "Bending instability of electrically charged liquid jets of polymer solutions in electrospinning." **Journal of Applied Physics** 87, 4531-4547.
- [38] Larrondo, L., and R. Mandley. (1981). "Electrostatic fiber spinning from polymers. II. Examination of the flow field in an electrically driven jet." **Journal of Polymer Science Part B: Polymer Physics** 19, 6 (June): 921-932.
- [39] Anton, F., et al. (1940). "Artificial thread and method of producing same." **U.S. Patent** 2, 187, 306 Issue date: January 16.
- [40] Greiner, A., and J. H. Wendorff. (2007). "Electrospinning: A Fascinating Method for the Preparation of Ultrathin Fibers" **Angewandte Chemie International Edition** 46, 30: 5670-5703.
- [41] Fridrikh, S. V., et al. (2003). "Controlling the Fiber Diameter during Electrospinning." **Physical Review Letters** 90, 14 (April 11): 144502.
- [42] Frenot, A., and I. S. Chronakis. (2003). "Polymer nanofibers assembled by electrospinning." **Current Opinion in Colloid & Interface Science** 8, 1 (March): 64-75.
- [43] Deitzel, J. M., et al. (2001). "The effect of processing variables on the morphology of electrospun nanofibers and textiles." **Polymer** 42, 1 (January): 261-272.
- [44] Doshi, J., and D. H. Reneker. (1995). "Electrospinning process and applications of electrospun fibers." **Journal of Electrostatics** 35, 2-3 (August): 151-160.

- [45] Fong, H., I. Chun, and D. H. Reneker. (1999). "Beaded nanofibers formed during electrospinning." **Polymer** 40, 16 (July): 4585-4592.
- [46] Hohman, M. M., et al. (2001). "Electrospinning and electrically forced jets. II. Applications." **Physics of Fluids** 13, 8 (August): 2221-2236.
- [47] Hayati, I., A. I. Bailey, and T. F. Tadros. (1987). "Investigations into the mechanisms of electrohydrodynamic spraying of liquids : I. Effect of electric field and the environment on pendant drops and factors affecting the formation of stable jets and atomization." **Journal of Colloid and Interface Science** 117, 1 (May): 205-221.
- [48] Xiaoyan Yuan, et al. (2004). "Morphology of ultrafine polysulfone fibers prepared by electrospinning." **Polymer International** 53, 11 (November): 1704-1710.
- [49] Yördem, O. S., M. Papila, and Y. Z. Menciloğlu. (2008). "Effects of electrospinning parameters on polyacrylonitrile nanofiber diameter: An investigation by response surface methodology." **Materials & Design** 29, 1: 34-44.
- [50] Deitzel, J. M., et al. (2002). "Electrospinning of polymer nanofibers with specific surface chemistry." **Polymer** 43, 3 (February): 1025-1029.
- [51] Bognitzki, M., et al. (2000). "Polymer, Metal, and Hybrid Nano- and Mesotubes by Coating Degradable Polymer Template Fibers (TUFT Process)." **Advanced Materials** 12, 9 (May): 637 - 640.
- [52] Teo, W. E. (2006). "A review on electrospinning design and nanofibre assemblies." **Nanotechnology** 17, 14 (June 30): R89.
- [53] Swart, M. (2007). "Synthesis and characterization of electrospun organic-inorganic hybrid graft copolymer nanofibers of poly(methyl methacrylate) and polydimethylsiloxane." MSc dissertation, Chemistry and Polymer Science, University of Stellenbosch.
- [54] Lee, K. Y., et al. (2009). "Electrospinning of polysaccharides for regenerative medicine." **Advance Drug Delivery Reviews** 61, 12 (October 5): 1020-1032.

- [55] Lifeng Zhang, T. J. Menkhaus, and Hao Fong. (2008). "Fabrication and bioseparation studies of adsorptive membranes/felts made from electrospun cellulose acetate nanofibers." **Journal of Membrane Science** 319, 1-2 (July 1): 176–184.
- [56] Kim, C., et al. (2005). "Preparation of submicron-scale, electrospun cellulose fiber via direct dissolution." **Journal of Polymer Science Part B: Polymer Physics** 43, 13 (July 1): 1673–1683.
- [57] Kim, C., et al. (2006). "Structural studies of electrospun cellulose nanofibers." **POLYMER** 47, 14 (June 28): 5097-5107.
- [58] Kulpinski, P. (2005). "Cellulose nanofibers prepared by the N-methylmorpholine-N-oxide method." **Journal of Applied Polymer Science** 98, 4 (November 15): 1473–1482.
- [59] Han, S. O., et al. (2008). "Electrospinning of ultrafine cellulose fibers and fabrication of poly(butylene succinate) biocomposites reinforced by them." **Journal of Applied Polymer Science** 107, 3 (February 5): 1954–1959.
- [60] Tungprapa, S., et al. (2007). "Electrospun cellulose acetate fibers: effect of solvent system on morphology and fiber diameter." **CELLULOSE** 14, 6 (December): 563–575.
- [61] Jarusuwannapoom, T., et al. (2005). "Effect of solvents on electro-spinnability of polystyrene solutions and morphological appearance of resulting electrospun polystyrene fibers." **European Polymer Journal** 41, 3 (March): 409–421.
- [62] Pattamaprom, C., et al. (2006). "The influence of solvent properties and functionality on the electrospinnability of polystyrene nanofibers." **Macromolecular Materials and Engineering** 291, 7 (July 14): 840–847.
- [63] Sundaray, B., et al. (2004). "Electrospinning of continuous aligned polymer fibers." **Applied Physics Letters** 84, 1222-1224.
- [64] Katta, P., et al. (2004). "Continuous Electrospinning of Aligned Polymer Nanofibers onto a Wire Drum Collector." **Nano Letters** 4, 11 (September 28): 2215-2218.

- [65] Theron, A. (2001). "Electrostatic field-assisted alignment of electrospun nanofibres." **Nanotechnology** 12, (August 28): 384.
- [66] Pokorny, M., K. Niedoba, and V. Velebny. (2010). "Transversal electrostatic strength of patterned collector affecting alignment of electrospun nanofibers." **Applied Physics Letters** 96, 193111.
- [67] Jaeger, R., et al. (1998). "Electrospinning of ultra-thin polymer fibers." **Macromolecular Symposia** 127, 1 (February): 141-150.
- [68] Kim, G. H. (2006). "Electrospinning process using field-controllable electrodes." **Journal of Polymer Science Part B: Polymer Physics** 44, 10 (May 15): 1426-1433.
- [69] Buttafoco, L., et al. (2006). "Electrospinning of collagen and elastin for tissue engineering applications." **Biomaterials** 27, 5 (February): 724-734.
- [70] Dan Li, Yuliang Wang, and Younan Xia. (2004). "Electrospinning Nanofibers as Uniaxially Aligned Arrays and Layer-by-Layer Stacked Films." **Advance Materials** 16, 4 (February): 361-366.
- [71] Dan Li, Yuliang Wang, and Younan Xia. (2003). "Electrospinning of Polymeric and Ceramic Nanofibers as Uniaxially Aligned Arrays." **Nano Letters** 3, 8 (July 8): 1167-1171.
- [72] Lihua L., and Y. A. Dzenis. (2008). "Analysis of the effects of the residual charge and gap size on electrospun nanofiber alignment in a gap method." **Nanotechnology** 19, 35 (September 3): 355307.
- [73] Jalili, R., M. Morshed and S. A. H. Ravandi. (2006). "Fundamental parameters affecting electrospinning of PAN nanofibers as uniaxially aligned fibers." **Journal of Applied Polymer Science** 101, 6 (September 15): 4350-4357.
- [74] Dayong Yang, et al. (2007). "Fabrication of Aligned Fibrous Arrays by Magnetic Electrospinning." **Advance Materials** 19, 21 (November): 3702-3706.
- [75] Yaqing Liu, et al. (2010). "Magnetic field-assisted electrospinning of aligned straight and wavy polymeric nanofibers." **Advance Materials** 22, 22 (June 11): 2454-2457.

- [76] Rošic, R., et al. (2012). "Properties, engineering and applications of polymeric nanofibers: current research and future advances." **Chemical and Biochemical Engineering Quarterly** 26, 4 (December): 417–425.
- [77] Leung, V., and F. Ko. (2011). "Biomedical applications of nanofibers." **Polymers for Advanced Technologies** 22, 3 (March): 350-365.
- [78] Rathinamoorthy, R. (2012). "Nanofiber for drug delivery system – principle and application." **Pakistan Textile Journal** 61, (February): 45-48.
- [79] Taepaiboon, P., U. Rungsardthong, and P. Supaphol. (2007). "Vitamin-loaded electrospun cellulose acetate nanofiber mats as transdermal and dermal therapeutic agents of vitamin A acid and vitamin E." **European Journal of Pharmaceutics and Biopharmaceutics** 67, 2 (September): 387-397.
- [80] Suwantong, O., et al. (2007). "Electrospun cellulose acetate fiber mats containing curcumin and release characteristic of the herbal substance." **Polymer** 48, 26 (December 13): 7546-7557.
- [81] Tuangprapa, S., et al. (2007). "Release characteristics of four model drugs from drug-loaded electrospun cellulose acetate fiber mats." **Polymer** 48, 17 (August 10): 5030-5041.
- [82] Zhuoxian Meng, et al. (2011). "Preparation and characterization of electrospun PLGA/gelatin nanofibers as a potential drug delivery system." **Colloids and Surfaces B: Biointerfaces** 84, 1 (May 1): 97-102.
- [83] Zhuoxian Meng, et al. (2011). "Fabrication, characterization and in vitro drug release behavior of electrospun PLGA/chitosan nanofibrous scaffold." **Materials Chemistry and Physics** 125, 3 (February 15): 606-611.
- [84] Zweig, G., and J. Sherma. (1976). "Paper and thin layer chromatography.", **Analytical Chemistry** 48, 5 (April): 66R-83R.
- [85] Lee, C. H., et al. (2005). "Nanofiber alignment and direction of mechanical strain affect the ECM production of human ACL fibroblast." **Biomaterials** 26, 11 (April): 1261-1270.

- [86] Chenwen Li, et al. (2013). "Silver nanoparticle/chitosan oligosaccharide/poly(vinyl alcohol) nanofibers as wound dressings: a preclinical study." **International Journal of Nanomedicine** 8, 1 (November 1): 4131-4145.
- [87] Xinhua Zong, et al. (2002). "Structure and process relationship of electrospun bioabsorbable nanofiber membranes." **Polymer** 43, 16 (July): 4403-4412.
- [88] Baji, A., et al. (2010). "Electrospinning of polymer nanofibers : Effects on oriented morphology, structure and tensile properties." **Composites Science and Technology** 70, 5 (May): 703-718.
- [89] Prabhakaran, M. P., L. Ghasemi-Mobarakeh, and S. Ramakrishna. (2011). "Electrospun composite nanofibers for tissue regeneration." **Journal of Nanoscience and Nanotechnology** 11, 4 (April): 3039-3057.
- [90] Choi, J. S., et al. (2008). "The influence of electrospun aligned poly(epsilon-caprolactone)/collagen nanofiber meshes on the formation of self-aligned skeletal muscle myotubes." **Biomaterials** 29, 19 (July): 2899-2906.
- [91] Xu He, et al. (2014). "Uniaxially Aligned Electrospun All-Cellulose Nanocomposite Nanofibers Reinforced with Cellulose Nanocrystals: Scaffold for Tissue Engineering." **Biomacromolecules** 15, 2: 618-627.
- [92] Prabhu, K., et al. (2011). "Isolation and spectral identification of arbutin from the roots of viburnum erubescens wall.ex.dc." **International Journal of Research in Ayurveda and Pharmacy** 2, 3: 889-892.
- [93] Subramanian, A., U. M. Krishnan, and S. Sethuraman. (2011). "Fabrication of uniaxially aligned 3D electrospun scaffolds for neural regeneration." **Biomedical Materials** 6, 2 (April): 025004.
- [94] Association of Southeast Asian Nation. (2005). **Identification and determination of hydroquinone in cosmetic products by TLC and HPLC.** Accessed 2014 January 8. Available from <http://www.asean.org/archive/MRA-Cosmetic/Doc-4.pdf>.
- [95] Association of Southeast Asian Nation. (2005). **Identification and determination of Retinoic acid (Tretinoin) in cosmetic products by**

TLC and HPLC. Accessed 2014 January 8. Available from <http://www.asean.org/archive/MRA-Cosmetic/Doc-1.pdf>







Table A.1 The diameter data of AR-loaded nanofibers (n = 50).

Random nanofibers	Semi-aligned nanofibers	Mostly aligned nanofibers
667.0819	667.0819	660.3774
596.6562	596.6562	566.0377
660.3774	573.8455	667.0819
632.8494	596.6562	573.8455
596.6562	573.8455	660.3774
604.0683	660.3774	667.0819
686.8028	573.8455	667.0819
680.2927	680.2927	680.2927
573.8455	632.8494	660.3774
550.0898	566.0377	632.8494
680.2927	660.3774	566.0377
667.0819	680.2927	667.0819
667.0819	680.2927	667.0819
660.3774	596.6562	566.0377
596.6562	667.0819	596.6562
632.8494	632.8494	680.2927
660.3774	573.8455	604.0683
604.0683	596.6562	667.0819
632.8494	596.6562	573.8455
596.6562	596.6562	660.3774
596.6562	566.0377	660.3774
596.6562	632.8494	632.8494
632.8494	604.0683	660.3774
632.8494	632.8494	573.8455
604.0683	573.8455	573.8455
680.2927	660.3774	660.3774
550.0898	604.0683	632.8494

Table A.1 The diameter data of AR-loaded nanofibers (n = 50) (continued).

Random nanofibers	Semi-aligned nanofibers	Mostly aligned nanofibers	
680.2927	604.0683	596.6562	
573.8455	604.0683	604.0683	
667.0819	596.6562	566.0377	
667.0819	667.0819	667.0819	
604.0683	596.6562	573.8455	
573.8455	680.2927	573.8455	
632.8494	604.0683	660.3774	
667.0819	596.6562	566.0377	
660.3774	573.8455	632.8494	
533.6655	680.2927	632.8494	
660.3774	667.0819	573.8455	
667.0819	566.0377	566.0377	
632.8494	596.6562	667.0819	
533.6655	632.8494	596.6562	
604.0683	604.0683	604.0683	
604.0683	632.8494	680.2927	
604.0683	632.8494	573.8455	
660.3774	573.8455	660.3774	
573.8455	680.2927	596.6562	
604.0683	566.0377	566.0377	
596.6562	604.0683	596.6562	
632.8494	596.6562	566.0377	
632.8494	604.0683	596.6562	
624.1498	616.7599	619.9277	Average
41.3979	38.0075	42.4999	Standard deviation

Table A.2 Layer thickness data of AR-loaded nanofibers (n = 10).

	Random nanofibers	Semi-aligned nanofibers	Mostly aligned nanofibers
	55.73	46.22	47.51
	53.17	48.80	45.59
	53.86	48.74	43.06
	55.71	46.24	41.79
	53.17	49.38	41.18
	54.43	49.40	39.25
	52.57	46.87	36.71
	55.06	46.84	38.61
	52.55	46.24	39.29
	53.80	48.11	45.64
Average	54.00	47.68	41.86
Standard deviation	1.19	1.34	3.54
	54.00 ± 1.19	47.68 ± 1.34	41.86 ± 3.54

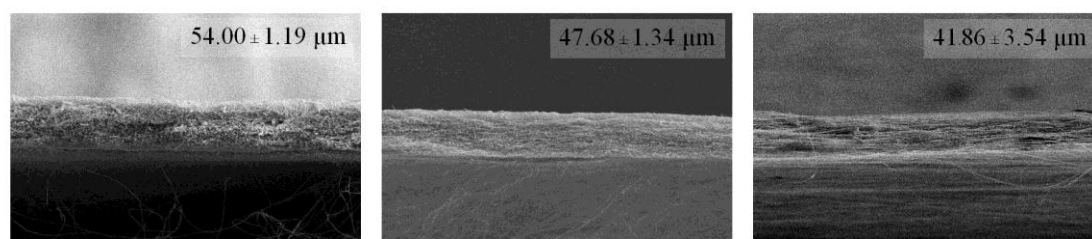


Figure A.1 Layer thickness of (a) random nanofibers, (b) semi-aligned nanofibers and (c) mostly aligned nanofibers.

Table A.3 Tensile strength (N/mm²) data of AR-loaded nanofibers (n = 5).

	Tensile strength (N/mm ²)	Tensile average	Standard deviation
Random nanofibers	14.04	19.00	3.19
(parallel)	20.01		
	22.83		
	18.53		
	19.58		
Random nanofibers	20.22	18.21	2.61
(perpendicular)	15.85		
	16.24		
	21.72		
	17.02		
Semi-aligned nanofibers	72.58	70.09	9.46
(parallel)	83.47		
	59.89		
	72.37		
	62.14		
Semi-aligned nanofibers	10.26	14.41	3.67
(perpendicular)	14.78		
	20.26		
	13.03		
	13.74		
Mostly aligned nanofibers	209.34	226.61	18.02
(parallel)	220.12		
	214.84		
	234.61		
	254.11		

Table A.3 Tensile strength (N/mm^2) data of AR-loaded nanofibers ($n = 5$) (continued).

	Tensile strength (N/mm^2)	Tensile average	Standard deviation
Mostly aligned nanofibers	7.87	8.27	0.95
(perpendicular)	9.85		
	7.35		
	7.99		
	8.30		



Table A.4 The % degree of swelling data in first 10 min of AR-loaded nanofibers.

	Time (min)	% degree of swelling	Standard deviation
Random nanofibers	1	144.00	17.92
	2	150.00	34.39
	4	170.00	19.48
	10	250.00	16.83
Semi-aligned nanofibers	1	122.00	17.54
	2	128.00	14.11
	4	133.00	12.95
	10	190.00	13.50
Mostly aligned nanofibers	1	107.00	17.64
	2	113.00	21.26
	4	115.00	28.50
	10	150.00	12.50

Table A.5 The % degree of swelling and % weight loss data in 24 h of AR-loaded nanofibers.

		% degree of swelling	Standard deviation	% weight loss	Standard deviation
Random nanofibers	24 h	381.07	0.22	8.25	0.01
Semi-aligned nanofibers		270.50	0.56	8.25	0.01
Mostly aligned nanofibers		202.70	0.13	8.00	0.00

Table A.6 Cumulative release (%) of AR release from 3% wt AR-loaded random nanofibers.

Random nanofibers (Actual Average)				
Time (min)	n = 1	n = 2	n = 3	% Cumulative release average
0	0	0	0	0
0.25	3.8616	8.2037	9.1999	7.0884
0.5	11.8461	23.0915	13.9104	16.2827
0.75	20.8937	29.6557	17.3237	22.6244
1	26.8353	38.3512	25.3355	30.1740
3	60.0897	61.8541	50.7853	57.5764
5	75.9275	78.7471	63.2713	72.6486
7	80.0571	82.2585	69.6117	77.3091
10	82.2421	85.1753	73.7234	80.3803
20	83.4486	85.8972	76.5322	81.9594
30	83.4222	85.7521	76.2528	81.8090
45	83.4687	85.6106	76.3020	81.7937
60	83.3542	85.7267	76.1701	81.7503
90	83.4970	85.8361	76.3372	81.8901

Table A.7 Cumulative release (%) of AR release from 3% wt AR-loaded semi-aligned nanofibers.

Semi-aligned nanofibers (Actual Average)				
Time (min)	n = 1	n = 2	n = 3	% Cumulative release average
0	0	0	0	0
0.25	7.4329	11.8386	10.8592	10.0436
0.5	28.5252	29.6016	28.6691	28.9320
0.75	43.6067	46.5546	45.2464	45.1359
1	52.8360	57.0490	53.8970	54.5940
3	71.9548	76.0066	77.1424	75.0346
5	81.9946	84.6436	83.5101	83.3827
7	84.8320	85.6296	85.2071	85.2229
10	85.8724	85.7779	85.7466	85.7990
20	85.8919	86.6942	85.6476	86.0779
30	85.8033	86.2920	85.8564	85.9839
45	85.4327	86.2462	85.7792	85.8194
60	86.0286	86.5185	85.7750	86.1074
90	86.1059	86.3775	85.8255	86.1030

Table A.8 Cumulative release (%) of AR release from 3% wt AR-loaded aligned nanofibers.

Mostly aligned nanofibers (Actual Average)				
Time (min)	n = 1	n = 2	n = 3	% Cumulative release average
0	0	0	0	0
0.25	20.7485	21.3961	20.4706	20.8717
0.5	53.3250	53.6568	51.5330	52.8383
0.75	71.2756	70.7855	67.0845	69.7152
1	76.6461	79.6507	74.8019	77.0329
3	85.4544	87.8596	80.1635	84.4925
5	86.3085	89.6205	82.0801	86.0030
7	86.3045	89.5596	82.0974	85.9872
10	86.5250	89.3282	82.0115	85.9549
20	86.2613	88.9140	82.0143	85.7299
30	86.0834	89.9973	81.8200	85.9669
45	85.6609	89.5707	81.8189	85.6835
60	85.7990	89.4851	81.8004	85.6948
90	86.2512	89.6629	81.6094	85.8412

Table A.9 Cumulative release (%) average of AR release from 3% wt AR-loaded nanofibers.

Actual content			
	Random nanofibers	Semi-aligned nanofibers	Mostly aligned nanofibers
Time (min)	% Cumulative release average	% Cumulative release average	% Cumulative release average
0	0	0	0
0.25	7.088403558	10.04355512	20.87170239
0.5	16.28268353	28.93196179	52.83829147
0.75	22.62437834	45.13588164	69.71517927
1	30.17400793	54.59402839	77.03289566
3	57.57637250	75.03458484	84.49250442
5	72.64864034	83.38274662	86.00303778
7	77.30909006	85.22286684	85.98717379
10	80.38026908	85.79898622	85.95489133
20	81.95935286	86.07790068	85.72987832
30	81.80900330	85.98389153	85.96687265
45	81.79374325	85.81937099	85.68347678
60	81.75033025	86.10739045	85.69482296
90	81.89007891	86.10297619	85.84116148

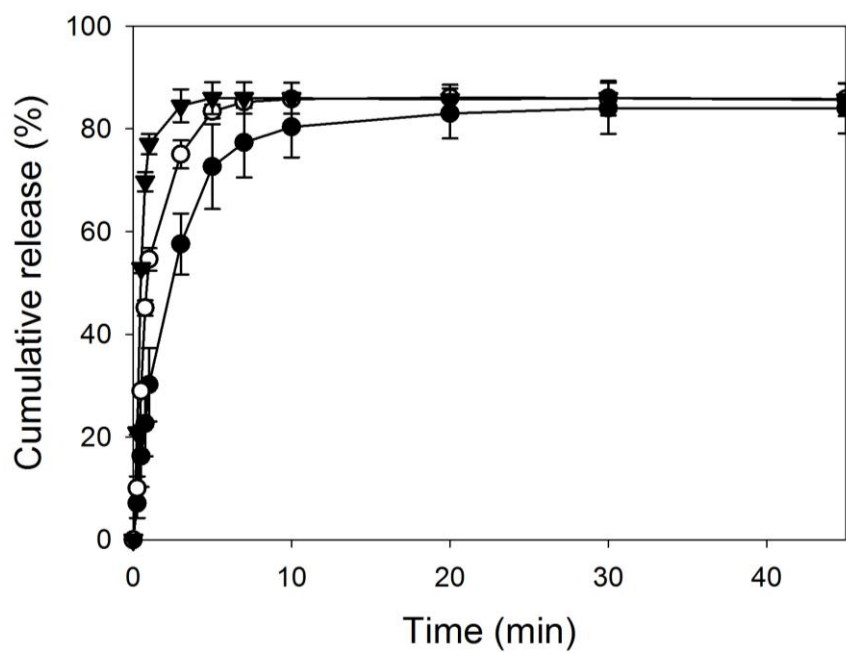


Figure A.2 Percent cumulative release of AR from nanofibers; (\blacktriangledown) mostly aligned, (\circ) semi-aligned, (\bullet) random nanofibers ($n = 3$) in 90 min.

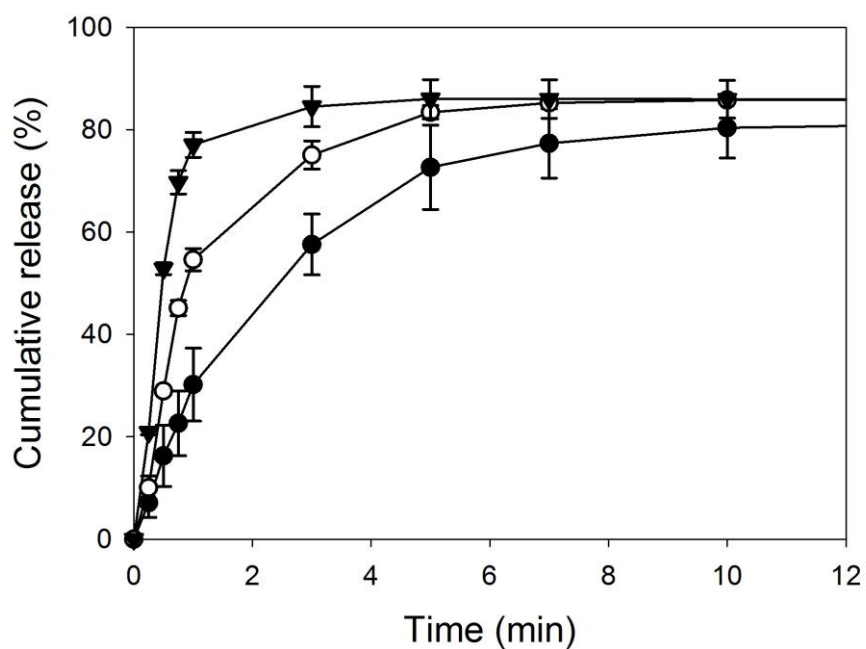
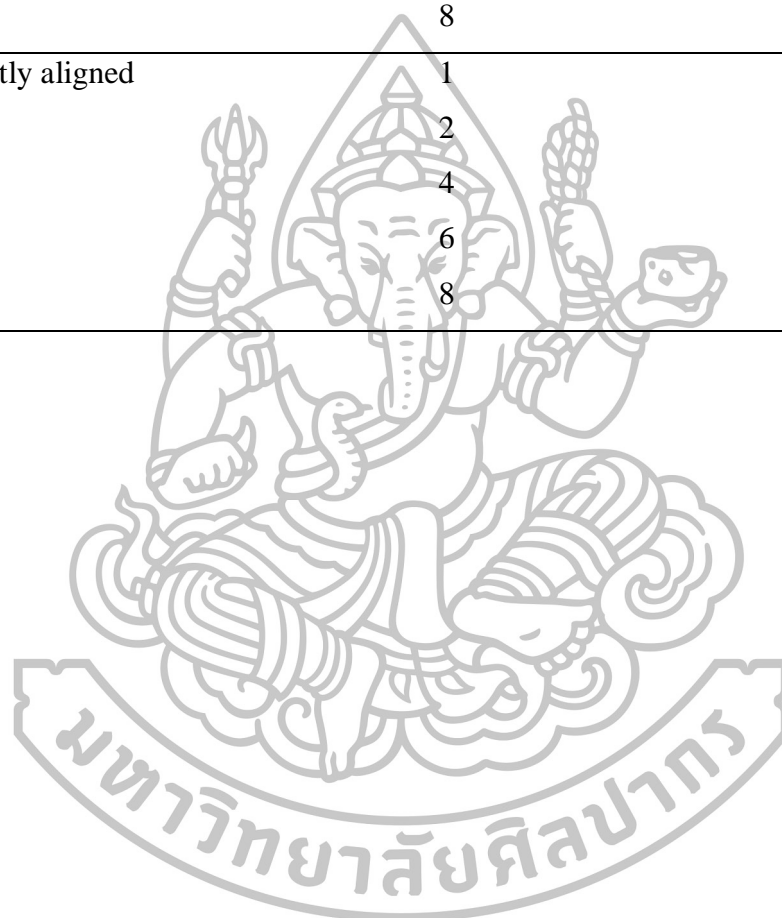


Figure A.3 Percent cumulative release of AR from nanofibers; (\blacktriangledown) mostly aligned, (\circ) semi-aligned, (\bullet) random nanofibers ($n = 3$) in first 10 min.

Table A.10 Layer thickness data of nanofibers in TLC application (n=10).

	Spin time (h)	Line length (μm)
Random	1	12.3585
	2	15.1887
	4	26.5094
	6	35.0943
	8	38.0189
Mostly aligned	1	4.0566
	2	8.9623
	4	9.6262
	6	12.9960
	8	20.8411





APPENDIX B



Uniaxially aligned electrospun cellulose acetate nanofibers for thin layer chromatographic screening of hydroquinone and retinoic acid adulterated in cosmetics



Siripran Tidjarat, Weerapath Winotapun, Praneet Opanasopit, Tanasait Ngawhirunpat, Theerasak Rojanarata*

Pharmaceutical Development of Green Innovations Group (PDGG), Faculty of Pharmacy, Silpakorn University, Nakhon Pathom 73000, Thailand

ARTICLE INFO

Article history:
Received 24 July 2014
Received in revised form
17 September 2014
Accepted 18 September 2014
Available online 28 September 2014

Keywords:
Uniaxially aligned
Nanofibers
Electrospinning
Cellulose acetate
TLC

ABSTRACT

Uniaxially aligned cellulose acetate (CA) nanofibers were successfully fabricated by electrospinning and applied to use as stationary phase for thin layer chromatography. The control of alignment was achieved by using a drum collector rotating at a high speed of 6000 rpm. Spin time of 6 h was used to produce the fiber thickness of about 10 μm which was adequate for good separation. Without any chemical modification after the electrospinning process, CA nanofibers could be readily devised for screening hydroquinone (HQ) and retinoic acid (RA) adulterated in cosmetics using the mobile phase consisting of 65:35:2.5 methanol/water/acetic acid. It was found that the separation run on the aligned nanofibers over a distance of 5 cm took less than 15 min which was two to three times faster than that on the non-aligned ones. On the aligned nanofibers, the masses of HQ and RA which could be visualized were 10 and 25 ng, respectively, which were two times lower than those on the non-aligned CA fibers and five times lower than those on conventional silica plates due to the appearance of darker and sharper of spots on the aligned nanofibers. Furthermore, the proposed method efficiently resolved HQ from RA and ingredients commonly found in cosmetic creams. Due to the satisfactory analytical performance, facile and inexpensive production process, uniaxially aligned electrospun CA nanofibers are promising alternative media for planar chromatography.

© 2014 Elsevier B.V. All rights reserved.

1. Introduction

Electrospinning is a facile, robust and versatile technique for the fabrication of nanofibers for laboratory and industrial use. In this process, polymer liquid, i.e. solution or melt, loaded in a syringe is charged by a high voltage. Once the electrostatic force overcomes the surface tension on the polymer droplet, the liquid is ejected from the nozzle tip towards the grounded collector while solvent evaporates or melt solidifies. This phenomenon results in the formation of extremely small fibers with high surface area, high porosity and controllable compositions and size. Taking advantages of these features, electrospun nanofibers are attractive for a wide array of applications ranging from filtration, medical wound

dressings, tissue engineering, drug delivery and so on [1]. So far, nanofibers electrospun by conventional methods are collected as nonwoven layers with randomly arranged structures. Later, aligned nanofibers can be produced through different means e.g. by using high speed rotating mandrel, electrostatic metallic staple and a pair of permanent magnets [2]. It is known that, for some applications, an ordered structure such as uniaxially or radially aligned nanofiber is more desirable. For instance, uniaxially aligned nanofibers with anisotropic properties has been shown to satisfy electrical, optical and mechanical purposes [3–5]. In addition, the aligned nanofiber scaffolds used in cell culture and tissue engineering not only mimic the parallel structure of fibrous tissues e.g. collagen in tendon or nerve, but also promote the migration and extension of cells [6,7].

In analytical chemistry, electrospun nanofibers have been currently applied to electrochemical and optical based detection systems, solid phase extraction and membrane separation [8]. Besides, electrospinning has recently become a new route to produce stationary phase for thin layer chromatography (TLC). There have been the reports about the fabrication and use of electrospun nanofibers as TLC stationary phase for the separation of amino

* Corresponding author at: Department of Pharmaceutical Chemistry and Pharmaceutical Development of Green Innovations Group (PDGG), Faculty of Pharmacy, Silpakorn University, Nakhon Pathom 73000, Thailand. Tel.: +66 34 255800; fax: +66 34 255801.

E-mail addresses: ttheerasak@yahoo.com, teerasak@su.ac.th (T. Rojanarata).

acids, laser dyes, steroidal compounds and food preservatives. However, the polymers used for the fabrication were limited to glassy carbon [9], polyacrylonitrile (PAN) [10–12], polyvinyl alcohol (PVA) [13] and cellulose acetate (CA) [14]. In other aspects, electrospun nanofiber layers were improved for the detection of ultraviolet-active compounds by incorporation of photoluminescence indicator and were hyphenated with electrospray-ionization mass spectrometry [12]. Concerning the aligned electrospun nanofibers, Olesik et al. reported the use of aligned PAN nanofibers to separate a mixture of β -blockers and steroidal compounds. Compared to those with random orientation, the aligned nanofibers improved reproducibility and separation efficiency as well as shortened run time [11]. The alignment of PAN nanofibers was also observed in the work done by Kampalanonwat et al. However, in that study the delicate investigation aimed to control the alignment such as the optimization of rotating speed of drum collector has not yet been conducted [12]. These reported performance enhancements motivate further pursuit of new electrospun TLC materials.

CA is an environmentally degradable material made from the most abundant biopolymer on earth i.e. cellulose [15]. It is much cheaper than some synthetic polymers such as PAN. In addition, nanofibers made from CA can be readily used after electrospinning process for TLC without additional steps such as pyrolysis or chemical crosslinking which are usually required for the fabrication of glassy carbon and PVA nanofibers, respectively. Recently, TLC plates made from non-aligned CA nanofibers have been prepared and used with eco-friendlier hydro-alcoholic mobile phases for the analysis of prohibited steroids in traditional medicines [14]. However, no reports related to the fabrication of aligned CA nanofibers used for TLC have been available.

The present study extends this work by optimizing drum collector rotation speed and spin time to produce new reversed-phase TLC plates with uniaxially aligned CA nanofibers. TLC performance of the aligned nanofibers was compared to that of non-aligned ones as well as commercially available silica based plates. Finally, their application was demonstrated by using them for screening hydroquinone (HQ) and retinoic acid (RA) adulterated in cosmetic creams since both of them are prohibited substances for use in cosmetics in many countries due to the side effects including scaling of skin, stinging, flushing and ochronosis [16,17]. From the study, the aligned CA nanofibers were proven to be the efficient TLC media for resolving the analytes within a shorter run time. Furthermore, this work reports for the first time about the advantage of aligned nanofibers over the non-aligned ones in the term of the lower mass of the analyte which could be visualized on the plates.

2. Materials and methods

2.1. Materials

Cellulose acetate (CA; $M_w = 30$ kDa; degree of acetylation ≈ 2.4), hydroquinone (HQ; purity $\geq 99.0\%$), retinoic acid (RA; purity $\geq 98.0\%$), vitamin C (VC; purity $\geq 99.0\%$), vitamin E (purity $\geq 96.0\%$), resorcinol (RS; purity $\geq 99.0\%$), α -arbutin (AR; purity $\geq 98.0\%$), sodium metabisulfite (purity $\geq 98.0\%$) and phosphomolybdic acid were purchased from Sigma–Aldrich, St. Louis, MO. Solvents used in this study i.e. *N,N*-dimethylacetamide (Labscan, Thailand; purity $\geq 99.5\%$), acetone (Carlo, Italy; purity $\geq 99.5\%$), glacial acetic acid (Merck, Germany; purity $\geq 99.8\%$), hexane (Merck, Germany; purity $\geq 99.0\%$), methanol and ethanol (Merck, Germany; purity $\geq 99.9\%$) were of analytical grade. Distilled water was used throughout the experiments. Commercial TLC plates i.e. silica gel 60 and silica gel 60 RP-18 plates (particle size of 10–12 μm , layer thickness of 200 μm on aluminum backing) were purchased from Merck. Cosmetic cream samples

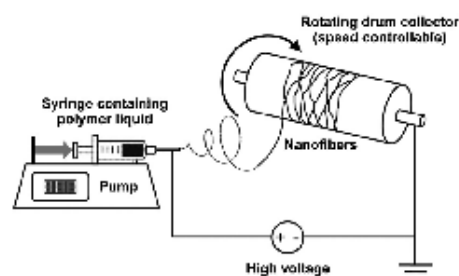


Fig. 1. Setup of electrospinning instrumentation for fabrication of nanofibers.

were collected from local markets in Nakhon Pathom province, Thailand, during January–March 2014.

2.2. Fabrication and characterization of electrospun CA nanofibers

2.2.1. Electrospinning of CA nanofibers

Initially, 17% (w/v) CA solution was prepared by dissolving 1.02 g of CA powder in 6 mL of 2:1 (v/v) acetone/*N,N*-dimethylacetamide at room temperature (30 °C). Then, 5 mL of the solution was loaded into a glass syringe equipped with a blunted stainless steel needle (diameter ≈ 0.9 mm) attached to a pump (Fig. 1). Electrospinning was performed by ejecting CA solution from the needle tip at the feeding rate of 0.4 mL h^{-1} towards the rotating drum which functioned as a grounded collector under the electric field using electrical potential of 17.5 kV from a high voltage supply. The distance between the needle tip and the aluminum foil (standard household quality with the thickness of about 15 μm) that was wrapped around the drum (circumference ≈ 19 cm) was 15 cm. To fabricate vertically aligned nanofibers, the drum was set to rotate at different high speeds (4500, 6000 and 7500 rpm) and the nanofibers were collected at different spin times (1, 2, 4, 6, and 8 h). Non-aligned nanofibers were prepared in a similar way except that the drum rotation speed was 350 rpm. After electrospinning, the aluminum foil containing CA nanofiber layer was removed from the collector and cut into rectangular shape (7.5 \times 2.5 cm^2) by selecting the area with the uniform thickness. The cut foil was then fixed onto the glass backing using double sided adhesive tape to produce CA nanofiber plate which was ready to use for TLC separation. It should be noted that this fixation is limited with regard to solvent resistance; thereby the use of thicker foils can be an option to avoid the tape.

2.2.2. Characterization of CA nanofibers

To observe the effect of drum rotation speed and spin time on the morphology and alignment, electrospun CA nanofibers fabricated under different conditions were subjected to scanning electron microscopy (SEM) (Camscan, MX-2000). The specimens for SEM were prepared by coating nanofibers with thin layer of gold (thickness ≈ 150 Å) by using sputtering device. The diameters of fibers and the thickness of layers were measured directly from SEM images ($n = 50$), using the image analysis software (JMicroVision V.1.2.7, University of Geneva, Geneva, Switzerland). The alignment of nanofibers was assessed as the number of fibers oriented in a determined direction with respect to a vertical reference line (0° angles). The angles from which individual fibers were deviated from this line were determined ($n = 50$) and then plotted as a function of frequency in a histogram. The narrow distribution of nanofiber angles indicated more alignment.

2.3. TLC screening method for HQ and RA

2.3.1. Preparation of standard and sample solutions

The standard solutions containing 0.125 mg mL^{-1} HQ and 0.67 mg mL^{-1} RA were freshly prepared in absolute ethanol. Cosmetic creams were extracted prior to TLC analysis following ASEAN guidelines [18,19]. Briefly, 1 mL of ethanol was added to 0.5 g of sample in a microcentrifuge tube. The mixture was then mixed and sonicated for 10 min to improve the dissolution and the release of HQ and RA from sample matrix. Subsequently, it was put on ice until the separation of wax occurred, centrifuged and the clear supernatant was finally collected for TLC. Since the adulteration level might vary among the collected samples, some extracts were further evaporated under nitrogen gas at room temperature to increase the concentration of target analytes for 2–10 folds.

2.3.2. TLC procedures

For general protocol, the separation of HQ and RA on electrospun CA nanofiber plate was carried out by manually spotting $0.5 \mu\text{L}$ of standard solutions of HQ and RA and sample solutions side by side, 1 cm from the bottom edge with the aid of calibrated micropipette and tips. The plate was then developed vertically in a closed chamber containing mobile phase (methanol/water/acetic acid) which was previously saturated at 30°C for 30 min. The mobile phase was allowed to migrate for a distance of 5 cm from the start. Subsequently, the plate was removed from the chamber and air-dried. The spots of HQ and RA were detected by spraying the plate with 5% (w/v) phosphomolybdic acid solution in ethanol following the ASEAN guidelines [18,19] and blowing with hot air (95°C) from hair dryer at 5 cm distance from the plate for 2.5 min. Alternatively, the plate might be incubated in hot air oven set at 95°C for 2.5 min. HQ and RA were directly visualized as grey spots under visible light. For comparison purposes, TLC was also run on two types of commercial plates i.e. silica gel 60 and silica gel 60 RP-18 plates using the same procedures, except that the volume of solutions spotted on the plate was increased to $2 \mu\text{L}$.

To investigate the optimal mobile phase, the solvents consisting of methanol and water at various ratios in the presence of 2.5% acetic acid were tested. The separation quality was evaluated from R_f values, the resolution between HQ and RA spots and the spot shape. In addition, the chromatographic performance of aligned and non-aligned CA nanofibers was compared in the aspects of run time, migration constant as calculated from $(\text{migration distance})^2/\text{time}$ and size of spot appeared on the plates. For this purpose, the images of the TLC plates ($n=4$) were captured by a scanner (HP Deskjet 1050, Hewlett Packard, China) at a resolution of 300 dpi and saved as TIF files. The image was then opened with Photoshop CS2 software (Adobe System, Mountain View, CA, USA). The mode of color was changed to grayscale and the threshold level was adjusted to 220. The area of spot was measured as pixels by using Magic Wand Tool and Histogram.

2.3.3. Method validation

The masses of HQ and RA which could be visualized on aligned and non-aligned CA electrospun nanofibers as well as commercial silica-based plates were determined by spotting series of standard solutions of HQ and RA on the plates to obtain 5, 10, 20, 40, 80 ng of HQ and 25, 50, 100, 200, 400 ng of RA. The specificity was validated by examining the interference effects from the ingredients commonly used in cosmetic creams i.e. VC, RS, AR, vitamin E and sodium metabisulfite. Finally, the analytical results obtained from TLC method run on the aligned CA nanofiber plates were verified by the confirmatory HPLC method according to ASEAN guidelines [18,19].

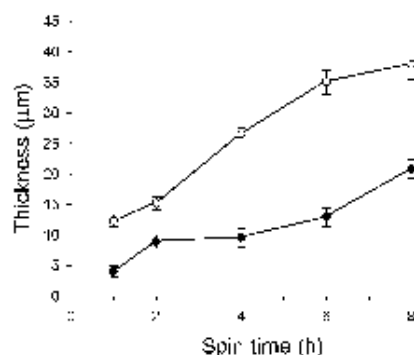


Fig. 2. Thickness of aligned (●) and non-aligned (○) nanofiber layers as a function of spin time.

3. Results and discussion

3.1. Morphological characteristics of CA nanofibers

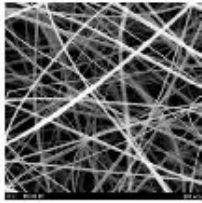
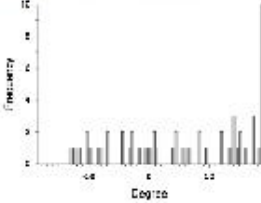
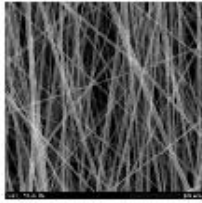
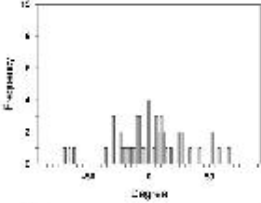
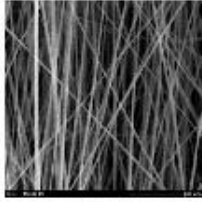
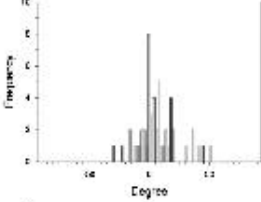
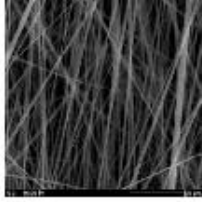
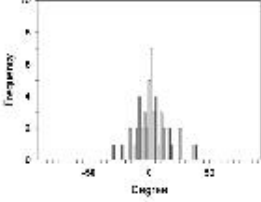
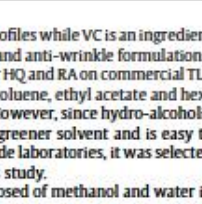
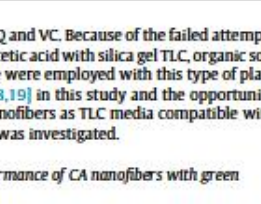
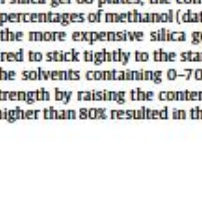
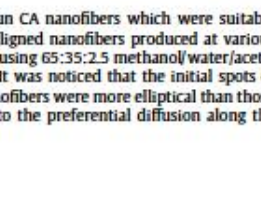
Of several means to control the alignment of electrospun nanofibers, a mechanical method through the use of a drum collector rotating at a high speed was employed in this study. As shown in Table 1, the drum rotation at 3500 rpm was apparently too slow to orient the deposited fibers in the uniaxial direction. By raising the collector speeds, nanofibers were found to be more aligned as indicated by the narrower distribution of nanofiber angles. Along with the improved alignment, the average diameter of nanofibers decreased with the increasing rotation speeds due to the higher stretch of the polymer jets wounded around the drum. Nonetheless, no evidence of fiber breakage was observed at all tested rotation speeds as seen under SEM. Since the nanofibers collected at 6000 rpm showed satisfactory alignment and insignificant morphological difference from those collected at the higher rpm, this rotation speed was chosen for the subsequent study.

To investigate the effect of spin time, the aligned nanofibers were electrospun at times of 1, 2, 4, 6, 8 and 10 h, maintaining the optimized collector rotation speed at 6000 rpm. Spin time is an important process parameter because the longer time generates more fibers on the collector and the electrical charge accumulated on the deposited fibers may interfere with the incoming ones resulting in the fibers with less alignment [20]. In another way, too short spin time produces insufficient thickness of fiber layers and may give rise to the poor chromatographic performance in terms of loading capacity of sample solution and separation quality. As shown in Fig. 2, the thickness of aligned nanofiber layers increased with the increasing spin time. Besides, the aligned nanofiber mats were thinner than the non-aligned ones which were electrospun at 350 rpm using the equal spin time. This effect was probably caused by the more compact deposit of aligned nanofibers with smaller diameter size on the aluminum backing. In this study, the alignment of nanofibers was not adversely affected by the increasing spin time, up to 10 h.

3.2. Silica gel TLC plates incompatible with green mobile phase

The separation of two target analytes namely HQ and RA and a possible interference VC was used for the evaluation of the chromatographic performance of different types of plates. HQ and RA are prohibited substances for use in cosmetics in many countries

Table 1
Effect of drum rotation speed on fiber morphology and alignment.

Speed of drum collector (rpm)	Characteristics of nanofibers		
	SEM	Diameter (nm)	Alignment
350		730 ± 60	
4500		650 ± 70	
			
6000		500 ± 40	
			
7500		500 ± 70	

due to their side effects and safety profiles while VC is an ingredient commonly found in skin whitening and anti-wrinkle formulations. Currently, the screening methods for HQ and RA on commercial TLC plates employ organic solvents e.g. toluene, ethyl acetate and hexane as mobile phase [18,19,21,22]. However, since hydro-alcoholic mixture is considered as safer and greener solvent and is easy to prepare and handle in the field outside laboratories, it was selected as the mobile phase of choice in this study.


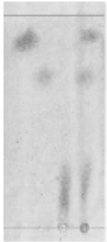




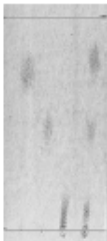
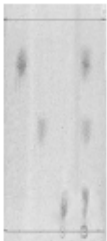
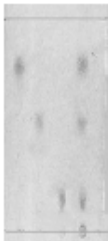
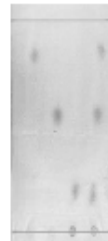
By using the mobile phase composed of methanol and water in the presence of 2.5% acetic acid with silica gel 60 plates, the compounds could not be resolved at any percentages of methanol (data not shown). After changing to use the more expensive silica gel 60 RP-18 plates, low polar RA appeared to stick tightly to the start spots and did not move up along the solvents containing 0–70% methanol. The increase of elution strength by raising the content of methanol in the mobile phase to higher than 80% resulted in the

poor resolution between HQ and VC. Because of the failed attempts at using methanol/water/acetic acid with silica gel TLC, organic solvents i.e. n-hexane/acetone were employed with this type of plate in the standard method [18,19] in this study and the opportunity of using electrospun CA nanofibers as TLC media compatible with safer and greener solvents was investigated.

3.3. Chromatographic performance of CA nanofibers with green mobile phase

To select the electrospun CA nanofibers which were suitable for TLC, aligned and non-aligned nanofibers produced at various spin times were evaluated using 65:35:2.5 methanol/water/acetic acid as the mobile phase. It was noticed that the initial spots of samples on the aligned nanofibers were more elliptical than those on non-aligned ones due to the preferential diffusion along the

Table 2
Effect of spin time on TLC separation of HQ, RA and VC.^a

Type of nanofibers	Spin time (h)					
	1	2	4	6	8	
Non-aligned						
	Run time (min)	47 ± 3	40 ± 4	38 ± 3	37 ± 3	35 ± 2
	Migration constant (cm ² /min) ^b	0.53	0.63	0.66	0.68	0.71
	Aligned					
		Run time (min)	34 ± 3	15 ± 2	13 ± 2	13 ± 2
Migration constant (cm ² /min) ^b		0.74	1.67	1.92	1.92	1.56

^a The order of spots from bottom to top was RA, HQ and VC.

^b Migration constant was calculated from (migration distance)²/time.

Table 3
Area of analyte spots on aligned and non-aligned CA nanofibers (n = 4).

CA nanofibers	Area of spot (pixel)	
	HQ	RA
Aligned	1260 ± 130	1020 ± 140
Non-aligned	2520 ± 300	1770 ± 330

vertical direction of nanofibers. Compared with the silica based plates, both aligned and non-aligned CA nanofibers were able to separate HQ, RA and VC with superior performance, as illustrated in Table 2. Good resolution without the solutes remaining at the initial spots was obtained from aligned and non-aligned nanofibers electrospun for at least 6 h and 4 h, respectively. The nanofibers collected at the shorter time than these periods were too thin for the efficient separation due to the inadequate chromatographic beds. Additionally, they took longer run time, probably related to the low capillary action to draw the solvent up the plate.

In spite of the comparable separation ability, the aligned and non-aligned nanofibers were found to be different in some aspects. By visual analysis, the spots on the aligned nanofibers were generally smaller and appeared darker compared to those on the non-aligned ones which were more diffused in broad areas (Table 2). The measurement of spot dimension by digital imaging software revealed that the spots on the non-aligned nanofiber plates were almost twice as large as those on the aligned ones in pixels (Table 3). This difference arose due to the fact that while the

solutes were moving up in the flow of mobile phase on the non-aligned nanofibers, they were likely to disperse in all directions due to the random arrangement of nanofiber mesh. On the other hand, the solute migration on the aligned nanofibers occurred preferentially along the vertical channels, giving rise to the lower extent of transverse (across-channel) diffusion. In addition, the reduced spot diffusion might associate with the lower thickness and higher density of the aligned media compared to the non-aligned one. For practical application, this feature offered the advantage of aligned nanofibers over the non-aligned ones in the terms of the ease of spot visualization and the lower mass of the analyte which could be detected.

Also interesting is the markedly faster separation ability of the aligned nanofibers. From the results, about two to three times reduction of developing time could be achieved by using the aligned nanofibers instead of the random ones (Table 2). In addition, the solvent migration on the aligned nanofibers used in this study (migration constant ≈ 1.9 cm²/min) was more rapid than that on the non-aligned ones reported in the previous work (migration constant ≈ 1.0 cm²/min), using the similar mobile phase [14]. It was hypothesized that the vertical channeling generated from the aligned nanofibers facilitated the solvent to move straight up the plate and minimized the lengthy distracted traveling along the random paths. In another point of view, the faster run time also lowered the chance of solute diffusion happening in the flow of mobile phase, thereby promoting the compact size of spots. In overall, since easy visual detection of spots and fast analysis are

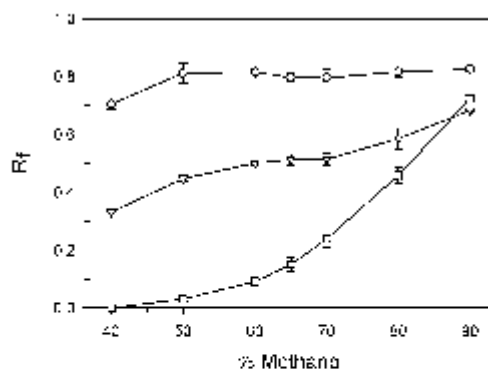


Fig. 3. TLC separation of RA (\square), HQ (∇) and VC (\circ) on aligned CA nanofiber plates (electrospun by using collector speed of 6000 rpm and spin time of 6 h) using mobile phases containing different percentages of methanol to water in the presence of 2.5% acetic acid.

Table 4
Masses of HQ and RA which could be visualized on different types of TLC plates.

Stationary phase	Mobile phase	Mass (ng)	
		HQ	RA
Aligned CA	65:35:2.5 methanol:water:acetic acid	10	25
Non-aligned CA	65:35:2.5 methanol:water:acetic acid	20	50
Silica gel 60	60:40 n-hexane:acetone	50	125

In all cases, 5% (w/v) phosphomolybdic acid in ethanol was used as a visualization reagent.

preferred for screening tasks, uniaxially aligned CA nanofibers with the adequate thickness were appropriate and practical for use.

3.4. Optimal conditions for TLC and method validation results

After the aligned CA nanofibers collected at the drum speed of 6000 rpm over 6 h of spin time were selected as the suitable stationary phase, the optimal mobile phase was investigated by varying the ratio of methanol to water. For reversed-phase separation, 2.5% acetic acid was added in the mobile phase to render the analytes non-ionized. The results showed that all solutes were eluted from the original application spots ($R_f > 0$) and well separated by using the mobile phase containing 60–70% methanol (Fig. 3). Therefore, 65:35:2.5 methanol/water/acetic acid was chosen as the optimized mobile phase.

To ascertain the analytical performance, TLC method was studied in the aspect of the masses of the analytes which could be visualized on the plates and the specificity. Interestingly, the masses of HQ and RA which could be visually detected on the aligned CA nanofiber plates were twice lower than those on the non-aligned nanofibers (Table 4) due to the darker spots on this type of fibers as previously discussed. Moreover, the masses of both compounds which could be detected on the aligned CA nanofibers were five times lower than those on typical silica plates which were used in the ASEAN method using the same visualization reagent. It was probable that the thinner chromatographic bed of electrospun nanofibers (8.5 μm) compared to that of commercial silica gel plates (200–250 μm) contributed to the better ability to visualize the analyte at the lower mass. To the best literature review, this is the first report about the advantage of nanofibrous stationary phases, especially in the aligned orientation, over conventional TLC plates in the aspect of the lower mass of the analyte which

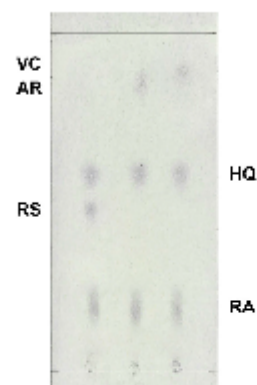


Fig. 4. Results of interference study for the proposed TLC screening method. The masses of HQ, RA, VC, AR and RS are 62, 335, 500, 500 and 50 ng per spot, respectively.

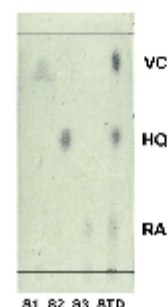


Fig. 5. TLC results for the analysis of three different samples on aligned CA nanofiber plates. S1 contained neither HQ nor RA whereas S2 and S3 were adulterated with HQ and RA, respectively. Standard (STD) VC, RA and HQ are in the right lane.

could be detected. For the specificity, the proposed method was free from the interference by the ingredients commonly found in cosmetic creams. As depicted in Fig. 4, HQ and RA were efficiently separated from the substances which could form colored spots with phosphomolybdic acid i.e. VC, RS and AR. For vitamin E and sodium metabisulfite, they did not react with phosphomolybdic acid and thus did not interfere with the test. Finally, the applicability of the proposed method was evaluated by the analysis of cosmetic creams collected from the local markets and it was found that the screening results were in agreement with the confirmatory HPLC method according to ASEAN guidelines [18,19]. Fig. 5 presents the TLC results of analysis of three different samples run on the aligned CA nanofiber plates. It was found that the sample S1 contained neither HQ nor RA whereas S2 and S3 were adulterated with HQ and RA, respectively.

4. Conclusion

Uniaxially aligned CA electrospun nanofibers were successfully fabricated by using high speed rotating drum collector and applied to use as TLC media. Besides the efficient separation ability, the aligned nanofibers with the appropriate layer thickness provided two to three times shorter run time than the randomly oriented ones. Furthermore, the masses of HQ and RA which could be detected on this material were two times lower than those on the

non-aligned nanofibers and five times lower than those on typical silica gel plates. In this work, the applicability of the aligned CA nanofibers was demonstrated in the screening of HQ and RA adulterated in cosmetics. Due to the satisfactory analytical performance as well as facile and inexpensive production process, aligned CA electrospun nanofiber is promising stationary phase for use in planar chromatography.

Acknowledgments

The authors acknowledge the financial support from Silpakorn University Research and Development Institute, Thailand under the grant agreement no. SURDI 55/01/19 and SURDI 56/01/11. Also, we thank Anon Chumphon-anan for his help in the laboratory and Eugene Kilayco for editing and proofreading the manuscript.

Appendix A. Supplementary data

Supplementary material related to this article can be found, in the online version, at <http://dx.doi.org/10.1016/j.chroma.2014.09.043>.

References

- [1] N. Bhardwaj, S.C. Kundu, Electrospinning: a fascinating fiber fabrication technique, *Biotechnol. Adv.* 28 (2010) 325–347.
- [2] W. Liu, S. Thomopoulos, Y. Xia, Electrospun nanofibers for regenerative medicine, *Adv. Healthcare Mater.* 1 (2012) 10–25.
- [3] H. Wu, et al., Electrospun metal nanofiber webs as high-performance transparent electrode, *Nano Lett.* 10 (2010) 4242–4248.
- [4] P. Wang, et al., Polymer nanofibers embedded with aligned gold nanorods: a new platform for plasmonic studies and optical sensing, *Nano Lett.* 12 (2012) 3145–3150.
- [5] K. Takazawa, J. Inoue, K. Mitsuishi, Self-assembled coronene nanofibers: optical waveguide effect and magnetic alignment, *Nanoscale* 6 (2014) 4174–4181.
- [6] D.P. Beason, et al., Fiber-aligned polymer scaffolds for rotator cuff repair in a rat model, *J. Shoulder Elbow Surg.* 21 (2012) 245–250.
- [7] H.B. Wang, M.E. Mullins, J.M. Clegg, C.W. McCarthy, R.J. Gilbert, Varying the diameter of aligned electrospun fibers alters neurite outgrowth and Schwann cell migration, *Acta Biomater.* 6 (2010) 2970–2978.
- [8] S. Chigome, N. Torto, A review of opportunities for electrospun nanofibers in analytical chemistry, *Anal. Chim. Acta* 706 (2011) 25–36.
- [9] J.E. Clark, S.V. Olesik, Electrospun glassy carbon ultra-thin layer chromatography devices, *J. Chromatogr. A* 1217 (2010) 4655–4662.
- [10] J.E. Clark, S.V. Olesik, Technique for ultrathin layer chromatography using an electrospun, nanofibrous stationary phase, *Anal. Chem.* 81 (2009) 4121–4129.
- [11] M.C. Beilke, J.W. Zewe, J.E. Clark, S.V. Olesik, Aligned electrospun nanofibers for ultra-thin layer chromatography, *Anal. Chim. Acta* 761 (2013) 201–208.
- [12] P. Kampaononwatt, P. Supaphol, G.E. Morlock, Electrospun nanofiber layers with incorporated photoluminescence indicator for chromatography and detection of ultraviolet-active compounds, *J. Chromatogr. A* 1299 (2013) 110–117.
- [13] T. Lu, S.V. Olesik, Electrospun polyvinyl alcohol ultra-thin layer chromatography of amino acids, *J. Chromatogr. B* 912 (2013) 98–104.
- [14] T. Rojanarata, S. Plianwong, K. Su-uta, P. Opasasopit, T. Ngawhirunpat, Electrospun cellulose acetate nanofibers as thin layer chromatographic media for eco-friendly screening of steroids adulterated in traditional medicine and nutraceutical products, *Talanta* 115 (2013) 208–213.
- [15] R. Komwarth, N. Karak, M. Misra, Electrospun cellulose acetate nanofibers: the present status and gamut of biotechnological applications, *Biotechnol. Adv.* 31 (2013) 421–437.
- [16] A.D. Katsambas, A.J. Stratigos, Depigmenting and bleaching agents: coping with hyperpigmentation, *Clin. Dermatol.* 19 (2001) 483–488.
- [17] S. Mukherjee, et al., Retinoids in the treatment of skin aging: an overview of clinical efficacy and safety, *Clin. Interv. Aging* 1 (2006) 327–348.
- [18] Association of Southeast Asian Nation (ASEAN). Available at: <http://www.asean.org/archive/MRA-Cosmetic/Doc-4.pdf> (accessed August 2013).
- [19] Association of Southeast Asian Nation (ASEAN). Available at: <http://www.asean.org/archive/MRA-Cosmetic/Doc-1.pdf> (accessed August 2013).
- [20] W.E. Teo, S. Ramakrishna, A review on electrospinning design and nanofiber assemblies, *Nanotechnology* 17 (2006) R89–R106.
- [21] O.N. Puzharitskaya, S.A. Ivanova, A.N. Shikov, V.G. Makarov, Separation and evaluation of free radical scavenging activity of phenol components of *Embilca* officinalis extract by using an HPTLC-DPPH method, *J. Sep. Sci.* 30 (2007) 1250–1254.
- [22] G. Ragnio, M. Veronico, R. Maddalena, C. Veluschi, Tretinoin assay in cosmetics and pharmaceuticals by carbon phase extraction, *J. Soc. Cosmet. Chem.* 47 (1996) 325–336.

BIOGRAPHY

- | | |
|-----------------------------|-------------------------|
| Name | Siripran Tidjarat, Miss |
| Date of Birth | February 20, 1986 |
| Place of Birth | Bangkok, Thailand |
| Nationality/Religion | Thai/Buddhism |
| E-mail address | tsiripran@gmail.com |
- Education**
- | | |
|-----------|--|
| 2010-2015 | Doctor of Philosophy, Ph.D. in Pharmaceutical Technology, Silpakorn University, Thailand |
| 2004-2008 | Bachelor of Pharmacy, in Pharmaceutical Technology, Silpakorn University, Thailand |
- Work experience**
- | | |
|-----------|--|
| 2009-2010 | Pharmacist at Sikarin Hospital, Thailand |
|-----------|--|
- Presentation**
- Poster**
1. **Siripran Tidjarat**, Winita Chaijaroenluk, Theerasak Rojanarata, Prasert Akkaramongkolporn, Tanasait Ngawhirunpat, Praneet Opanasopit. "Molecularly Imprinted Polymers: new technique to synthesis propranolol selective beads" The 2nd Current Drug Development International conference, 2nd – 3rd May 2012, Phuket, Thailand.

 2. **Siripran Tidjarat**, Praneet Opanasopit, Tanasait Ngawhirunpat, Theerasak Rojanarata. "Effect of Ionic and Covalent Crosslinking on Solubility and Copper Ion Adsorption Capability of Chitosan Beads" The 9th KU-KPS Conference, 6th – 7th December 2012, Kasetsart University (Kamphaeng Saen Campus), Thailand.

 3. **Siripran Tidjarat**, Kwanrutai Waewsang-nga, Thanawit Muangchang, Phudinan Ratanakreethakul, Theerasak Rojanarata. "Development of

Reversed Phase Paper Chromatography for Screening of Hydroquinone and Retinoic Acid in Cosmetics” The 3rd Current Drug Development International Conference, 1st – 3rd May 2014, Krabi, Thailand.

4. **Siripran Tidjarat**, Tanasait Ngawhirunpat, Praneet Opanasopit, Theerasak Rojanarata. “Preparation of Doubly Crosslinked Chitosan by The Use of Environmentally Friendly Crosslinkers_for Enzyme Immobilization” The 30th Annual Research Conference in Pharmaceutical Sciences, 10th – 12th Jan 2014, Chulalongkorn University, Thailand.

Scientific Publication:

1. **Siripran Tidjarat**, Tanasait Ngawhirunpat, Praneet Opanasopit, Theerasak Rojanarata,. Uniaxially aligned electrospun cellulose acetate nanofibers for thin layer chromatographic screening of hydroquinone and retinoic acid adulterated in cosmetics. *Journal of Chromatography A*. 2014; 1367: 141-147.

